The Dissertation Committee for Brian Scott Chen certifies that this is the approved version of the following dissertation:

TOP-LATERAL BRACING SYSTEMS FOR TRAPEZOIDAL STEEL BOX-GIRDER BRIDGES

Committee:

Joseph A. Yura, Supervisor

Karl H. Frank, Co-Supervisor

Michael D. Engelhardt

Stelios Kyriakides

Eric B. Williamson

TOP-LATERAL BRACING SYSTEMS FOR TRAPEZOIDAL STEEL BOX-GIRDER BRIDGES

by

Brian Scott Chen, M.S.

Dissertation

Presented to the Faculty of the Graduate School of

The University of Texas at Austin

in Partial Fulfillment

of the Requirements

for the Degree of

Doctor of Philosophy

The University of Texas at Austin

December 2002

This One Was for Me

ACKNOWLEDGEMENTS

I would like to express my sincerest gratitude to all those who helped me navigate this long and fruitful journey. This research project was funded by Texas Department of Transportation, with additional financial assistance provided by the College of Engineering at the University of Texas. Special assistance was provided by Bill West and his crew at J. D. Abrams during the field studies phase. The laboratory test specimen was graciously donated by Grand Junction Steel in Grand Junction, Colorado.

I would like to recognize the numerous individuals whose help was integral to the success of this research endeavor. To Ben Cheplak for enduring all the obstacles we encountered in the field studies; Cem Topkaya for all his work on the analytical side; Mike Hagenberger and Greg Cohen for keeping the office environment interesting and continually expanding my vocabulary; Jenny Tanner and Nat Ativitas for always being willing to help me test; Widianto for his countless hours of volunteer work and for always having a smile on his face.

I am especially indebted to Dr. Yura for not only being a patient and understanding advisor, but for also being a true teacher and mentor both in and outside of the classroom.

To my family, for their providing their continual advice and support.

Finally, to Christine, Kaffee, and Hogan for always being there.

October 27, 2002

TOP-LATERAL BRACING SYSTEMS FOR TRAPEZOIDAL STEEL BOX-GIRDER BRIDGES

Publication No. _____

Brian Scott Chen, Ph.D.

The University of Texas at Austin, 2002

Supervisors: Joseph A. Yura and Karl H. Frank

Trapezoidal steel box girders are becoming increasingly popular as a bridge system due to their torsional efficiency and aesthetic appearance. These bridge systems utilize one or more trapezoidal steel girders with a cast-in-place composite concrete roadway. The critical design stage occurs during pouring of the bridge deck, when the steel superstructure must support the weight of the fresh concrete. Top-lateral bracing systems are used to provide both strength and stiffness during construction.

A method for the design of top-lateral bracing systems was developed through field and laboratory experiments conducted on full-scale trapezoidal steel box-girders. The top-lateral bracing systems investigated included traditional single-diagonal truss systems and stay-in-place metal deck forms used during deck casting. Results include torsional girder stiffnesses, brace forces, and load-deflection responses. Design issues, limitations, and guidelines for truss, metal-deck, and combined top-lateral systems are presented.

TABLE OF CONTENTS

LIST OF TABLES

LIST OF FIGURES

CHAPTER 1
INTRODUCTION

1.1 GENERAL

Trapezoidal box girder systems are being used more frequently for curved bridges because of their torsional stiffness and aesthetic appearance. A typical system consists of one or more U-shaped girders, usually called "tub" girders, placed side-by-side with a concrete slab connecting the top flanges as shown in Figure 1.1.

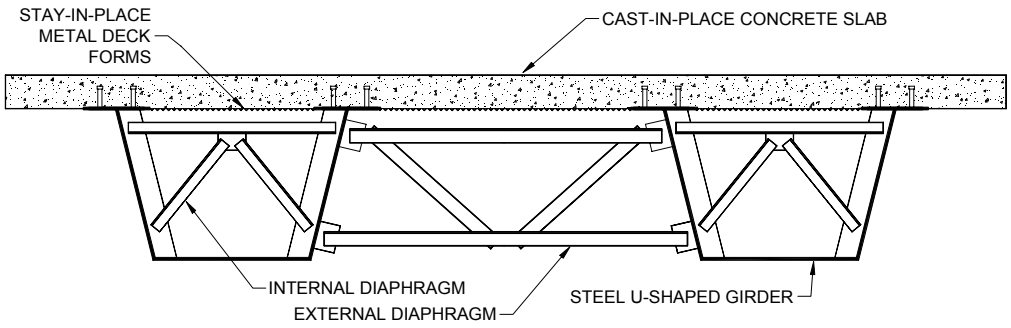

FIGURE 1.1 CROSS SECTION OF TRAPEZOIDAL BOX-GIRDER BRIDGE SYSTEM (CHEPLAK, 2001)

Construction of box-girder systems occurs in several stages. The steel girders are first assembled in a fabrication shop by cutting the webs and flanges from plates and welding them together. The girders are typically fabricated in lengths of 40 to 120 ft. so they can easily be transported to the construction site. At the job site, the segments are lifted into place and can be either bolted or

welded together. Field bolting has been the connection choice in most applications due to its ease of installation in comparison with field welding.

Stay-in-place or permanent metal-deck forms are placed across the top of the girders, as shown in Figure 1.2. These corrugated steel panels serve as the formwork when pouring the concrete slab and offer the advantage of speedy installation and freedom from having to be removed. The panels are normally supported on seat angles that are welded or strapped to the top-flanges as shown in Figure 1.3. The use of the support angles allows for the vertical adjustment of the deck panels and is used to correct for differences between the specified and as-built flange elevations.

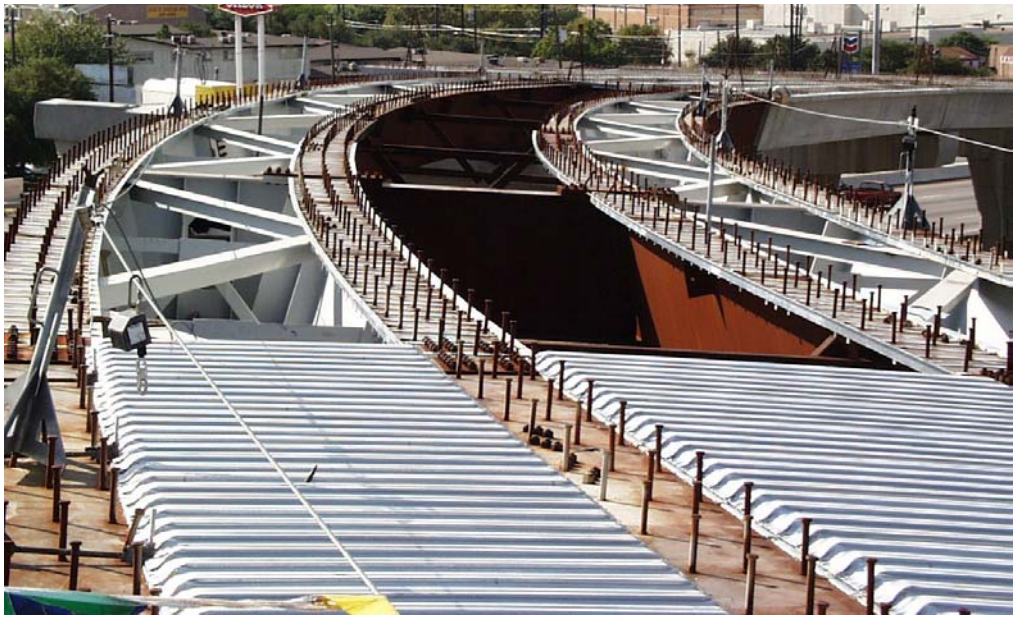

FIGURE 1.2 PERMANENT METAL DECK FORMS

The bridge deck is poured in stages to control both girder stresses and concrete shrinkage. When the concrete cures, shear studs previously placed on the top flanges allow the girder and deck to act compositely. The hardened deck

provides continuous lateral bracing for the top flanges and also closes the cross-section of each U-girder. The closed-section characteristic provides a path for shear flow around the cross section, which dramatically increases the torsional rigidity. For comparison, closed cross-sections can often have torsional stiffnesses thousands of times greater than similar open sections (Basler and Kollbrunner, 1969).

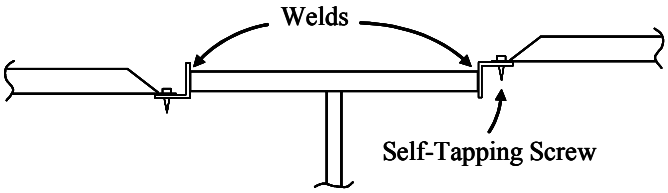

a.) Support With Welding

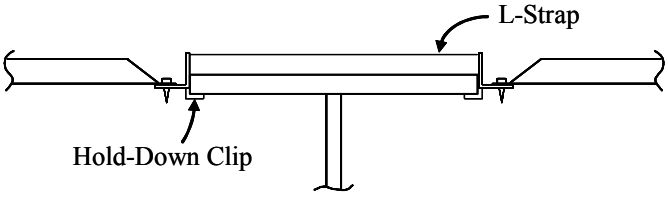

b.) Support Without Welding

FIGURE 1.3 METAL DECK SUPPORT DETAILS

The critical design stage for the steel members of these bridge systems occurs during pouring of the bridge deck, when the steel superstructure must support the entire construction load, including the weight of the fresh concrete. Lateral bracing is necessary to stabilize the narrow top flanges and provide sufficient torsional rigidity.

Current design guides provide little or no guidance for the design of top-lateral bracing systems. This lack of guidance has led many engineers to develop

either overly conservative or, in some instances, inadequate bracing designs. Recent failures such as the one pictured in Figure 1.4, have demonstrated the need for a comprehensive and rational design methodology.

FIGURE 1.4 FAILURE OF TOP-LATERAL BRACE DURING BRIDGE ERECTION

1.2 OBJECTIVE AND SCOPE

The objective of this research project is to develop guidelines for the design of top-lateral bracing systems for steel box-girder bridge systems. In addition to traditional truss systems, an alternative bracing system utilizing the stay-in-place metal deck forms is be evaluated. Although the idea of using permanent metal-deck forms as lateral bracing was first presented in the 1970's, little research to date has been conducted.

Heins and Blank (1973) investigated the torsional stiffness of open box beams closed by corrugated decking. A procedure was developed to replace the

decking with an equivalent flat plate. This equivalent-plate approximation, first introduced by Dabrowski (1968), enabled the braced section to be analyzed using existing thin-walled closed-section theories. Experiments included in-plane shear tests on the corrugated deck panels as well as box-beam torsion tests. Torsional stiffnesses estimated using the equivalent-plate approximations were between 0.8 and 1.3 times measured values. Procedures to determine the equivalent plate thickness of the corrugated decking were complicated and difficult to implement in design.

Luttrell (1981) developed a diaphragm design manual for the Steel Deck Institute (SDI) which enabled designers to estimate the shear strength and stiffness of a particular deck diaphragm based on the physical properties of the deck sheets and the fastener arrangement. These design formulations, which were based on extensive experimental tests on various steel deck profiles, have been used extensively in the building industry for the design of roof and floor diaphragms (Luttrell and Huang, 1981). A schematic of metal-deck forms spanning between girder flanges is shown in Figure 1.5.

Currah (1993) tested various types of bridge-deck forms and compared the results with predictions using the SDI Manual. Modifications of the design formulations were made to account for the specific arrangement of bridge deck diaphragms versus roof or floor diaphragms. Results indicated that the modified formulations produced reasonably reliable stiffness and strength values. It was also discovered that the shear stiffness of the decking was greatly influenced by the supporting system used to attach the deck panels. In some cases, the support-angle systems commonly used in the industry (Figure 1.3) reduced the overall diaphragm stiffnesses by more than 80%.

Soderburg (1994) developed modified connection details to improve the overall stiffness of the deck diaphragms. Jetann et al. (2002) proposed using a

stiffening-angle to which the sheet-to-sheet sidelap connectors could be attached. Overall diaphragm shear stiffnesses using this detail exhibited increases on the order of 50%.

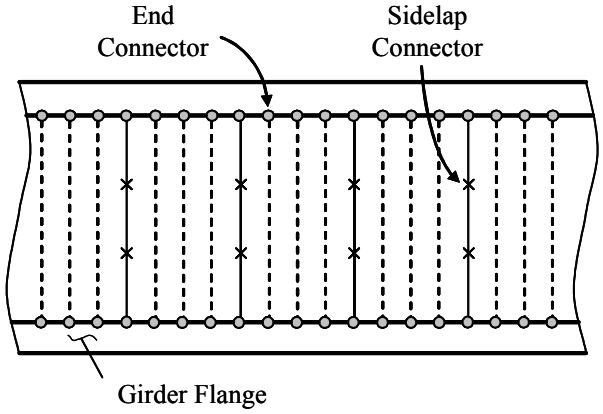

FIGURE 1.5 SCHEMATIC LAYOUT OF A BRIDGE DECK FORM

Helwig (1994) developed a design approach for using stay-in-place metal deck forms as lateral-bracing in bridge girders during the construction of the concrete deck. The scope of the research, however, was limited to I-girder bridge systems.

A primary emphasis of this research study is to investigate the application of metal-deck forms as lateral-bracing in box-girder bridge systems. The capabilities and limitations of metal-deck bracing systems will be examined. The lateral-bracing design guidelines developed will encompass metal-deck systems, traditional truss-systems, as well as combined systems using both truss and metal decking.

Chapter 2 of this dissertation presents background information related to torsion of thin-walled sections and describes the equivalent plate approximation used to model box-girders with top-lateral bracing systems. Chapter 3 presents

field tests conducted on a highway interchange that utilized trapezoidal steel box-girders. These tests provided verification of analytical models as well as insight into the behavior of these bridge systems. In addition, these tests were used to evaluate the feasibility of metal-decking as a lateral-bracing system. Laboratory tests conducted on a straight box-girder test specimen are reported in Chapters 4 and 5 with analysis of results in Chapter 6. The proposed design method for the various lateral-bracing systems is outlined in Chapter 7 along with a discussion on special issues and limitations related to metal-deck bracing. Numerical design examples for straight and curved bridges are included in the appendices. A final summary and conclusion of the research study is given in Chapter 8.

CHAPTER 2
BACKGROUND

2.1 TORSION OF THIN-WALLED SECTIONS

Members subjected to torsion have a distinguishing feature in that plane sections do not remain plane when loaded. This phenomenon causes the cross sections of members to warp. Certain sections that do not warp include circular sections and thin-walled sections in which all elements intersect at one point, such as a cruciform, angle, or tee. Depending on whether the cross section is free to warp, there is a distinction that is made between *uniform* (also referred to as pure or St. Venant) and *nonuniform* (or warping) torsion. Pure torsion resists the applied load through shear stresses in the plane of the cross sections. During loading, displacements occur both in and out-of-plane. If warping is unrestrained, the out-of-plane displacements do not induce any normal stresses. If warping is restrained, however, the out-of-plane displacements cause normal stresses to develop. The resulting normal stresses induce warping shears, which provide an additional torsional restraining moment. This moment, known as the warping torsional moment, along with the pure torsional moment combine to keep the system in equilibrium.

2.1.1 Pure Torsion

The basic governing equation for an elastic member subjected to pure torsion is given by (Basler and Kollbrunner, 1969)

$$T = GK_T\theta' \tag{2.1}$$

where T is the applied torque, G is the shear modulus of the material, K_T is the pure torsional constant, and θ' is the twisting angle per unit length. The pure

torsional constant for open sections comprised of narrow rectangular elements can be approximated by (Basler and Kollbrunner, 1969)

$$K_{T_{open}} = \frac{1}{3}\sum_{i=1}^{n} b_i t_i^3 \tag{2.2}$$

where b_i and t_i are the width and thickness of each element, respectively. For closed sections, the pure torsional constant is

$$K_{T_{closed}} = \frac{4A_o^2}{\oint \frac{1}{t(s)} ds} \tag{2.3}$$

where A_o is the area enclosed by the centerline of the walls and $t(s)$ is the wall thickness along the member arc length s. If the hollow cross section is made up of n elements, each of thickness t_i and width b_i, then the contour integral can be replaced with

$$\oint \frac{1}{t(s)} ds = \sum_{i=1}^{n} \frac{b_i}{t_i} \tag{2.4}$$

The expression for the pure torsional constant for closed shapes then becomes

$$K_{T_{closed}} = \frac{4A_o^2}{\sum_{i=1}^{n} \frac{b_i}{t_i}} \tag{2.5}$$

2.1.2 Warping Torsion

The basic governing equation for an elastic member subjected to warping torsion is given by (Basler and Kollbrunner, 1969)

$$T = -EI_w\theta''' \tag{2.6}$$

where E is the modulus of elasticity and I_w is the warping torsion constant. The warping torsional properties for any general shape can most readily be obtained

using a numerical procedure, which utilizes finite difference relations. Many cross sections can be simplified by considering the section to be composed of a series of interconnected narrow, rectangular elements (Basler and Kollbrunner, 1969). Details of this procedure are presented in various references (Basler and Kollbrunner, 1969; Heins 1975).

2.1.3 Combined Pure and Warping Torsion

In most engineering applications, a member will resist torsional loads with both pure and warping torsional stresses. The combined torsional resistance becomes the sum of both the pure and warping components. As a result, the governing differential equation becomes

$$T = GK_T\theta' - EI_w\theta''' \tag{2.7}$$

The relative proportion of each type of torsion present in a member depends on both its length and cross section. The parameter χ is used to determine whether pure or warping torsion predominates. This parameter is related to the member length as well as the ratio of the pure torsional rigidity GK_T and the warping torsional rigidity EI_w.

$$\chi = L\sqrt{\frac{GK_T}{EI_w}} \tag{2.8}$$

The torsional predominance of a member based on the value of the parameter χ is given in Table 2.1 (Basler and Kollbrunner, 1969).

TABLE 2.1 PURE AND WARPING TORSIONAL PREDOMINANCE

Torsional Predominance	χ
Pure Warping	< 0.3
Dominating Warping	0.3 - 2
Mixed	2 - 5
Dominating Pure Torsion	5 - 10
Pure Torsion	> 10

Members dominated by one type of torsion can be approximately analyzed by neglecting the other type of torsion. For thin-walled open cross sections, Saint-Venant torsion dominates long members and warping in short ones (Basler and Kollbrunner, 1969). For idealized systems, the boundary conditions for twist and warping are summarized in Table 2.2.

TABLE 2.2 IDEALIZED BOUNDARY CONDITIONS

Twist Restrained	$\theta = 0$
Warping Restrained	$\theta' = 0$
Warping Unrestrained	$\theta'' = 0$

2.2 EQUIVALENT-PLATE METHOD

The analysis of pseudo-closed or quasi-closed box girders is generally performed using an equivalent-plate approximation. In this method, the top-lateral truss system is treated as a fictitious plate. This allows the torsional properties of the girder to be approximated during structural analysis. The thickness of the fictitious plate is used in Eqn. (2.5) to determine the pure torsion

constant for the section. The resulting torsional properties are used to determine the distribution of torsional moments in the girder.

2.2.1 Truss Systems

Truss bracing systems can be approximated as an equivalent plate of thickness t_{eq}. Solutions have been developed for a variety of commonly used arrangements (Basler and Kollbrunner, 1969; Dabrowski, 1968). For single-diagonal (SD) arrangements, the equivalent plate thickness is

$$t_{eq} = \frac{E}{G} \frac{s\,b}{\frac{d^3}{A_d} + \frac{2}{3}\frac{s^3}{A_f}} \tag{2.9}$$

where A_f and A_d are the areas of the top flange and diagonal brace, respectively. The variables s, w, and d define the geometry of the bracing as shown in Figure 2.1. Expressions for other truss arrangements are presented elsewhere (Heins, 1975).

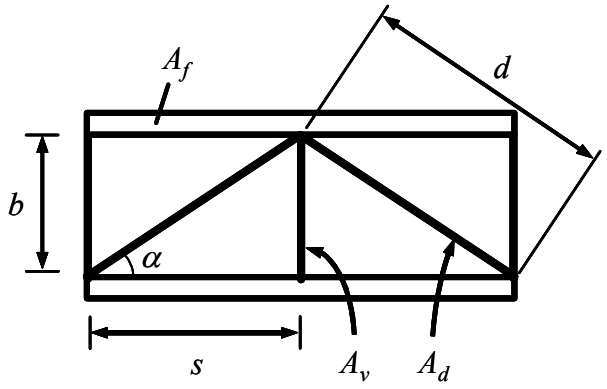

FIGURE 2.1 TOP-LATERAL SINGLE-DIAGONAL TRUSS SYSTEM

2.2.2 Metal Decking

The *Steel Deck Institute Diaphragm Design Manual* or SDI Manual (Luttrell, 1987) has procedures to determine the shear stiffness of metal decking with various geometries and fastener arrangements. The permanent metal deck forms, when used as top-lateral bracing, can be approximated as an equivalent plate. The thickness of the plate is determined by equating the shear stiffness of decking and the plate. The validity of this assumption will be evaluated in this research project.

The shear stiffness of metal decking is not linear with respect to the thickness of the deck material. Therefore the deck stiffness determined using the SDI Manual is presented as an effective shear modulus, G', and is defined as

$$G' = Gt_{eq} \tag{2.10}$$

where G is the shear modulus of steel. The thickness of the equivalent plate representing the metal decking can be approximated as the effective shear modulus determined from the SDI Manual divided by the shear modulus of steel. The equivalent plate thickness of metal decking is routinely one order of magnitude smaller than the base metal thickness of the decking. For 20-gauge decking (0.036 in.), a typical equivalent plate thickness might be 0.005 inches.

2.2.3 Combined Truss-Deck Systems

When a top-lateral truss system is used in conjunction with a metal deck system, the thickness of the equivalent plate closing the section is assumed to be equal to the algebraic sum of the individual plate thicknesses. The validity of this assumption is evaluated in this research project. The shear force induced in each bracing system is then proportional to the relative shear stiffness of each system, which corresponds to the relative thickness of each equivalent plate. The force in a diagonal used in conjunction with metal decking can be calculated as

$$P_d = \left[\frac{(t_{eq})_{diag}}{(t_{eq})_{diag} + (t_{eq})_{deck}} \right] \frac{Td}{2A_o} \tag{2.11}$$

where $(t_{eq})_{diag}$ and $(t_{eq})_{deck}$ refer to the equivalent plate thicknesses of the diagonal truss member and decking, respectively. The enclosed area, A_o, for the combined system is affected by the location of the combined equivalent plate. Although the true location of the combined system lies between the individual plate locations, a conservative design approach would be to select the smallest enclosed area.

2.3 TOP-LATERAL BRACE FORCES

2.3.1 Brace Forces Due to Torsion

The forces in top-lateral bracing systems due to torsion are related to the torsional shear flow within the psuedo-closed cross section. The shear flow in the elements of a closed section is given by

$$q = \frac{T}{2A_o} \tag{2.12}$$

The total shear force on a brace panel is

$$V = \frac{T}{2A_o} b \tag{2.13}$$

where b is the brace panel width defined in Figure 2.1. If metal deck is used as lateral bracing, it must be designed to carry the total shear force given by Eqn. (2.13). For truss bracing, the transverse shear can be resolved into a diagonal brace force

$$P_d = \frac{Td}{2A_o} \tag{2.14}$$

The diagonal force, P_d, is independent of the brace member size and depends only the vertical placement (A_o) and geometry (d) of the bracing. For X-type systems,

the brace forces are one-half the magnitude of those with single-diagonals and are equal and opposite in magnitude.

2.3.2 Truss Forces Due to Bending

Fan and Helwig (1999) developed equations to determine the forces generated in top-lateral truss systems due to box-girder bending. These formulations were in excellent agreement with finite-element predictions. For convenience, these equations are reproduced below (refer to Figure 2.1):

For SD-Type Trusses

$$D_{bend} = \frac{f_{x_{top}} s \cos\alpha}{K_1} = \frac{f_{x_{top}} s^2}{K_1 d} \tag{2.15}$$

$$S_{bend} = -D_{bend} \sin\alpha = -\frac{D_{bend} b}{d} \tag{2.16}$$

$$f_{L_{bend}} = \frac{1.5s}{b_f^2 t_f} S_{bend} \tag{2.17}$$

For X-Type Trusses

$$D_{bend} = \frac{f_{x_{top}} s \cos\alpha}{K_2} = \frac{f_{x_{top}} s^2}{K_2 d} \tag{2.18}$$

$$S_{bend} = -2D_{bend} \sin\alpha = -\frac{2D_{bend} b}{d} \tag{2.19}$$

$$f_{L_{bend}} = 0 \tag{2.20}$$

where K_1 and K_2 are parameters defined by

$$K_1 = \frac{d}{A_d} + \frac{b}{A_s}\sin^2\alpha + \frac{s^3}{2b_f^3 t_f}\sin^2\alpha = \frac{d}{A_d} + \frac{b^3}{A_s d^2} + \frac{s^3 b^2}{2b_f^3 t_f d^2} \qquad (2.21)$$

$$K_2 = \frac{d}{A_d} + \frac{2b}{A_s}\sin^2\alpha \qquad (2.22)$$

and where

f_{xtop} = the longitudinal stress at the middle of the top flange

D_{bend} = diagonal brace force

S_{bend} = strut brace force

$f_{L_{bend}}$ = lateral bending stress in top flange due to S_{bend}

s = the spacing of the struts (panel length)

α = angle between the top flange and diagonal brace

b_f = top flange width

t_f = top flange thickness

d = length of a diagonal

b = distance between the middle of the top flanges

A_d = area of diagonal

A_s = area of strut

2.4 SUMMARY

A review of torsion of thin-walled sections has been presented. The concept of the equivalent-plate approximation is used to apply these principles to pseudo-closed sections. The formulas presented to determine the equivalent-plate thickness and associated brace forces for various types of top-lateral systems will be used in the subsequent section of this report.

CHAPTER 3
FIELD TESTS

This chapter presents the results of a series of experimental field tests conducted on a full-scale trapezoidal steel box-girder bridge during construction. The main objective of these tests was to evaluate the potential of permanent metal deck forms as a lateral-bracing system, verify the accuracy of finite-element models, and obtain experimental data on a bridge structure with real-world boundary conditions. These tests were performed in conjunction with a companion research project sponsored by the Texas Department of Transportation. Additional details are reported by Cheplak (2001) and Memberg (2002).

3.1 BRIDGE UNDER STUDY

The bridge under study was located at the north interchange for Interstate Highway 35 (IH-35) and State Highway US 290 in Austin, Texas. The interchange was comprised of four bridge connects, each consisting of twin trapezoidal steel box-girder systems for the curved spans and concrete box-girders for the straight spans. The portion of the bridge under study was bridge Connect K, which connected southbound IH-35 to eastbound US 290 and is highlighted in Figure 3.1.

The steel spans of bridge Connect K had a radius of curvature of approximately 575 ft. and span lengths of 168 ft., 242 ft., and 168 ft., as shown in Figure 3.2. Typical cross-sectional dimensions are given in Figure 3.3. The bridge utilized a single-diagonal top-lateral bracing system with internal K-diaphragms at every panel point. External diaphragms were placed between the

two adjacent girders at every other panel point. One elastomeric bearing was located under the center of each girder at pier locations.

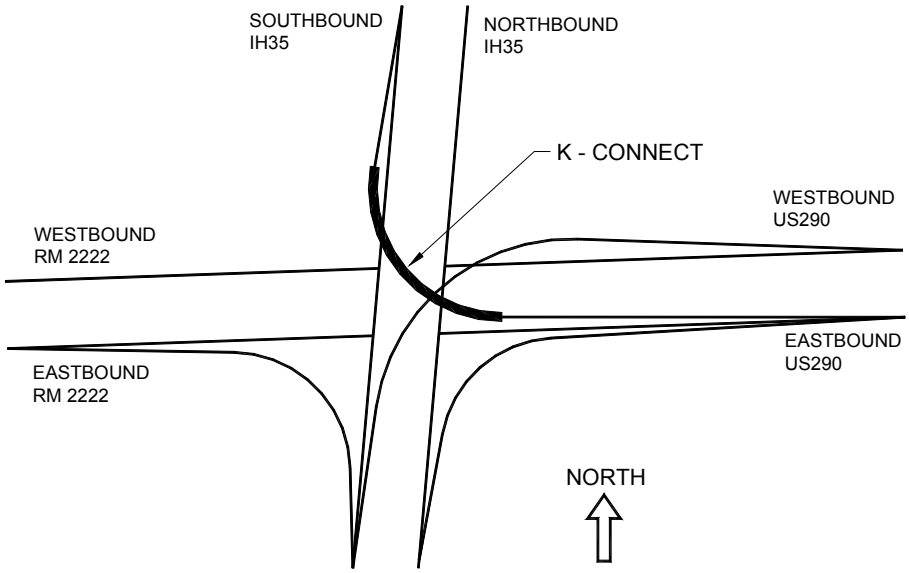

FIGURE 3.1 SITE LOCATION (CHEPLAK, 2001)

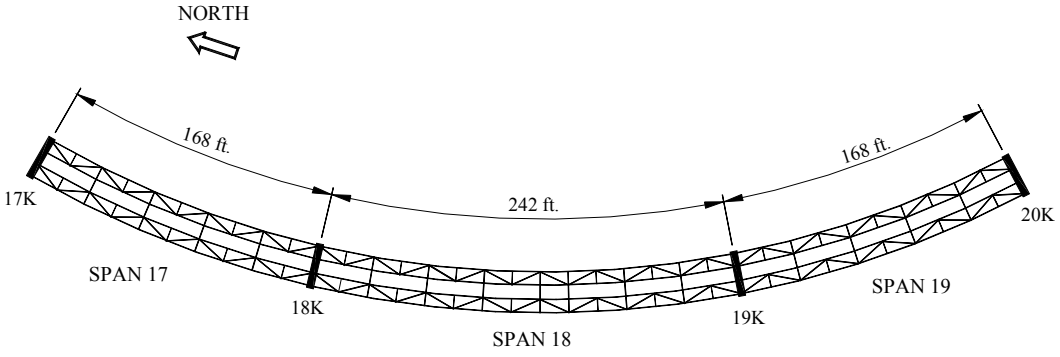

FIGURE 3.2 PLAN VIEW FOR BRIDGE (CHEPLAK, 2001)

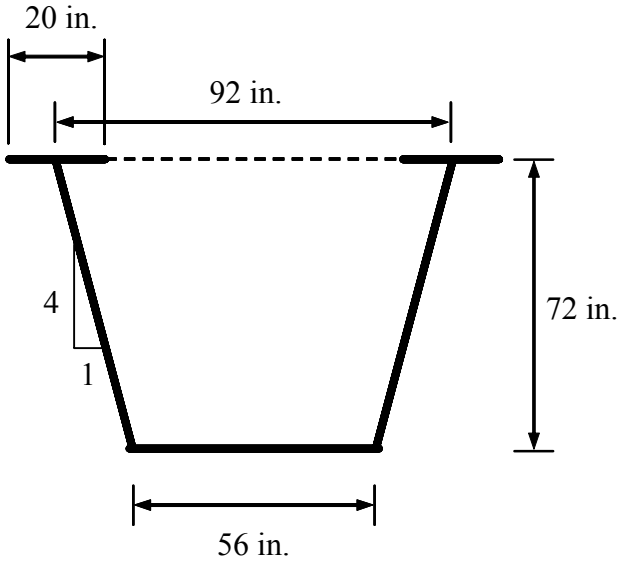

FIGURE 3.3 TYPICAL CROSS-SECTION

3.2 TEST DESCRIPTION

3.2.1 Overview

The field tests on bridge Connect K involved applying a known concentrated load to the erected steel superstructure using a construction crane fitted with a load cell. Selected top-lateral braces were instrumented to measure brace forces. One test was conducted on the bare steel and a second replicate test was conducted with permanent metal deck forms placed over the instrumented braces. Differences in the brace forces measured in the two tests were used to evaluate the effectiveness of the metal decking as a potential bracing system. Finally, measured values were compared with analytical models.

3.2.2 Loading

Loading of the bridge was accomplished by attaching the lifting apparatus used for girder erection to the top flange of one of the bridge girders as seen in Figure 3.4. The crane used to apply the concentrated loads had an internal load

cell capable of measuring the applied load with an accuracy of 500 lbs. The two lifting clamps were attached to the exterior flange of the exterior girder at the fourth brace panel point as shown in Figure 3.5.

FIGURE 3.4 LOADING CRANE & TOP-FLANGE ATTACHMENT

3.2.3 Instrumentation

The first three top-lateral diagonal braces in each girder, highlighted in Figure 3.5, were each instrumented with strain gauges. Three gauges were placed at two different cross-sections on each member for redundancy. Brace forces were obtained by assuming a planar strain distribution. All gauge measurements were compensated for induced strains resulting from thermal effects of the bridge structure (Cheplak, 2001).

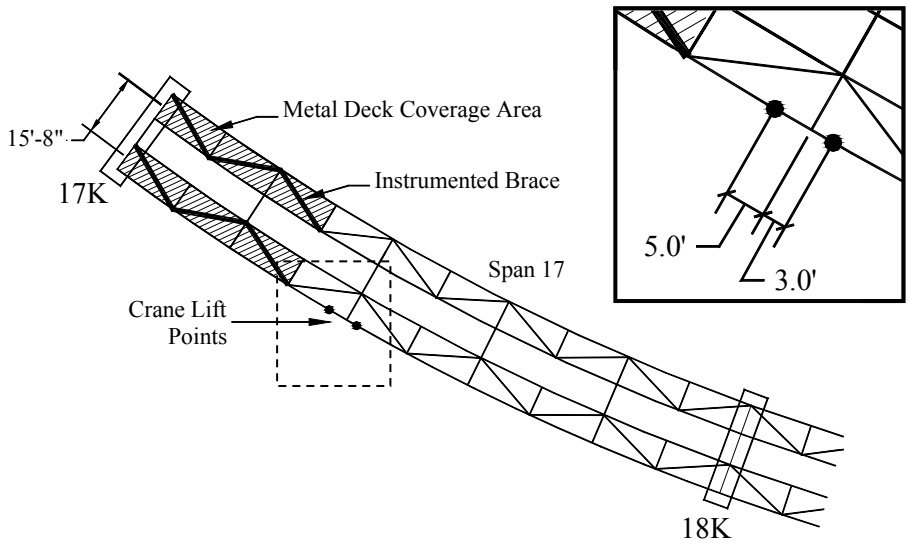

FIGURE 3.5 LOCATION OF APPLIED CRANE LOAD

3.2.4 Permanent Metal Deck Forms

The permanent metal deck forms used in the field tests were 2.5 in. deep 16-gauge galvanized steel bridge forms. These deck forms were manufactured by the Wheeling Corrugated Company and were identical to those used by the contractor except that the gauge thickness was increased from 20-gauge. The thicker 16-gauge decking was selected so a "best-case" metal-deck bracing system could be evaluated.

Each deck sheet was 96 in. long with a 32 in. cover width. Cross-sectional dimensions for the deck panels are given in Appendix B. A schematic of the connection detail used in the field tests is shown in Figure 3.6. In current practice, a light-gauge angle member is attached to the top flange either by welding directly to the flanges in compression zones or using strap details if the flange is in tension (see Figure 1.3).

For Connect K, the deck panels were fastened directly to the top flanges using Hilti ENPH2-21-L15 powder actuated fasteners. The purpose of this direct

attachment was to eliminate the eccentricity between the decking and flange. These eccentricities have been shown to dramatically reduce the effective stiffness of deck panels (Soderberg, 1994). Elimination of the support angle would provide the optimal brace connection upon which to evaluate the bracing potential of the decking. For the field tests, one fastener was placed in the center of each corrugation valley while two fasteners were used at each lap seam as shown in Figure 3.7. No sheet-to-sheet stitch fasteners were used to connect adjacent deck panels.

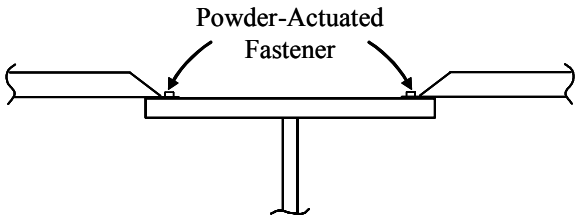

FIGURE 3.6 METAL DECK ATTACHMENT DETAILS

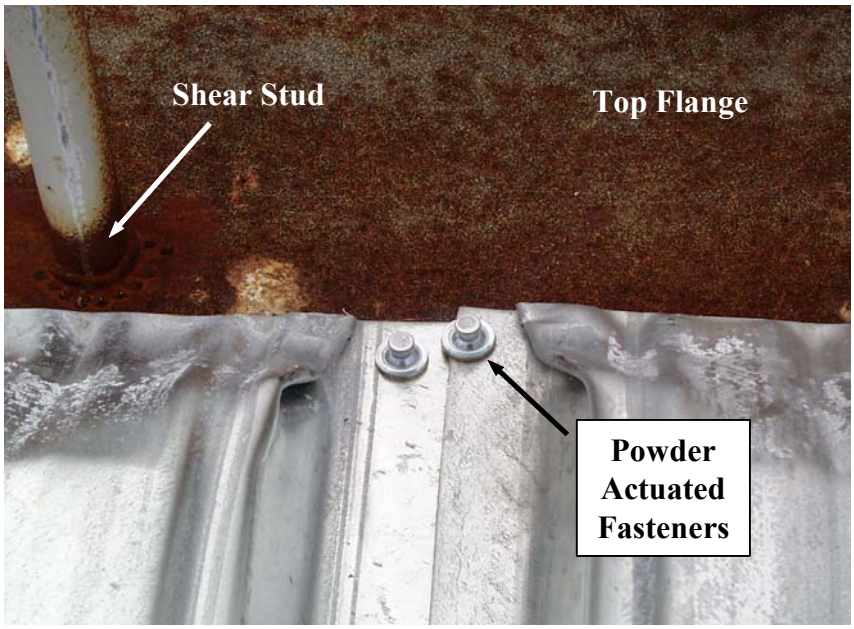

FIGURE 3.7 DECK-TO-FLANGE ATTACHMENT AT SIDELAP SEAM

3.2.5 Test Procedure

Load was applied to the bridge incrementally and held constant for one minute at each load step to allow for any settlement or redistribution. This was done during both the loading and unloading stages. The maximum applied load was limited to prevent uplift at any support or damage to any structural element.

The first test was conducted on the bare steel superstructure with no permanent metal deck forms present. Deck forms were then installed over the instrumented braces, as shown in Figure 3.5, and a second test was conducted. For each test case, two trials were conducted to ensure repeatability.

3.3 FINITE ELEMENT MODELS

The bridge under study was analyzed using the commercially available finite element program ABAQUS. The model for Connect K was developed jointly with a concurrent Texas Department of Transportation research study investigating early stiffness of bridge deck concrete (Topkaya, 2002). The finite element model incorporated eight-noded quadratic shell elements with reduced integration (S8R5) for the top and bottom flanges, webs, pier diaphragms, and metal decking. Four shell elements were used in webs and bottom flanges and two shell elements were used for each top flange as seen in Figure 3.8. Three-dimensional 2-node linear beam elements (B31) were used to model the internal diaphragms, external diaphragms, and top-lateral bracing members. A layer of eight shell elements was used between each internal brace locations. The crane load was represented using two concentrated loads placed at the centerline of the top flange. All analyses were linear.

The metal deck panels were modeled using the equivalent flat plate approximation described in Chapter 2. The calculated equivalent plate thickness was equal to 0.01168 in. Detailed calculations are given in Appendix B.

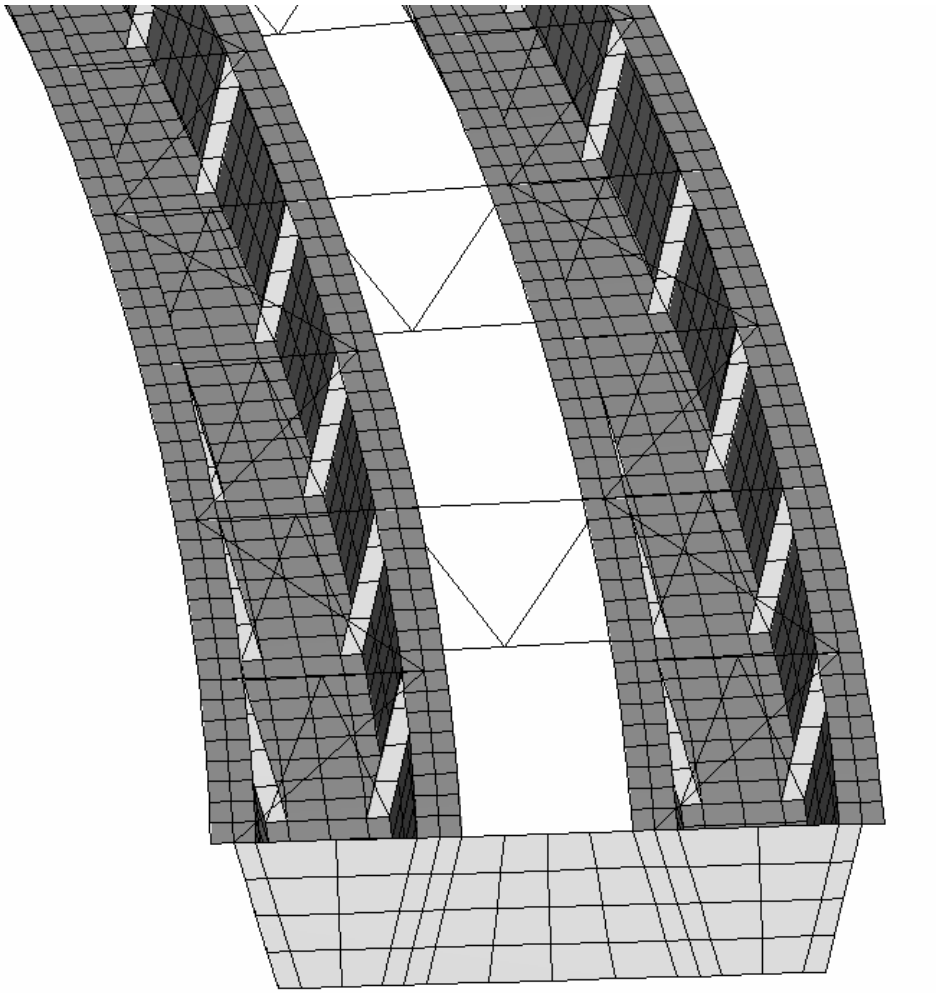

FIGURE 3.8 FINITE ELEMENT MODEL FOR BRIDGE CONNECT K

3.4 TEST RESULTS

3.4.1 Top-Lateral Forces

The top-lateral brace forces measured during the field tests were compared with predicted forces from ABAQUS. A typical brace force response is shown in Figure 3.9. The measured response is generally linear for both the loading and

unloading stages. The solid line plotted represents the response predicted using ABAQUS. The modified ABAQUS prediction includes an adjusted external diaphragm stiffness and is discussed in Section 3.4.2.

The brace force responses summarized in Table 3.1 represent the brace forces in kips per unit applied crane load and is simply the slope in Figure 3.9. Field test values were obtained using a linear regression of the experimental data. Brace member labels are given in Figure 3.10.

It was observed that the measured forces for the outer girder (A, B, & C) were all greater than the predicted values while the inner girder forces (D, E, & F) were all smaller than predicted. This phenomenon was also observed in similar tests conducted on bridge Connect Z at the same site (Cheplak, 2001). It was believed that the cause for this discrepancy was due to the flexibility of the connection between the external diaphragms and girders.

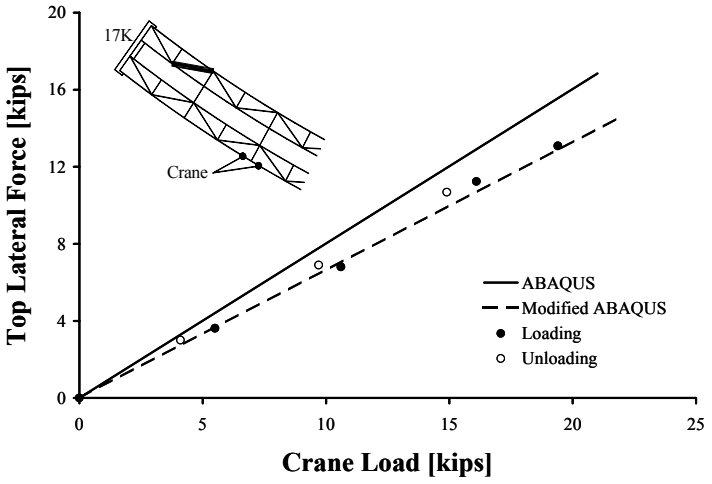

FIGURE 3.9 TYPICAL TOP-LATERAL BRACE FORCE RESPONSE

TABLE 3.1 BRACE FORCES (KIPS) PER UNIT APPLIED CRANE LOAD FOR VARIOUS EXTERNAL DIAPHRAGM STIFFNESSES

BRACE MEMBER	FIELD TEST (no deck)	ABAQUS External Diaphragm Brace Area [in^2]					
		4.75 (actual)		1.13		0.50	
A	-1.00	-0.91	-9%	-0.94	-6%	-0.97	-3%
B	0.98	0.93	-5%	0.97	-1%	1.00	3%
C	-0.70	-0.63	-10%	-0.66	-6%	-0.69	-1%
D	-0.64	-0.79	24%	-0.73	14%	-0.66	3%
E	0.69	0.80	17%	0.74	7%	0.67	-3%
F	-0.41	-0.47	12%	-0.43	3%	-0.38	-8%

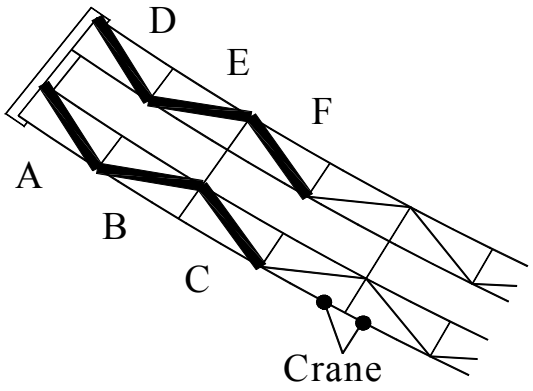

FIGURE 3.10 TOP-LATERAL BRACE MEMBER LABELS

3.4.2 Effect of External Diaphragm Stiffness

The external diaphragm-to-girder connection incorporated a WT stub bolted to the web of the girder as shown in Figure 3.11. When loaded in tension, the distortion of the WT stub, shown in Figure 3.12, reduced the effective stiffness of

the diaphragm. As a result, a smaller proportion of the applied crane load was transmitted to the inner girder.

An approximate analysis was conducted to investigate the effect of the external diaphragm stiffness on the distribution of top-lateral brace forces. The stiffness of the connection was determined by considering the portion of the WT stub between the bolt lines to be a simply supported beam. A fixed-end condition was also considered to establish the bounding limits of the connection stiffness. The connection stiffness in series with the axial truss member stiffnesses were used to ascertain an overall diaphragm stiffness. Analysis indicated the connection reduced the overall diaphragm stiffness between 1.6 and 3.3 times.

The stiffness of the external diaphragms was modified by altering the area of the bracing members. Table 3.1 summarizes the predicted brace force responses for different brace areas. For each brace area, the brace force response per unit applied crane load and percent difference from the experimental values is listed. The area of the actual brace members used in the bridge was 4.75 in^2. Brace areas equal to 2.01 in^2 represent the average of the simply supported and fixed-fixed analysis results. For a brace area equal to 0.50 in^2, the predicted forces were within 3% of experimental values and represents the modified ABAQUS analysis shown in Figure 3.9.

Although the connection stiffness could not account for the entire brace force discrepancy, it represents only one of many differences between the field structure and the analytical model. Other simplifications in the analytical model include attachment of the external diaphragm at the web-flange intersection, exclusion of the dapped ends at pier 17K, and idealized support conditions.

Since the primary goal of the field tests was to investigate the effectiveness of metal-deck bracing, comparisons between the bare steel and decked girder were made using the calibrated model (brace area = 0.5 in^2).

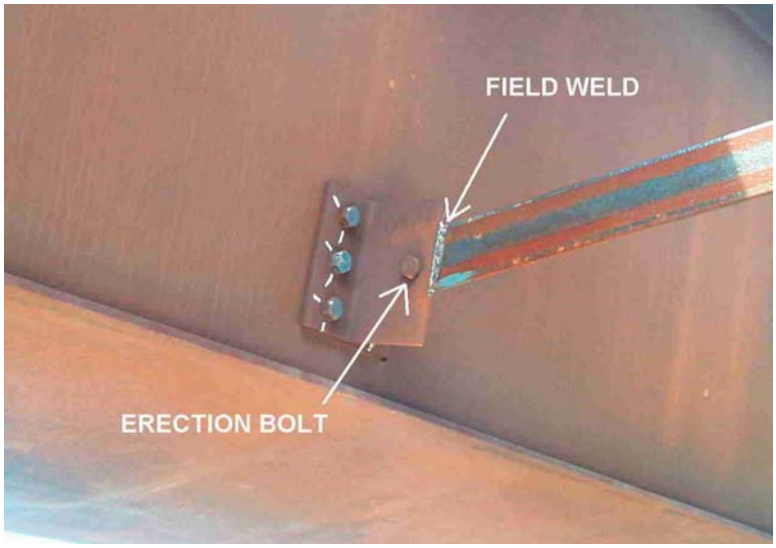

FIGURE 3.11 EXTERNAL DIAPHRAGM CONNECTION (CHEPLAK, 2001)

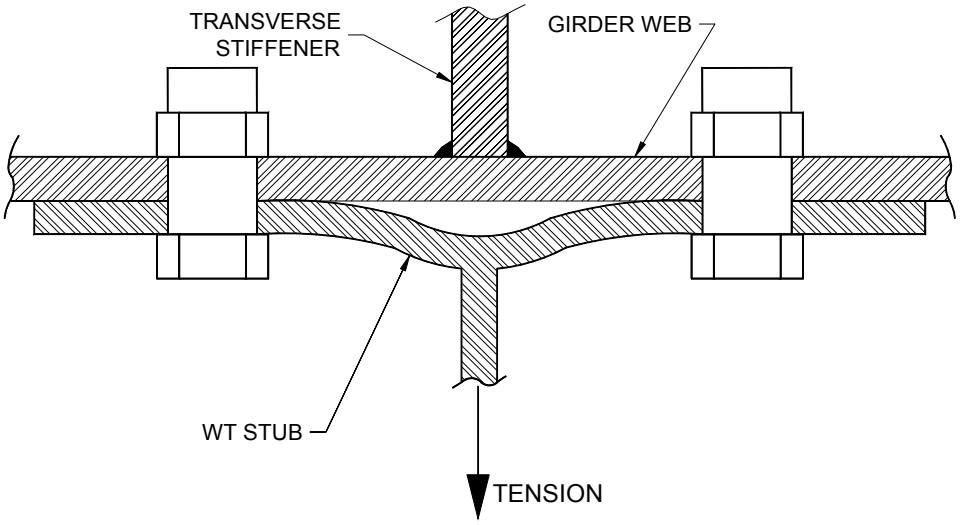

FIGURE 3.12 DISTORTION OF WT STUB (CHEPLAK, 2001)

3.4.3 Effect of Permanent Metal Deck Forms

Table 3.2 summarizes the diagonal brace force responses when the permanent metal deck forms were present. Brace forces predicted using the equivalent flat plate approximation showed reasonable agreement with measured values. Brace forces with decking present were between 23% and 34% smaller than the forces measured with no decking present. This significant reduction in the truss bracing demonstrated the substantial potential of the metal deck forms as a lateral bracing system. As such, further laboratory investigation was warranted to study additional parameters that could not be controlled in the scope of the field studies.

TABLE 3.2 BRACE FORCES PER UNIT APPLIED CRANE LOAD (KIPS) WITH METAL DECKING PRESENT

BRACE MEMBER	ABAQUS*	FIELD TEST (with Deck)	% Diff from ABAQUS	% Diff from No Deck
A	-0.79	-0.75	-6%	-25%
B	0.87	0.72	-22%	-27%
C	-0.52	-0.48	-9%	-32%
D	-0.52	-0.48	-8%	-25%
E	0.56	0.53	-6%	-23%
F	-0.29	-0.27	-4%	-34%

**Uses Modified External Diaphragm Brace Area = 0.5 in^2*

3.5 SUMMARY OF FIELD TESTS

A series of unique field tests were conducted on a full-scale twin box-girder bridge during construction. Loading was applied to the top flange of one girder

using a construction crane fitted with a load cell. Girder cross-sections and top-lateral braces were instrumented to extract brace forces. A three-dimensional finite-element model was developed and verified against the experimental measurements.

Analysis indicated that the distribution of brace forces in the adjacent girder was affected in part by the stiffness of the external diaphragms connecting them. Model calibration was achieved by adjusting the stiffness of the external diaphragms. The calibrated model was then used to evaluate the bracing potential of permanent metal deck forms.

Application of the deck forms resulted in significant decreases in measured top-lateral brace forces, demonstrating its potential effectiveness as a bracing system. Finite-element analysis using the equivalent-plate approximation and SDI shear stiffness of the deck panels reasonably predicted the brace force response of the decked bridge.

CHAPTER 4
LABORATORY TEST PROGRAM

This chapter describes the laboratory tests conducted on a full-scale trapezoidal steel box-girder test specimen. The specimen was tested with various top-lateral truss and metal deck bracing configurations under pure bending and pure torsion.

4.1 GENERAL

The test specimen used in the laboratory test program was a straight trapezoidal steel box-girder measuring 54 ft. in length. The specimen was fabricated and donated by Grand Junction Steel located in Grand Junction, Colorado. The general cross-sectional dimensions were based on bridge Connect Z at the highway interchange described in Chapter 3. The test girder was supported in a diving board configuration over a 12 ft. length and was cantilevered 40 ft. as shown in Figure 4.1. The end support and load point were located 1 ft. from the ends of the specimen.

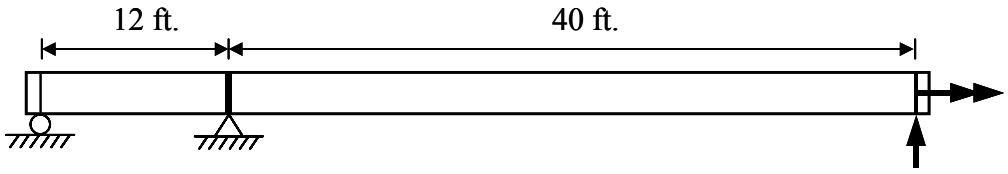

FIGURE 4.1 PROFILE VIEW OF TEST SETUP

4.2 SPECIMEN DIMENSIONS & PROPERTIES

The test specimen was fabricated using A572 Gr. 50 steel for the flanges and A36 steel for the webs. The cross-sectional dimensions were constant over the entire length of the specimen and are shown in Figure 4.2. The lab specimen cross-sectional area and moment of inertia (x-axis) were approximately 70% and 60% of bridge Connect Z, respectively. These differences were primarily due to larger 24 in. wide top flanges in Connect Z. The webs and flanges of the specimen were attached using one-sided exterior 5/16 in. E70 fillet welds.

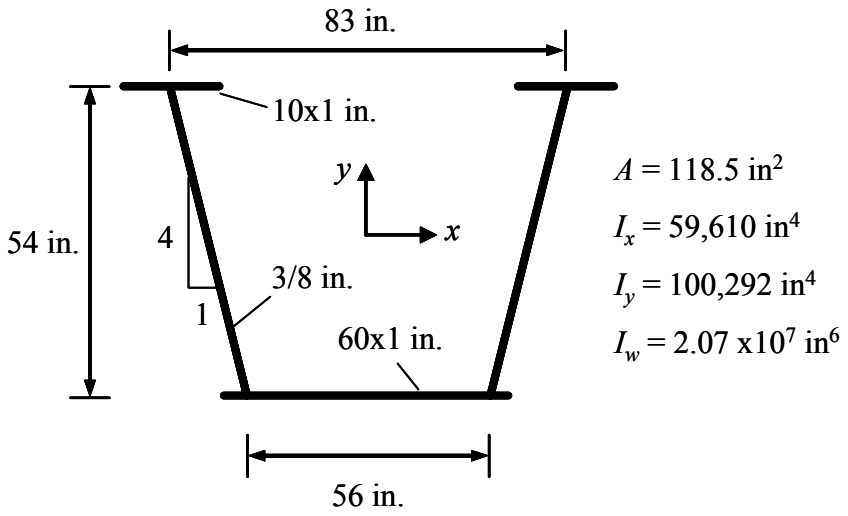

FIGURE 4.2 CROSS-SECTIONAL DIMENSIONS AND PROPERTIES

Vertical web stiffeners were located at the load and support points to eliminate web crippling and local buckling failure modes. In addition, three pairs of evenly spaced web stiffeners were used within the support span to handle the large shear forces inherent with the test configuration. All stiffeners were fabricated from 7-1/2 in. by 11/16 in. A572 Gr. 50 material. The stiffeners were fit-to-bear against the bottom flange and terminated 2 in. below the bottom face of

the top flange. A 1/2 in. thick A572 Gr. 50 plate diaphragm was located at the interior support and was welded directly to the web stiffeners and bolted angles on the bottom flange as shown in Figure 4.3. This plate diaphragm was used to distribute the large tensile reaction from the bottom flange to the webs.

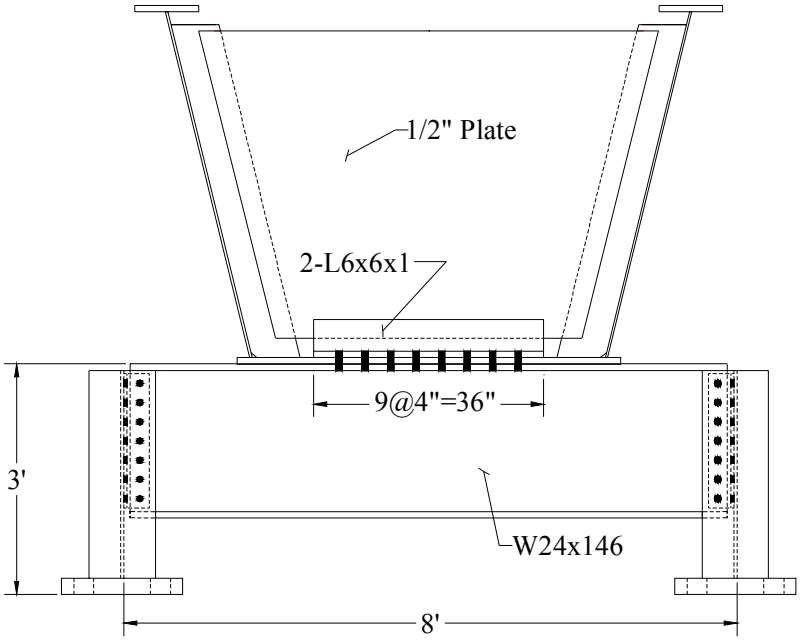

FIGURE 4.3 INTERIOR SUPPORT DETAILS

The out-of-straightness and imperfections of the top flange plates were recorded prior to testing and are given in Appendix A. The initial lateral out-of-straightness of the top flanges was measured by stringing a wire along the length of the flange. The flange position at the interior support and load point web stiffeners served as the reference points. The imperfections were caused by cooling contraction of the one-sided bottom flange-to-web welds. The maximum out-of-straightness occurred near the center of the cantilever span and was roughly equal to $L/300$, where L equals 40 ft.

4.3 LOADING AND SUPPORT SYSTEM

The test specimen supports were 36 in. high and extended beyond the full width of the bottom flange as shown in Figure 4.3. The interior support beam was a W24x146 and was attached to the girder using 16 one-inch diameter A325 bolts. Two 1 in. diameter A325 bolts were used to attach the bottom flange of the specimen to the end support. These bolts were placed symmetrically inline with the end web stiffener, 13 in. from the outside edge of the bottom flange as shown in Figure 4.4. The end support consisted of a W36x160 and also extended beyond the full width of the bottom flange of the girder. The initial imperfection of the bottom flange created gaps between the bottom flange and support beam near the outer edges. Hydrostone was used to fill in these gaps.

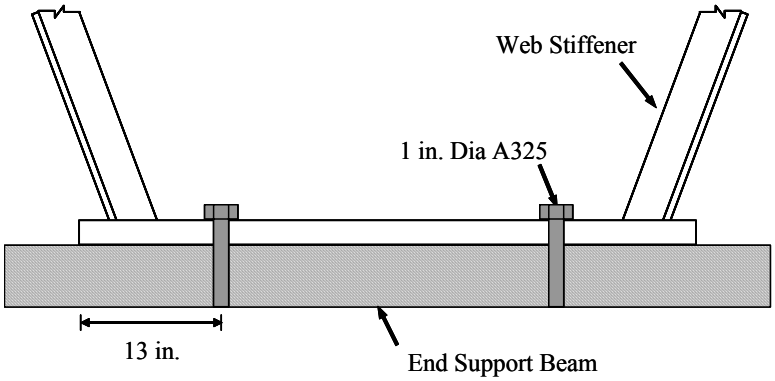

FIGURE 4.4 END SUPPORT DETAIL

Both the torsional and bending loads were applied 12 in. from the end of the test specimen. Torsional loading of the specimen was achieved using two 100 kip push-pull hydraulic rams. These rams, shown in Figure 4.5, were capable of applying equal force in both tension and compression for a given hydraulic

pressure. The rams were connected in parallel to a single pump to ensure equal and opposite force was being applied by each ram at all times. A loading beam placed across the top flanges was used to transfer the load from the rams to the test specimen.

Bending of the specimen was achieved using two 200 kip hydraulic compression rams placed below the bottom flange as shown in Figure 4.5. These rams were also connected in parallel to maintain equal force at all times. Roller bearing assemblies were placed in between the ram and the girder to maintain a vertical line-of-action of the ram force and are pictured in Figure 4.6. During bending tests, the torsion rams were configured to move freely while still being attached to the loading beam. During torsion tests, the bending rams were retracted to avoid interference.

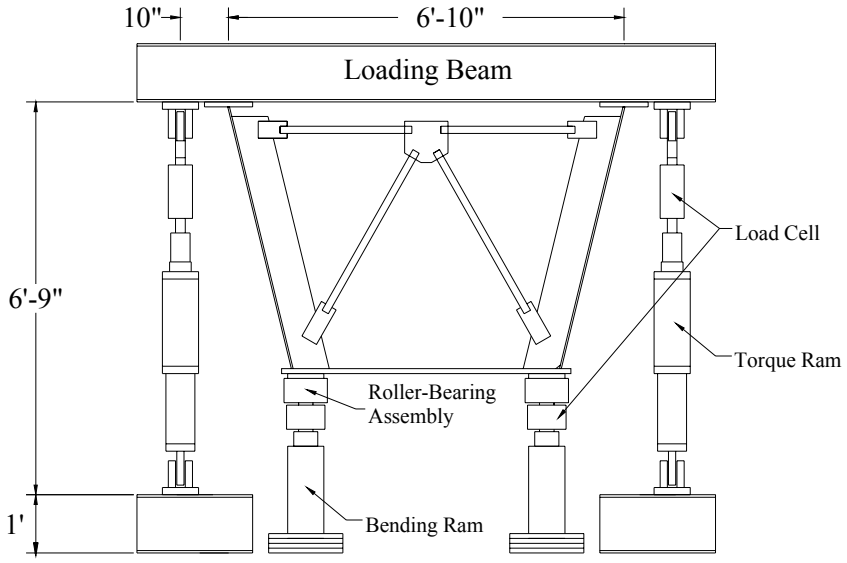

FIGURE 4.5 SCHEMATIC OF LOADING SYSTEM

FIGURE 4.6 ROLLER-BEARING ASSEMBLY

FIGURE 4.7 PICTURE OF LOADING SYSTEM

An end diaphragm constructed from 1.5 in. diameter standard weight schedule 40 steel pipe was installed at the load point and was welded directly to

the web stiffeners. This diaphragm was used to prevent distortion of the cross-section at the load point and is pictured in Figure 4.7.

4.4 INSTRUMENTATION

Ram load, hydraulic pressure, strain, and deflection data were collected using a computerized data acquisition system. Loads were obtained from load cells placed in series with each of the rams. Each load cell was calibrated prior to testing. Hydraulic pressure was monitored using a pressure transducer as a secondary measure of load.

Vertical displacements of the specimen were measured using linear string potentiometers attached to the outside edges of the bottom flange at the quarter points, load point, and interior support as shown in Figure 4.8. The string potentiometers were located on the test floor 36 in. below the bottom flange to minimize error introduced by horizontal displacement of the girder during torsional loading. This error was less than 1% for the largest expected displacements. Two linear spring potentiometers placed at the edge of the bottom flange were used to measure vertical displacements at the end support.

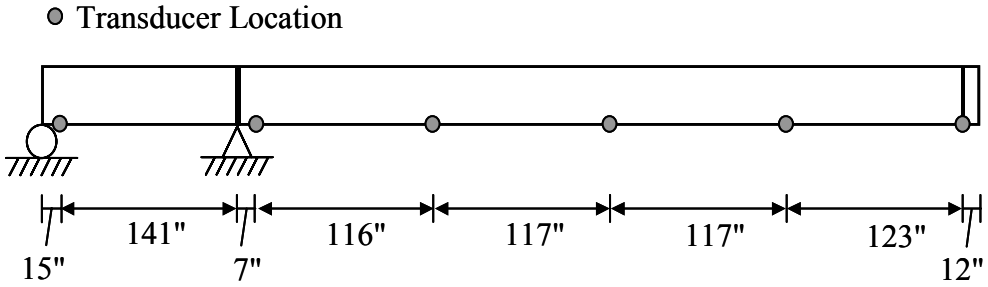

FIGURE 4.8 VERTICAL DISPLACEMENT TRANSDUCER LOCATIONS

Three-wire temperature compensated uniaxial strain gauges were used to obtain girder and brace member strains. Girder stresses and brace forces were calculated using the measured strain data. The gauges placed on the girder flanges had a 6 mm gauge length, while the gauges placed on the bracing members had a 3 mm gauge length. The girder gauges were placed at mid-thickness of the outer edges of both top flanges and the bottom flange at midspan, the north quarter point, and the interior support as shown in Figure 4.9. All girder gauges were oriented to measure strains along the long axis of the specimen. Each bracing member was instrumented with four strain gauges placed equally spaced along the circumference. Each brace member of the end diaphragm, intermediate diaphragm, and top-lateral truss system was instrumented.

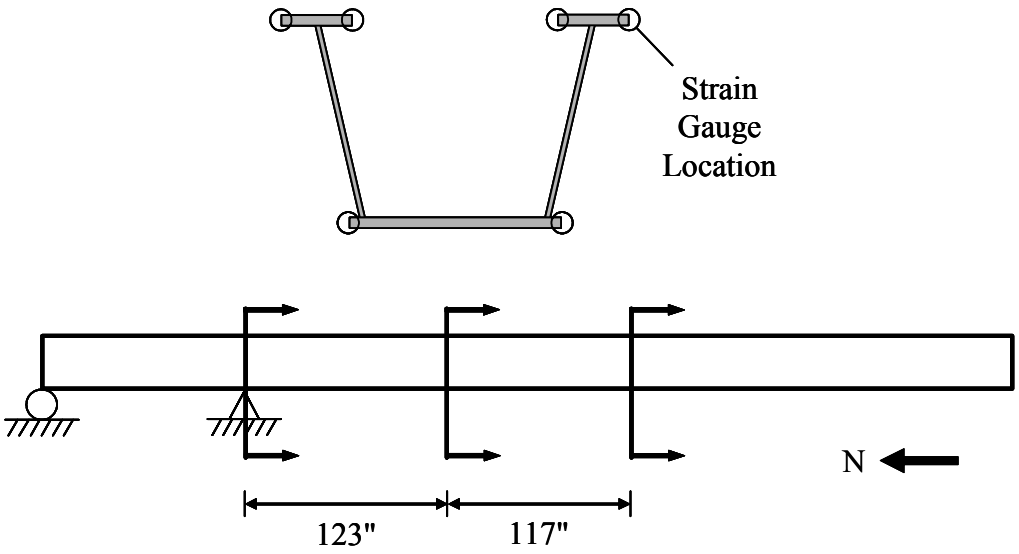

FIGURE 4.9 STRAIN GAUGE LOCATIONS ON TEST SPECIMEN

4.5 BRACING

4.5.1 Top-Lateral Truss

The top-lateral truss bracing used in the laboratory experiments were single-diagonal Warren truss configurations as shown in Figure 4.10. All bracing members were constructed from standard weight schedule 40 steel pipe. Two-inch diameter pipe was used for the diagonals in the 4-panel configuration as well as all for all the strut members. Three-inch diameter pipe was used for the diagonals in the 2-panel configuration. The cross-sectional areas for the 2 in. and 3 in. diameter bracing members were 1.07 and 2.23 in^2, respectively. By comparison, the brace members used in Connect Z were WT7x21.5 (6.31 in^2).

The bracing was designed with slip-critical bolted connections to facilitate removal and installation for various test cases. The tube members were slotted at their ends and welded to a single 1/2 in. thick gusset plate that was connected to the web of the test specimen using connection mounts pictured in Figure 4.11. The bracing members were attached to the connection mounts using 7/8 in. diameter A325 bolts. Each of the connection mounts was attached to the webs of the girder using three 3/4 in. A325 bolts. The diagonal brace connections in the end panels were placed 6 in. to the inside of the plate and load point diaphragms as shown in Figure 4.10. The centerline of the brace was located 3 in. (vertically) below the center of the top flange. All brace gusset plates and connection mounts were unpainted and blast-cleaned for improved slip-critical performance. All bolts were brought to the required tension using the turn-of-the-nut method.

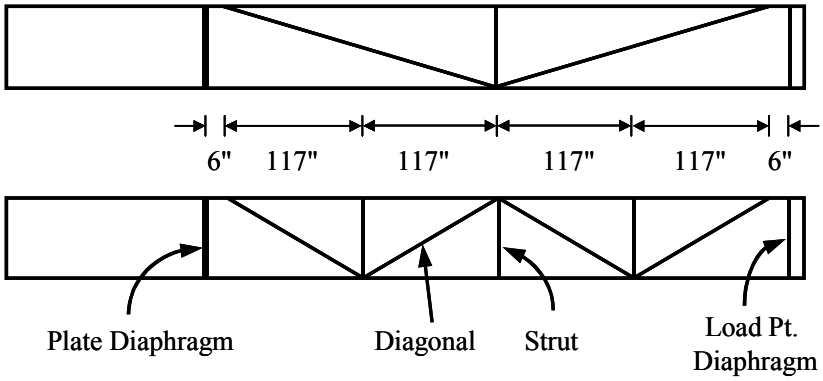

FIGURE 4.10 TOP-LATERAL TRUSS BRACING CONFIGURATIONS

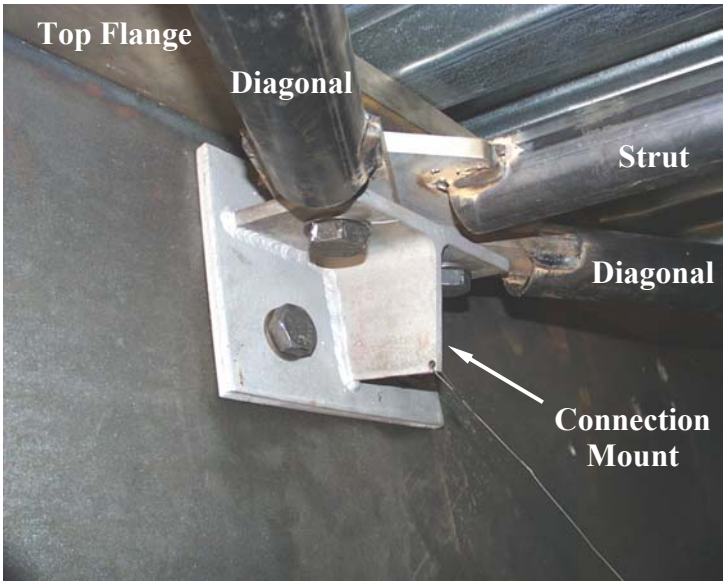

FIGURE 4.11 TRUSS BRACE CONNECTION VIEWED FROM BELOW

4.5.2 Permanent Metal Deck Forms

The permanent metal deck forms used in this study were 2.5 in. deep 16-gauge (0.0598 in.) and 20-gauge (0.0359 in.) panels and were manufactured by the Wheeling Corrugated Company. The cross-sectional dimensions of the deck were idealized by straight lines and are shown in Figure 4.12. The actual

measured dimensions may be found in Appendix B. Each deck panel was 90 in. long with a 32 in. cover width and had tapered ends as shown in Figure 4.13. Fifteen panels were used to cover the cantilever portion of the test specimen.

The deck panels were oriented with the ribs perpendicular to the length of the girder and were fastened to the top flanges using Hilti ENPH2-21-L15 powder actuated fasteners. One fastener was placed at the center of every corrugation valley 1.5 in. from the panel edge. Occasionally, during installation the head of a fastener would break while the fastener was being driven. For these cases, a replacement fastener would be placed near the broken fastener as pictured in Figure 4.14. The new fastener would still be located in the center of the valley and have a slightly increased edge distance.

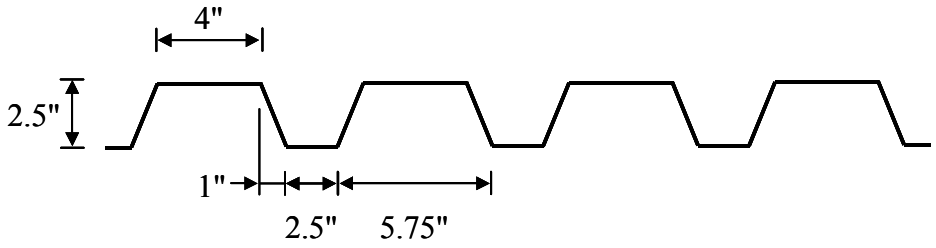

FIGURE 4.12 IDEALIZED CROSS-SECTIONAL DIMENSIONS OF DECKING

FIGURE 4.13 TAPERED END OF DECKING WITH CABLE ACCESS HOLE

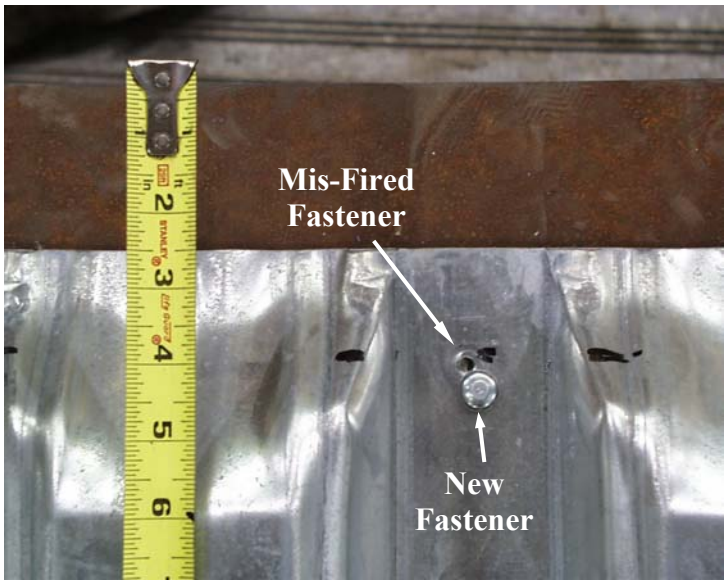

FIGURE 4.14 MIS-FIRED END FASTENER

Adjacent deck panels were attached to one another using four #14 x ¾ Buildex TEKS self-drilling screws spaced at 18 in. Although the screws were self-drilling, they were not capable of drilling through two layers of 16-gauge decking. To ensure proper clamping of the sheets and to ensure the sidelap fasteners did not thread into the upper sheet before penetrating the lower sheet, 13/64 in. pilot holes were drilled for each fastener. This was done for all test cases to maintain consistency. Particular attention was given to ensure that the recommended 1/2 in. distance from the screw centerline to the panel edge was maintained.

A stiffening angle detail proposed by Jetann et al. (2002) was used in one test configuration to augment the performance characteristics of the metal decking. These stiffening angles were placed under the deck panels along a seam so the sidelap fasteners could be directly attached to them as shown in Figure 4.15. The stiffeners were located at every third lap seam as shown in Figure 4.16. The stiffeners were 2x3x10-gauge (0.1345 in.) galvanized steel angles and are what is typically used as deck support angles for deck construction. The angles were coped at each end to accommodate the flanges and extended 1.5 in. beyond the edge of the deck panels. To avoid interference with the top-lateral truss bracing, the 2 in. legs were oriented vertically for the four intermediate stiffening angles. For the two end stiffeners, the 3 in. leg was oriented vertically.

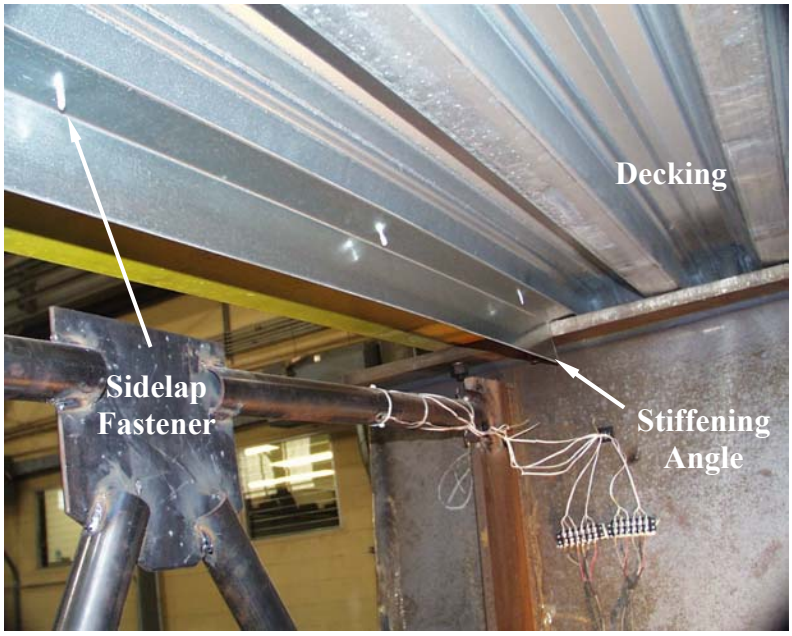

FIGURE 4.15. STIFFENING ANGLE SEEN FROM BELOW

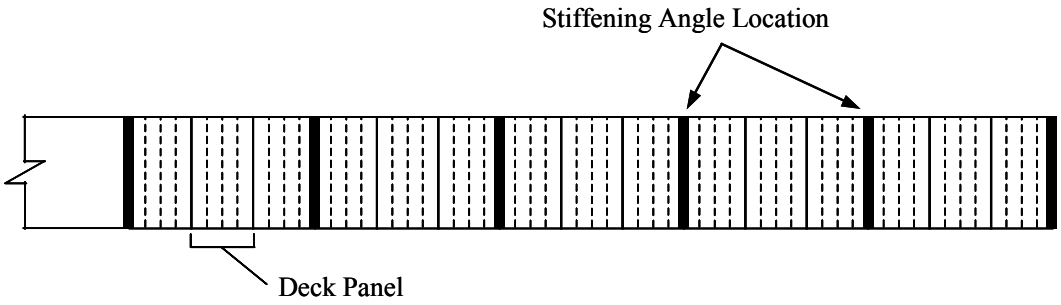

FIGURE 4.16 STIFFENING ANGLE LOCATIONS

The cumulative thickness of the deck sheets and stiffening angle in the test configuration were near the maximum limit recommended by the fastener manufacturer. Driving fasteners through material thicker than the recommended limit can result in inadequate penetration into the base metal. This generally results in poor pullout and shear performance. To ensure the stiffening angle was

adequately attached to the top flange, a single fastener was placed into the extended portion of the stiffening angle only as shown in Figure 4.17. Additionally, two fasteners were used to attach the deck panels to the flanges instead of a single fastener. The second deck fastener was used only at locations where stiffening angles were present. This was done to reduce the demand on the end lap fastener and minimize the possibility of pullout.

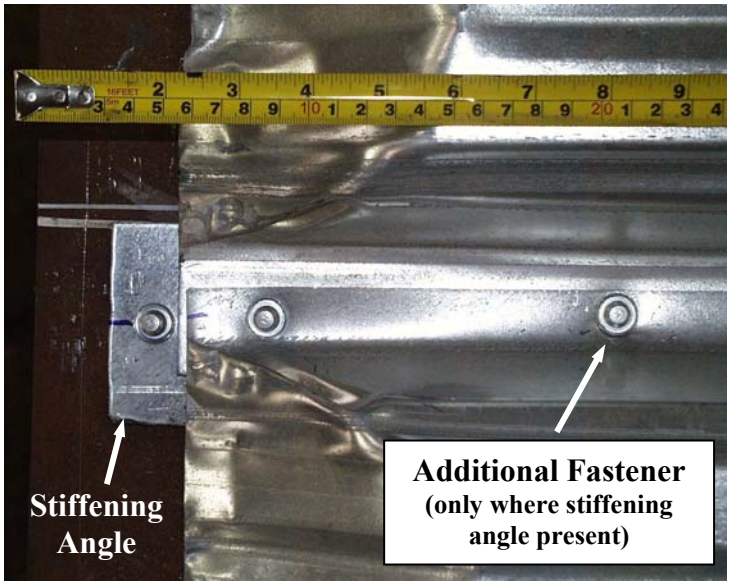

FIGURE 4.17 END FASTENER DETAIL AT STIFFENING ANGLE

Several holes were cut into the crimped ends of the decking to provide access for instrumentation wiring as shown in Figure 4.13. These holes were cut into the ends of various sheet ribs and ranged in size from 1/2 to 1-1/8 in. in diameter.

4.5.3 Internal Diaphagm

An intermediate internal K-diaphragm similar to the end diaphragm described in Section 4.3 was fabricated from 2 in. diameter standard weight

schedule 40 pipe. Like the top-lateral truss bracing, the end connections were designed as slip-critical bolted connections to allow for easy removal and installation. The internal diaphragm, when used, was located at the midpoint of the cantilever span.

4.6 TEST CASES

The parameters investigated in the experimental program included two top-lateral truss geometries, two different metal deck gauge thicknesses, the use of a stiffening angle for the metal decking, and the use of an internal truss diaphragm. The bracing configurations for the various test cases are summarized in Table 4.1. For each test configuration or test case, several trial runs were conducted. The naming convention for each trial run is described in Figure 4.18.

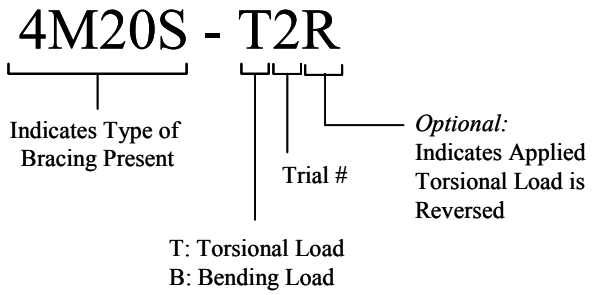

FIGURE 4.18 NAMING CONVENTION FOR TEST TRIALS

4.7 TEST PROCEDURE

Each of the test configurations shown in Table 4.1 was loaded in both pure bending and pure torsion. For all configurations, bending tests were conducted prior to torsion tests. The unbraced test case was first conducted to establish the control case. The maximum applied loads for all of the subsequent braced

configurations were limited to the maximum load in the unbraced test to ensure the specimen remained within the elastic range. Additional unbraced tests were conducted after each metal deck test series.

The order of test cases involving metal decking was chosen to minimize potential damage to fasteners prior to testing the deck to failure. For each gauge thickness, the first test after deck installation was the combined decking and 4-diagonal truss configuration. The truss bracing was then removed and the specimen was tested with only the metal decking present. In these tests, two replicate bending tests were performed followed by four torsion tests. The maximum applied load for the first three torsion tests was limited to the maximum load applied in the unbraced test case. In addition, the direction of the applied torque was reversed for the second torsion test. Loading in the fourth torsion test was applied until the end rotation was equal to that achieved in the unbraced case and generally resulted in failures of one or more of the metal deck fasteners. This test procedure was identical for the 16-gauge, 20-gauge, and stiffened 20-gauge metal deck configurations.

TABLE 4.1 SUMMARY OF TEST CASES

Test Prefix	Top-Lateral Truss	Metal Deck	Internal Diaphragm
U	--	--	--
D	--	--	Yes
2	2-Diagonals	--	--
4	4-Diagonals	--	--
4D	4-Diagonals	--	Yes
4M16	4-Diagonals	16-Gauge	--
M16	--	16-Gauge	--
4M20	4-Diagonals	20-Gauge	--
M20	--	20-Gauge	--
4M20S	4-Diagonals	20-Gauge (with stiffening angle)	--
M20S	--	20-Gauge (with stiffening angle)	--

Legend:

U – *Unbraced*
D – *Internal Diaphragm Present*
– *Number of Top-Lateral Diagonal Braces*
M## – *Metal Deck Gauge*
S – *Stiffening Angle Present*

CHAPTER 5
LABORATORY TEST RESULTS

This chapter presents the results of the laboratory experiments conducted on a full-scale trapezoidal steel box girder test specimen. The specimen was tested with various bracing configurations in both pure bending and pure torsion. The results reported include torsional and bending stiffnesses, brace forces, and load-deflection responses.

5.1 TORSION TESTS

The rotation of each cross section was calculated by dividing the relative vertical displacement of the ends of the bottom flange by the width of the bottom flange. Since the shear center or center of twist for the open and pseudo-closed section was located below the bottom flange (see Appendix A), horizontal displacements were observed during testing. The location of the string potentiometers 54 in. below the bottom flange minimized errors associated with the horizontal displacements of the girder. The error in determining the rotation of the girder was less than 1% for the maximum twist encountered during all the experimental tests.

5.1.1 Support Movements

In order to make meaningful comparisons with analytical models that have idealized boundary conditions, it was necessary to correct the measured displacements for support movements. Comparisons between adjusted and unadjusted experimental results were made to illustrate the affect and validity of the support movement corrections employed. Support movements at both the interior and end support affected the measured displacements in the cantilever

span of the test specimen. These interior and end support movements were each corrected for individually.

Vertical movements at the interior support resulted in rigid body rotation of the cantilever portion of the test specimen. Corrections for these movements were made by subtracting the rotation at the interior support from the rotations measured at all other locations. The interior support rotations were generally 2-4% of the measured rotations at the tip of the cantilever under the maximum the applied torque in each test case. The most significant interior support rotations were seen in the combined truss-deck test configurations (4M20 and 4M16) where the support rotations were approximately 7% of the tip rotations.

Vertical movements at the end support had a very significant effect on the displacements measured in the cantilever span. Small vertical movements at the end support were magnified at the cantilever tip due to the relative lengths of the cantilever span and span between supports. These support movements increased the relative tip rotations by up to 45%. The support movements were due to both the curved imperfection of the bottom flange and the use of two bolts away from the flange edges as seen in Figure 5.1.

The effect of the end support movements on the girder rotations in the cantilever span were facilitated by the support condition at the interior support. Figure 5.2 shows a finite-element mesh of the bottom flange of the test specimen (all other plate elements are hidden, but still present). Although the interior support provided significant restraint against vertical and horizontal displacements, rotation about axis BE was relatively free. Therefore, vertical displacements at points C and F caused displacements along the cantilever span as seen in Figure 5.3.

The corrections for the end support movements were determined using the finite-element model developed to analyze the laboratory tests, which is described

in detail in Chapter 6. Translational restraints, shown in Figure 5.2, were used to model the interior and end supports. The bottom-flange mesh was selected so that the end support restraints coincided with the location of the end support bolts. A unit upward displacement at point C would result in a downward displacement of 2.35 at point A and a small upward displacement of 0.20 at point D. These displacements produce a perceived girder rotation, which were generally very significant compared with measured rotations. For example, for the 4-diagonal brace configuration (4-T3), the measured displacements at points F and C were 0.03 in. and -0.01 in, respectively (positive indicates upward movement). The resulting perceived rotation at the cantilever tip was equal to 0.073 deg and represents approximately 27% of the measured tip rotation of 0.27 deg (adjusted for interior support movements).

The correction for end support movements was accomplished using the finite-element displacement field from a unit displacement at point C. The actual measured displacements at points C and F were then used to determine the resulting displacements in the cantilever span. These displacements were then subtracted from the displacements measured in the torsion tests.

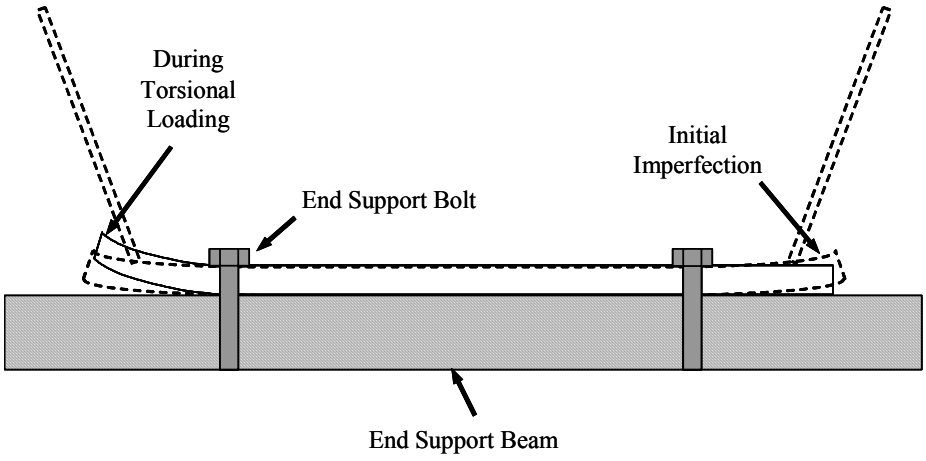

FIGURE 5.1 SECTION VIEW OF END SUPPORT

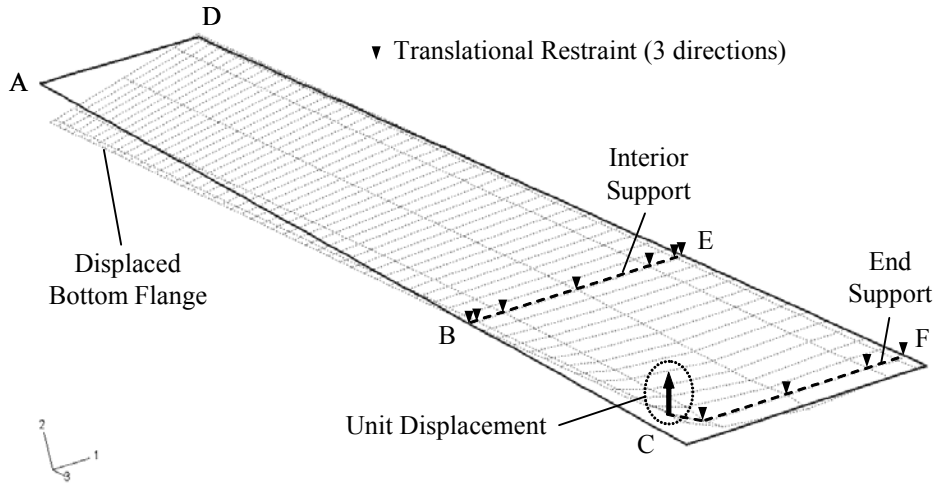

FIGURE 5.2 BOTTOM-FLANGE DISPLACEMENTS DUE TO END SUPPORT MOVEMENTS

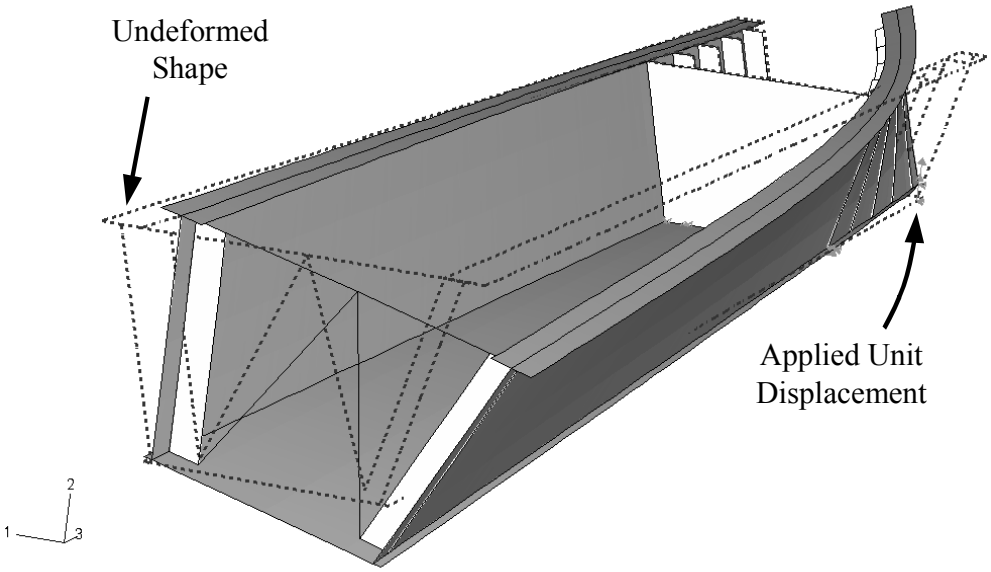

FIGURE 5.3 GIRDER ROTATIONS DUE TO END SUPPORT MOVEMENTS

The torque versus relative twist at the tip of the girder for the unbraced test case is shown in Figure 5.4. Adjusted values refer to experimental rotations that are corrected for end support movements. The adjusted experimental rotations compared favorably with finite-element predictions. Adjusted rotations along the length of the girder also agreed reasonably well with finite-element predictions as shown in Figure 5.5. Consequently, all subsequent test results presented herein utilize measured displacements that have been adjusted for end support movements. Additional torque-twist and rotation plots for other test configurations can be found in Appendix C.

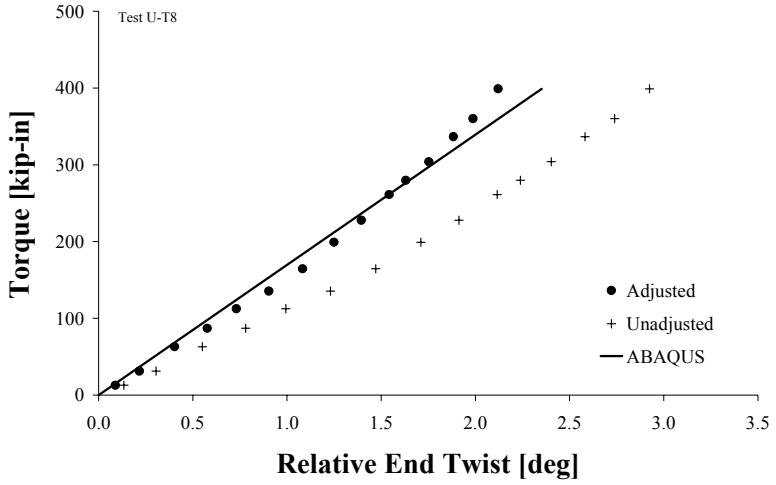

FIGURE 5.4 TORQUE-TWIST RESPONSE FOR UNBRACED GIRDER

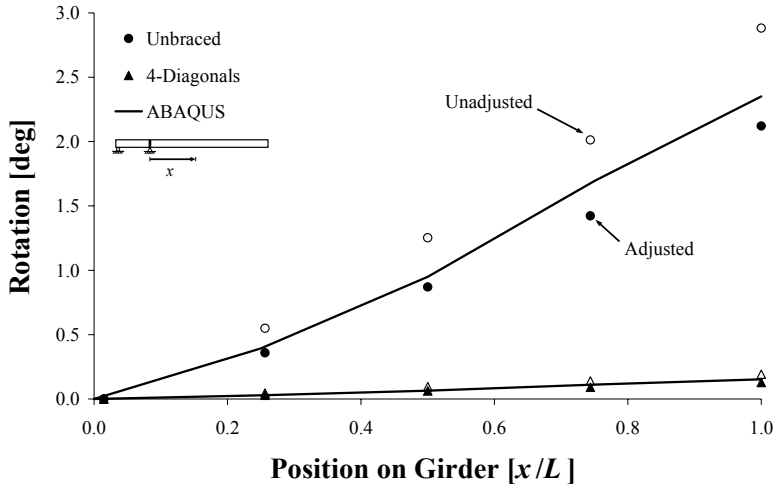

FIGURE 5.5 ROTATIONS ALONG GIRDER LENGTH

5.1.2 Load-Deflection Responses

Typical torque-twist responses for the unbraced and metal-deck test configurations are shown in Figure 5.6. Significant increases in the torsional stiffness of the girder were achieved when top-lateral bracing systems were present. Quantification of the stiffness increases is presented in Section 5.1.3.

The load-deflection responses for the various test configurations were generally linear. A typical response is shown in Figure 5.7 where the loading branch is denoted by solid data points. Overlapping loading and unloading responses were observed for the unbraced, diagonal truss, and combined truss-deck configurations. For the three metal-deck-only test configurations, however, a discernable separation was present. This phenomenon is apparent in Figure 5.8 when the horizontal scale is magnified and was likely due to fastener slip. This slip is further evidenced by a permanent rotation after unloading.

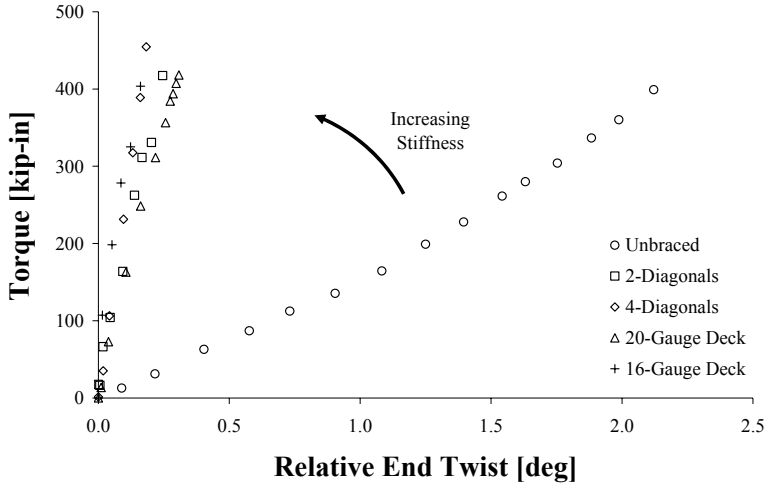

FIGURE 5.6 TYPICAL TORQUE-TWIST RESPONSES FOR VARIOUS TOP-LATERAL BRACING CONFIGURATIONS

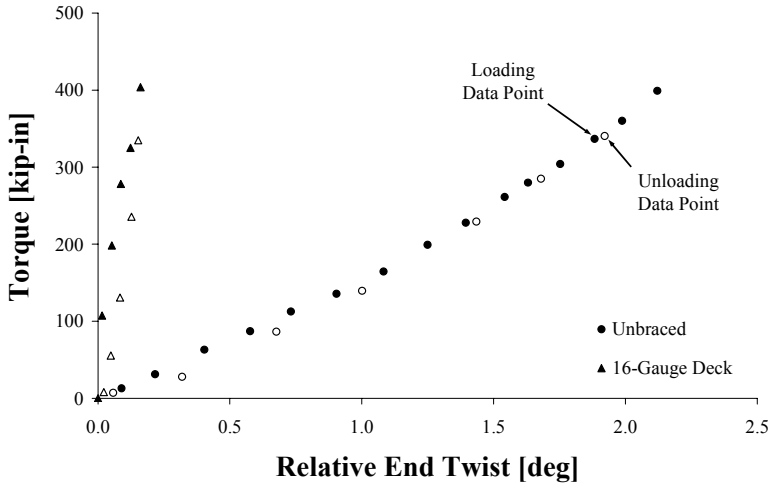

FIGURE 5.7 TYPICAL LOADING & UNLOADING TORQUE-TWIST RESPONSES

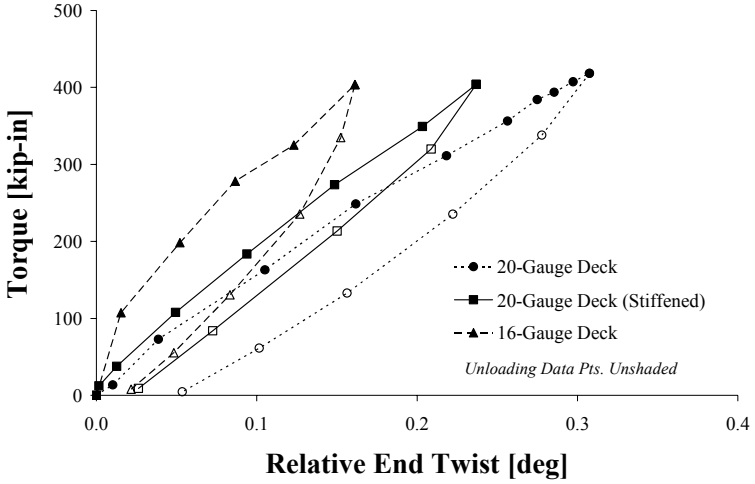

FIGURE 5.8 LOAD-DEFLECTION SEPARATION FOR METAL-DECK-ONLY CONFIGURATIONS RESPONSES

For each metal-deck-only test configuration, four load cycles were conducted as described in Section 4.7. A typical load-deflection response is given in Figure 5.10. Three initial loading cycles were conducted where the maximum applied torque was kept below the maximum torque applied in the unbraced test cases. The fourth cycle imposed an end rotation equal to the rotation imposed in the unbraced test cases.

The torsional stiffness of the braced girder, which is the slope of load-deflection curve, decreased with increasing applied load. Permanent end rotations were present after unloading. Fastener distress was observed in all cases and is reported in Section 5.1.5. The girder stiffness decreased with increasing load, eventually approaching that of the unbraced case. This behavior can be more readily visualized by removing the torque contribution associated with the unbraced girder. For the braced test configurations, the measured torque at a given tip rotation can be subdivided into the torque contribution associated with

the unbraced girder and the additional torque contribution associated with the bracing as illustrated in Figure 5.10. The adjusted load-deflection responses for the three metal-deck-only cases shown in Figure 5.11 were obtained by subtracting the torque contribution for the unbraced girder from each data point. The unbraced stiffness shown in Figure 5.10 represents the average of the unbraced test cases and is discussed in further in Section 5.1.3.

For all three metal-deck-only configurations, the load-deflection responses seen in Figure 5.11 become nearly horizontal for large end rotations. This indicates that the stiffness contribution of the bracing approaches zero and the incremental stiffness response of the girder is as if it were unbraced.

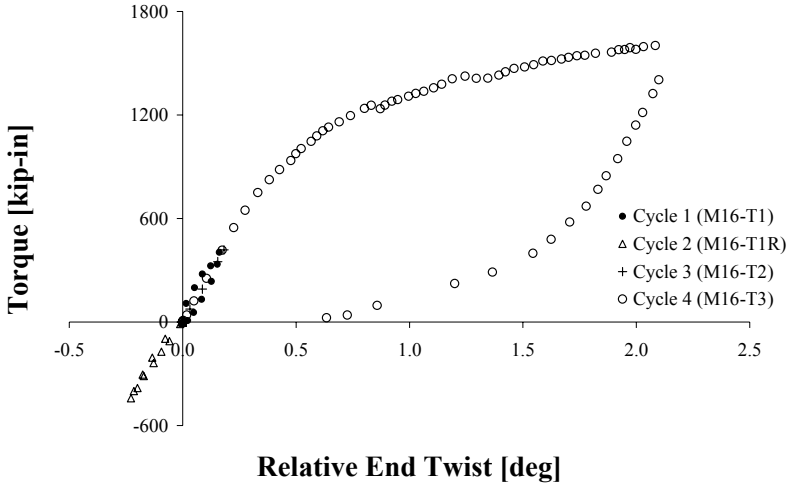

FIGURE 5.9 TYPICAL TORQUE-TWIST RESPONSE AND LOAD CYCLES FOR 16-GAUGE METAL-DECK-ONLY BRACING CONFIGURATION

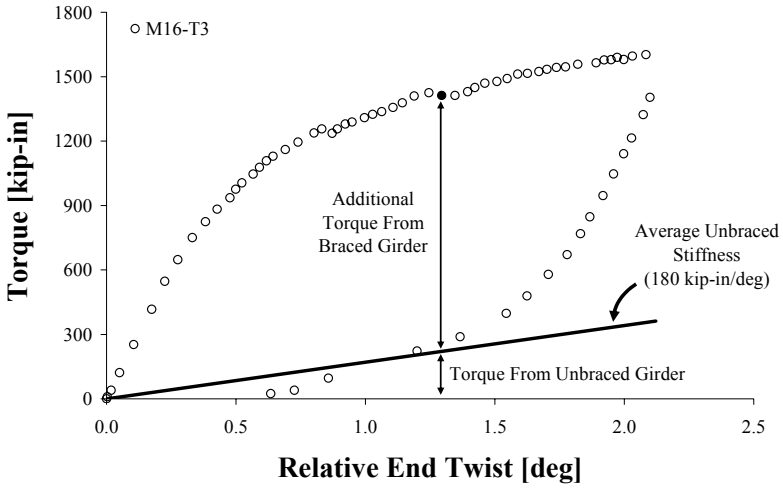

FIGURE 5.10 TORQUE CONTRIBUTIONS FROM UNBRACED GIRDER AND BRACED GIRDER

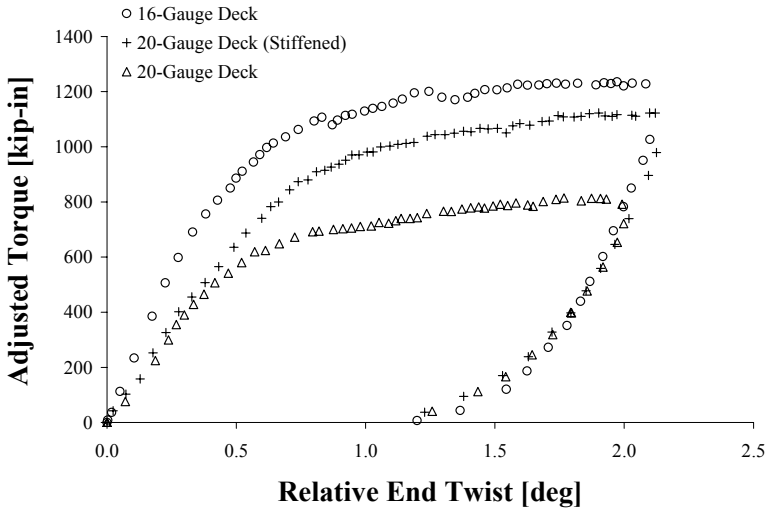

FIGURE 5.11 ADJUSTED TORQUE-TWIST RESPONSES FOR METAL-DECK-ONLY TESTS WITH TORQUE CONTRIBUTION FROM UNBRACED GIRDER REMOVED

5.1.3 Torsional Stiffness

The torsional stiffness of the laboratory test specimen was determined for the various bracing configurations from the slope of a best-fit line on the torque-twist curves. Only the data points during the loading stage were used to calculate the torsional stiffness values. Figure 5.12 summarizes the average experimental torsional stiffnesses of each brace configuration relative to the unbraced test case. Torsional stiffness values for the individual test trials are listed in Table 5.1. On average, the 2-diagonal and 4-diagonal truss systems increased the unbraced girder torsional stiffness by approximately 9 and 14 times, respectively. The metal-deck bracing systems increased the stiffness between 8 and 12 times, while the combined metal-deck and truss systems increased the stiffness between 18 and 24 times. The use of an internal diaphragm had no appreciable effect on the torsional stiffness in either the unbraced (D-T1) or 4-diagonal (4D-T3) test configurations.

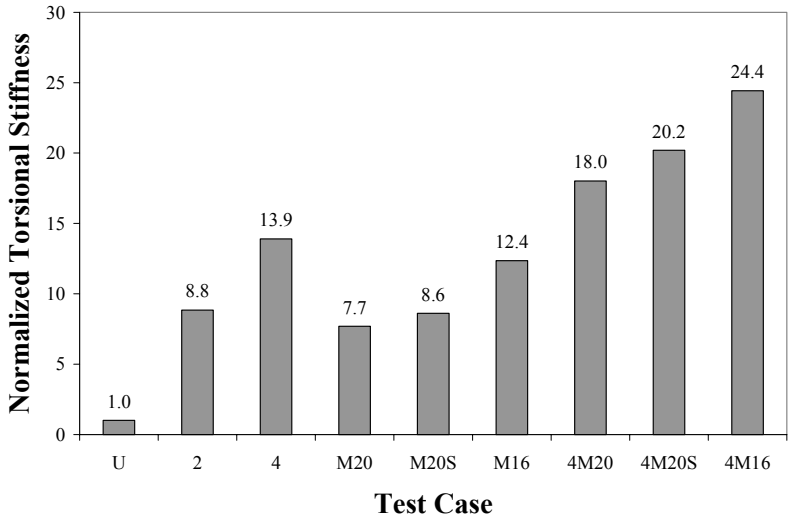

FIGURE 5.12 NORMALIZED AVERAGE EXPERIMENTAL TORSIONAL STIFFNESS VALUES

TABLE 5.1 EXPERIMENTAL TORSIONAL STIFFNESS VALUES

Bracing Configuration	Test Trial	Torsional Stiffness [kip-in/deg]	% Diff from Ave
Unbraced	U-T7	220	23%
	U-T7R	194	8%
	U-T8	150	-17%
	U-T8R	154	-14%
	(Ave)	*(180)*	--
2-Diagonals	2-T1	1647	4%
	2-T2	1530	-4%
	Ave	*(1588)*	--
4-Diagonals	4-T3	2467	-1%
	4-T3R	2428	-3%
	4-T4	2560	3%
	4-T5	2528	1%
	Ave	*(2496)*	
Diaphragm	D-T1	221	--
4-Diagonals + Diaphragm	4D-T3	2438	--

TABLE 5.1 EXPERIMENTAL TORSIONAL STIFFNESS VALUES (CONTINUED)

Bracing Configuration	Test Trial	Torsional Stiffness [kip-in/deg]	% Diff from Ave
20-Gauge Deck	M20-T1	1388	0%
	M20-T1R	1290	-7%
	M20-T2	1381	0%
	M20-T3	1468	6%
	Ave	*(1382)*	--
20-Gauge Deck (Stiffened)	M20S-T1	1682	9%
	M20S-T1R	1622	5%
	M20S-T2	1294	-16%
	M20S-T3	1591	3%
	Ave	*(1547)*	--
16-Gauge Deck	M16-T1	2281	3%
	M16-T1R	1903	-14%
	M16-T2	2281	3%
	M16-T3	2412	9%
	Ave	*(2219)*	--
4-Diagonals + 20-Gauge Deck	4M20-T1	3134	-3%
	4M20-T1R	3335	3%
	Ave	*(3234)*	--
4-Diagonals + 20-Gauge Deck (Stiffened)	4M20S-T1	3932	8%
	4M20S-T1R	3321	-8%
	Ave	*(3626)*	--
4-Diagonals + 16-Gauge Deck	4M16-T1	4595	5%
	4M16-T1R	4180	-5%
	Ave	*(4387)*	--

5.1.4 Brace Forces

The top-lateral diagonal and strut brace members were each instrumented with four uniaxial strain gauges oriented along the long axis of the member. The force in each brace member was determined by averaging the four measured strain readings. The typical response for the gauges of a brace member is shown in Figure 5.13. The strain readings for each gauge were linear with respect to the applied torque on the girder.

The predicted diagonal forces were determined using the methods outlined in Chapter 2. Forces predicted from the finite-element model were within 5% of those computed from simple hand methods. The equivalent plate thicknesses for the truss and metal-deck configurations are summarized in Table 5.2 and ranged between 0.004 and 0.01 in. The equivalent plate thickness for the two top-lateral truss geometries were determined using Eqn. (2.9). The equivalent thickness for the metal decking was determined from the SDI shear stiffness. Detailed calculations can be found in Appendix B.

For the single-diagonal configurations used in the laboratory tests, the predicted forces in each diagonal brace were equal in magnitude and alternated between tension and compression. The predicted diagonal brace forces for the various bracing configurations are summarized in Table 5.3. Column (2) lists the total equivalent plate thickness for each configuration. Column (3) lists the fraction of the total plate thickness that the truss bracing represents and was used in determining the diagonal forces for combined systems. The predicted diagonal brace forces, P_d, per unit torque, T, calculated using Eqn. (2.11) are listed in column (4). The location of the equivalent plate for truss only and combined truss-decking configurations was assumed to be at the centerline of the truss bracing, 3 in. below the top flange.

The top-lateral brace force responses are shown in Figures 5.14 through 5.18. Measured truss forces are designated by the symbols located beneath the corresponding brace panel. Measured forces compared favorably with theoretical predictions. Measured strut forces for all torsion tests were equal to zero, corresponding to theoretical predictions.

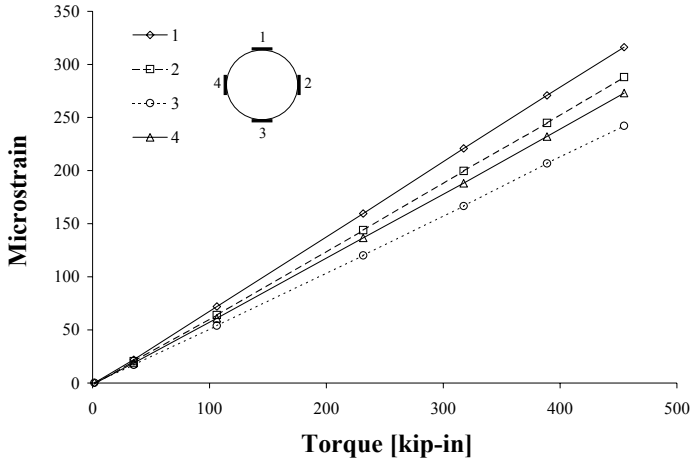

FIGURE 5.13 TYPICAL STRAIN GAUGE RESPONSE FOR BRACING MEMBERS

TABLE 5.2 EQUIVALENT PLATE THICKNESSES FOR BRACING SYSTEMS

Bracing System	t_{eq} [in]
2-Diagonals	0.00651
4-Diagonals	0.00877
20-Gauge Deck	0.00387
16-Gauge Deck	0.01149

TABLE 5.3 PREDICTED DIAGONAL BRACE FORCES PER UNIT APPLIED TORQUE [KIPS/KIP-IN]

(1) **Bracing Configuration**	(2) t_{eq} [in]	(3) $\frac{(t_{eq})_{diag}}{(t_{eq})_{diag}+(t_{eq})_{deck}}$	(4) P_d/T
2-Diagonals	0.0064	100%	0.0334
4-Diagonals	0.0089	100%	0.0191
4-Diagonals + 20-Gauge Deck	0.0135	66%	0.0126
4-Diagonals + 16-Gauge Deck	0.0206	43%	0.0082

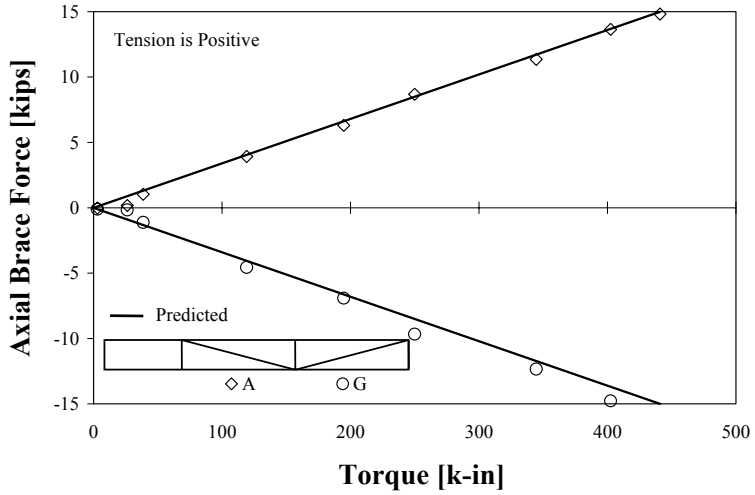

FIGURE 5.14 DIAGONAL BRACE FORCES, TORSIONAL LOADING, 2-DIAGONALS

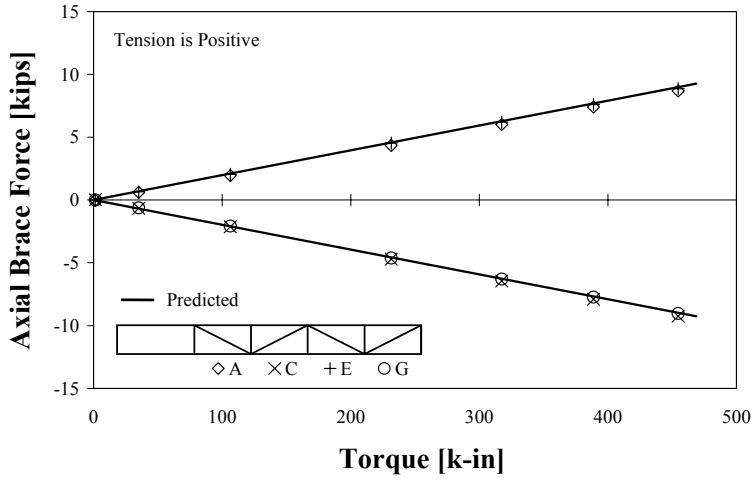

FIGURE 5.15 DIAGONAL BRACE FORCES, TORSIONAL LOADING, 4-DIAGONALS

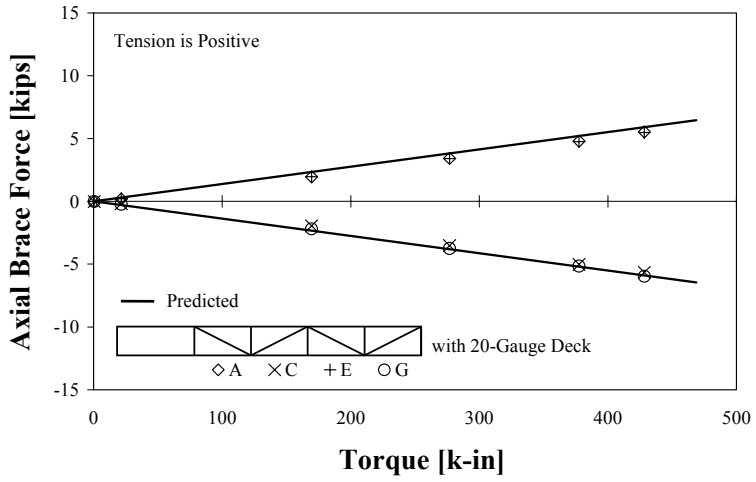

FIGURE 5.16 DIAGONAL BRACE FORCES, TORSIONAL LOADING, 4-DIAGONALS WITH 20-GAUGE METAL DECK

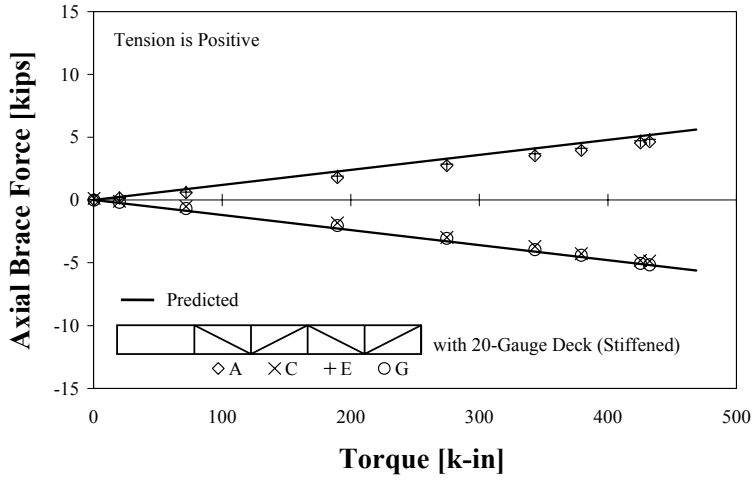

FIGURE 5.17 DIAGONAL BRACE FORCES, TORSIONAL LOADING, 4-DIAGONALS WITH 20-GAUGE STIFFENED METAL DECK

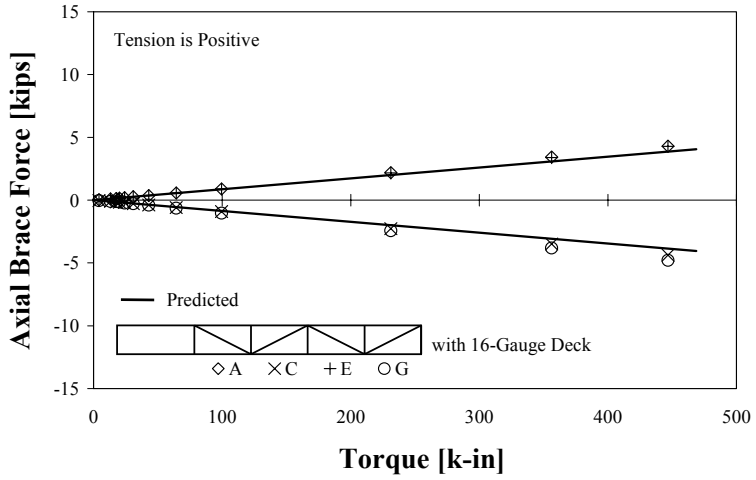

FIGURE 5.18 DIAGONAL BRACE FORCES, TORSIONAL LOADING, 4-DIAGONALS WITH 16-GAUGE METAL DECK

5.1.5 Performance of Metal-Deck Fasteners

Fastener distress was observed in the final T3 trial of the three metal-deck-only test cases. End fastener failures were observed in the 16-gauge and 20-gauge unstiffened deck trials, but not the 20-gauge stiffened deck. Stitch fastener tipping was observed in all cases, except at stitch seams where stiffening angles were present.

The stitch fasteners in the two unstiffened metal-deck tests exhibited a "tipping" phenomenon. This phenomenon is well documented and occurs when two relatively thin sheets connected by screw fasteners, are pulled apart (Luttrell, 1987). Figure 5.19 shows typical observed tipping of a stitch fastener. The screw head and tip protruding from the underside of the decking has tipped dramatically. Prior to testing, each fastener was spray painted to facilitate observation of fastener movements. Bearing deformation in the top sheet can be seen as the screw head has shifted to expose the unpainted deck surface below.

The use of a stiffening angle in the M20S test configuration eliminated the tipping of the stitch fasteners at seams where stiffening angles were present. Figure 5.20 shows a stitch fastener at the location where a stiffening angle was present. The inset pictures show the screw head and tip maintaining a vertical orientation at the maximum applied load for the test. All other stitch fasteners at seams without stiffening angles exhibited the tipping shown in Figure 5.19. In addition, buckling of the deck sheets where stiffening angles were present was observed at some stitch fasteners and is shown in Figure 5.21.

End fastener slip occurred in all three metal-deck tests as seen in Figure 5.22. Figure 5.23 summarizes the locations where fastener slip was observed. Slip of the end fasteners for the middle 13 deck panels for the 16-gauge test was not recorded.

Three end fasteners in test M16-T3 and four end fasteners in test M20-T3 failed. The fasteners in the 16-gauge deck test failed by both fracture and pullout. Figure 5.24 shows an end fastener that has pulled out from the flange with the nail still intact. The fasteners in the 20-gauge deck test all failed by fracture.

The four end fastener failures in test M20-T3, however, were due to improper installation as they were inadvertently fired into locations where previous fasteners had been driven. This caused the fasteners to improperly imbed into the flange or fracture beneath the surface of the decking. The locations of these fasteners are shown in Figure 5.23. Figure 5.25 shows a deck sheet that has been moved after the T3 trial to expose the embedment point of the fastener. The location of the subsequent fastener coincided with the embedment location of a previous fastener. As the fastener was being driven, the tip was driven into the flange at an angle. This either fractured the fastener immediately or damaged the fastener to cause premature failure during testing. The head of the subsequent fastener, pictured at the bottom of Figure 5.25, showed no indications of distress after installation. Figure 5.26 shows the ends of the two deck panel sheets where the improperly installed fasteners were located. With the fasteners fractured, the ends of the deck panels visibly buckled away from the top flange as load was increased. This sheet buckling was localized to the area where the four damaged fasteners were located. No other end fastener failures were observed in the M20-T3 test.

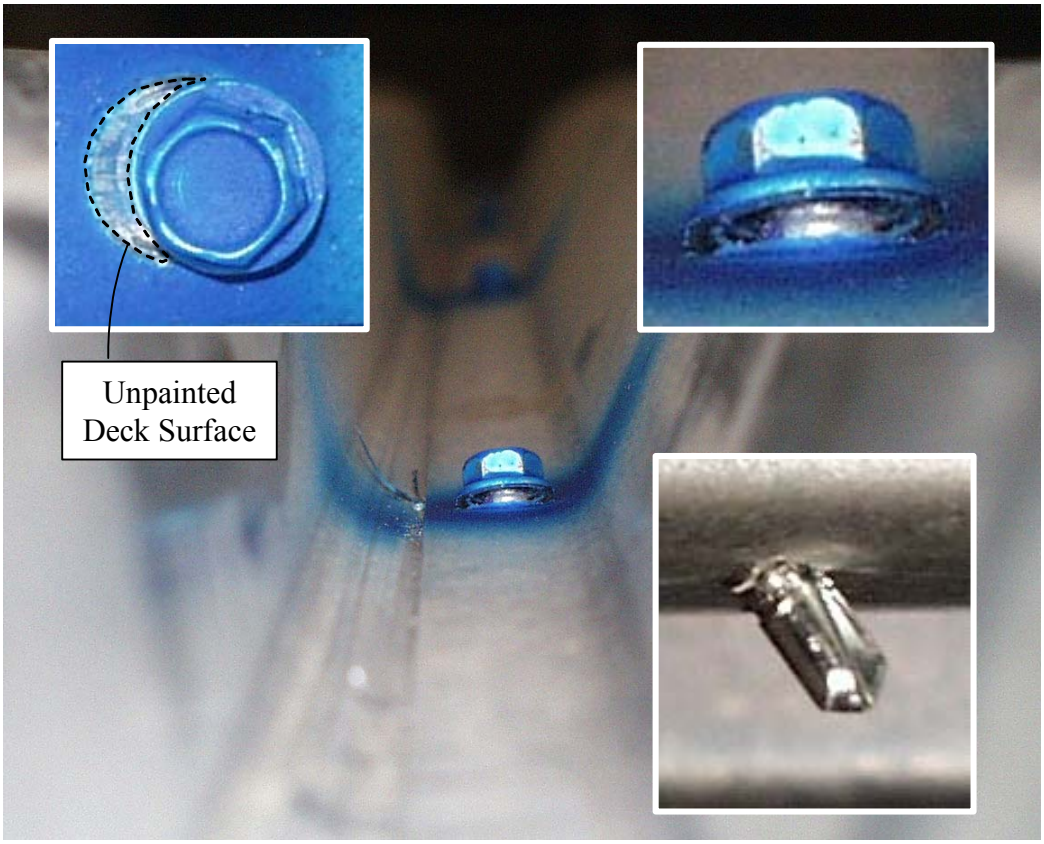

FIGURE 5.19 TYPICAL STITCH FASTENER TIPPING AND BEARING DEFORMATION.

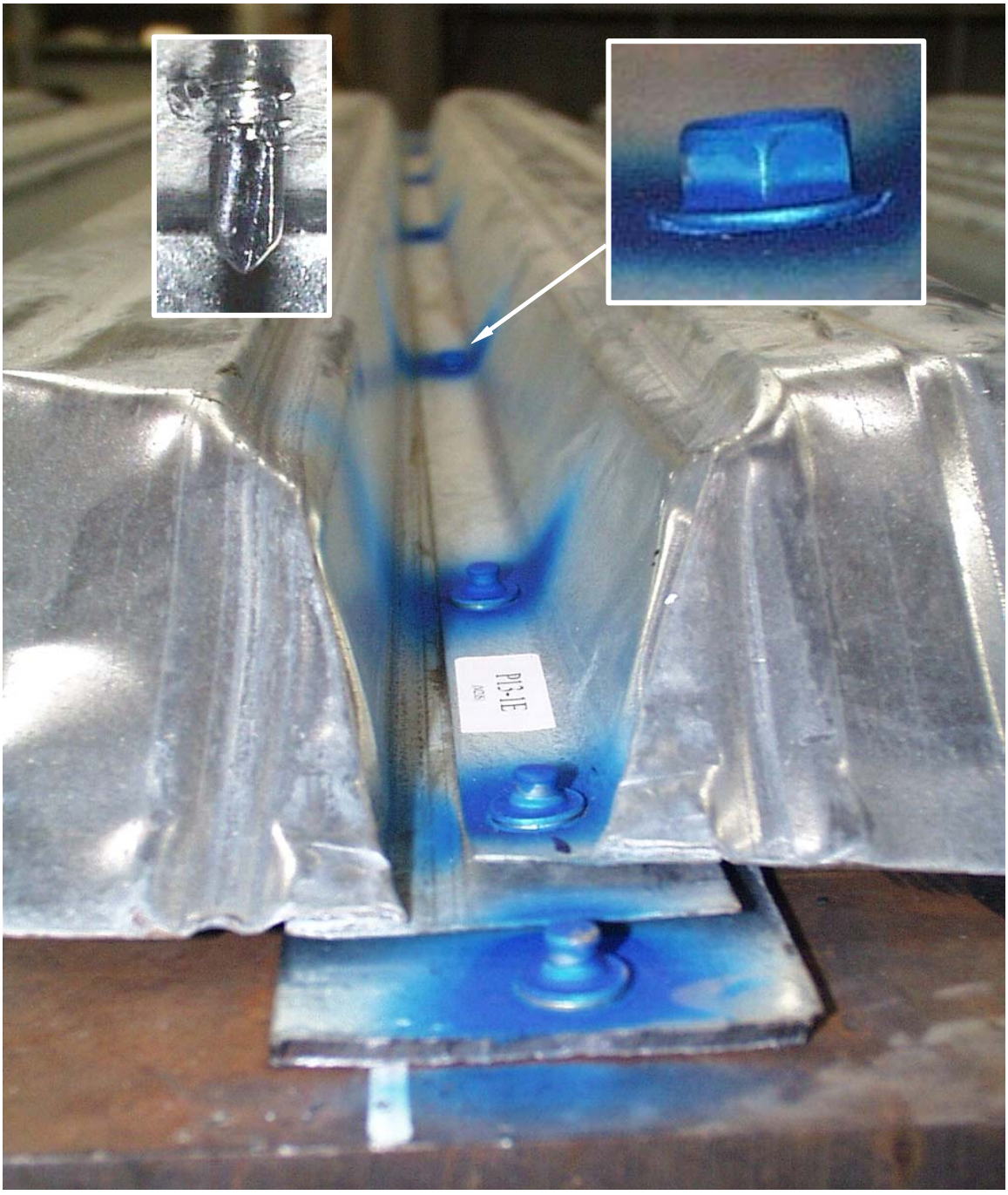

FIGURE 5.20 STITCH FASTENER AT STIFFENING ANGLE UNDER MAXIMUM APPLIED LOAD

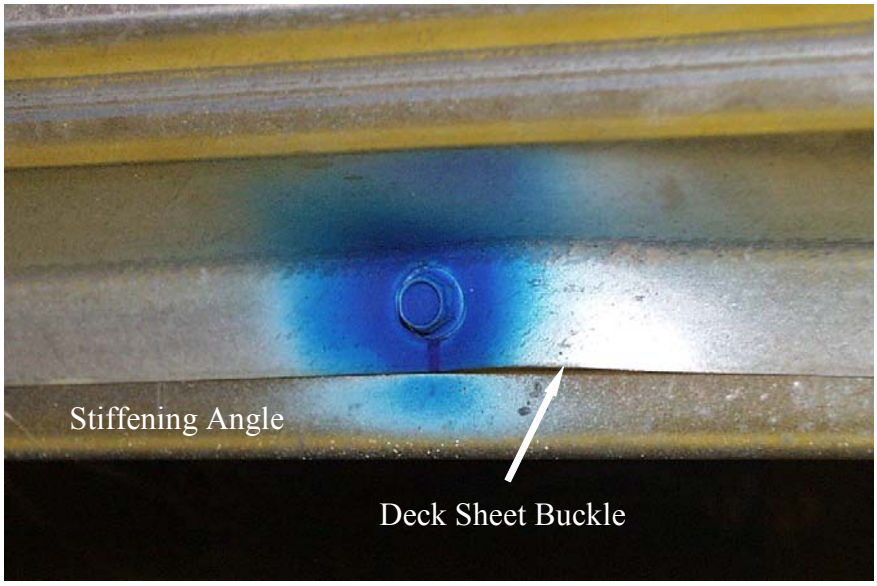

FIGURE 5.21 BUCKLING OF DECK AT STITCH FASTENER WITH STIFFENING ANGLE.

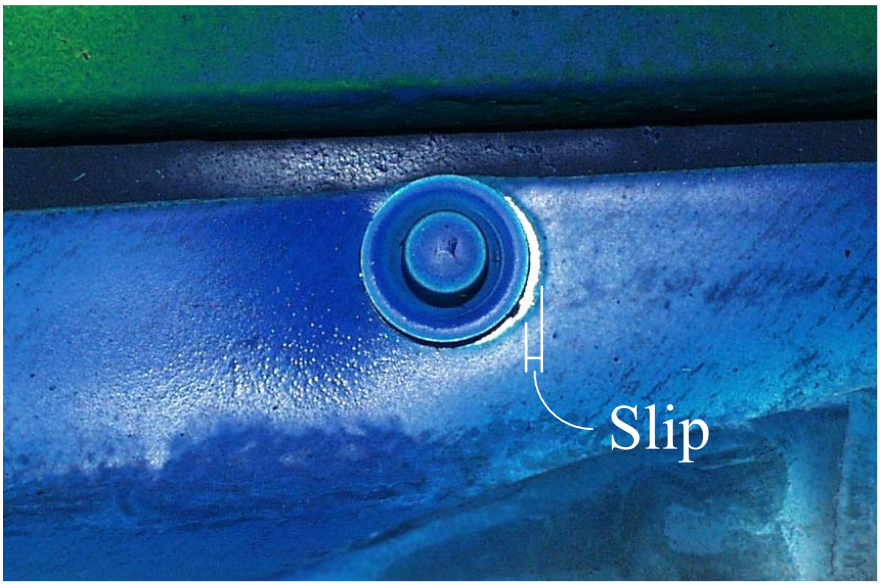

FIGURE 5.22 SLIP IN END FASTENER EXPOSING UNPAINTED DECK SURFACE

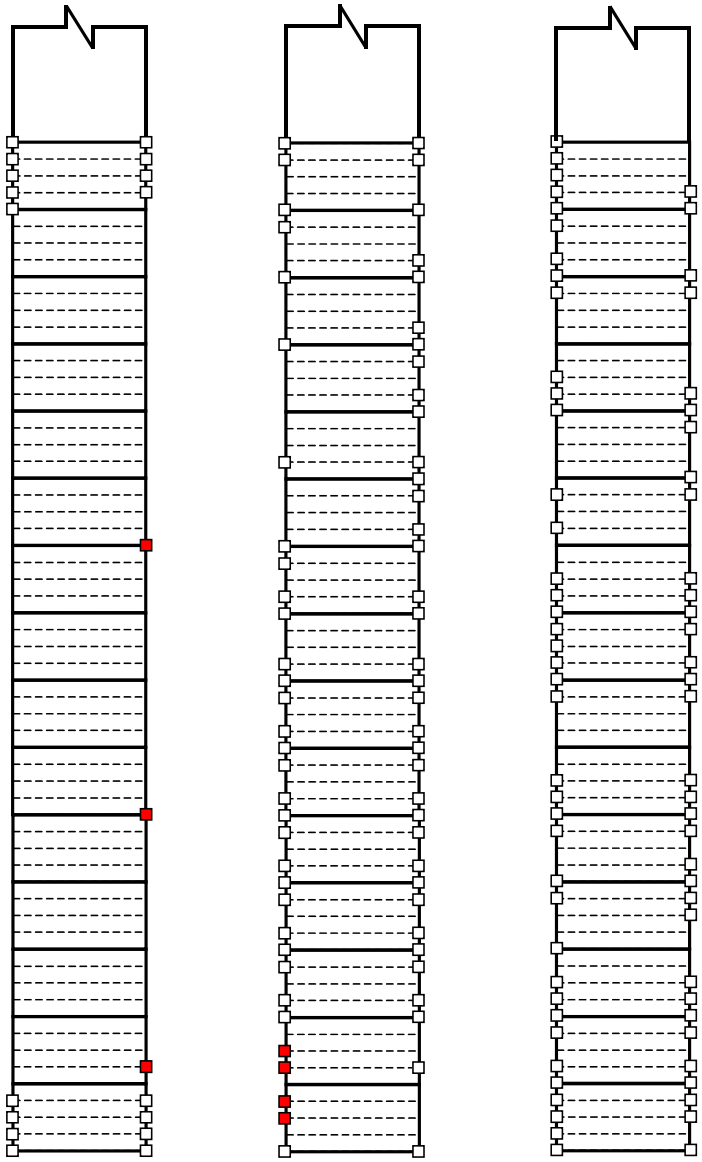

FIGURE 5.23 FASTENER CONDITION AT PEAK LOAD FOR METAL-DECK TESTS

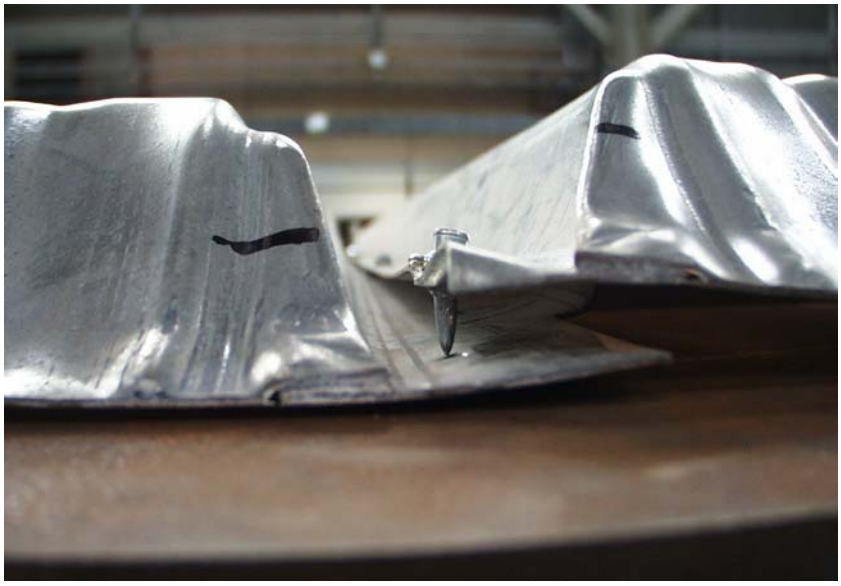

FIGURE 5.24 PULLOUT OF AN END FASTENER AT A LAP SEAM IN TEST M16-T3

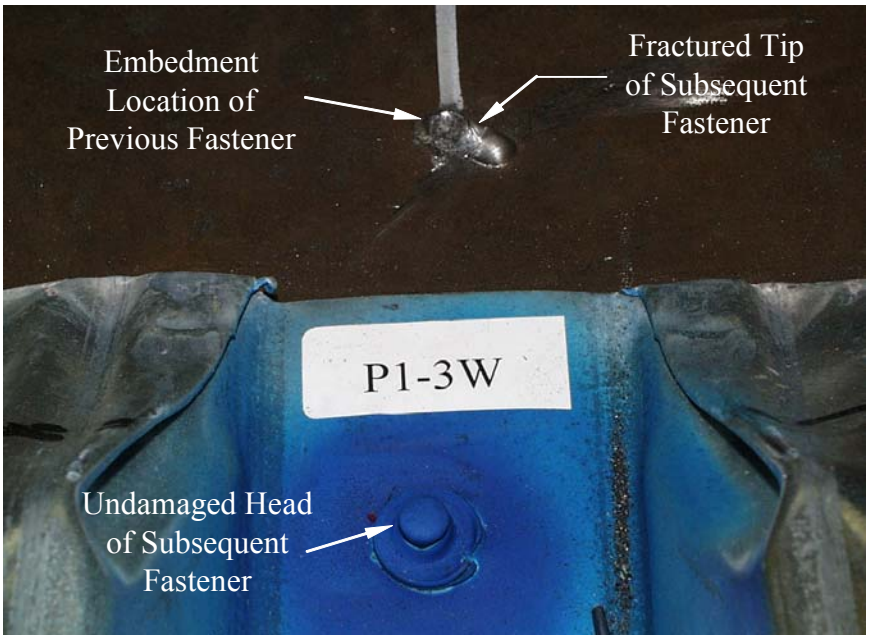

FIGURE 5.25 FASTENER DRIVEN INTO LOCATION OF PREVIOUS FASTENER

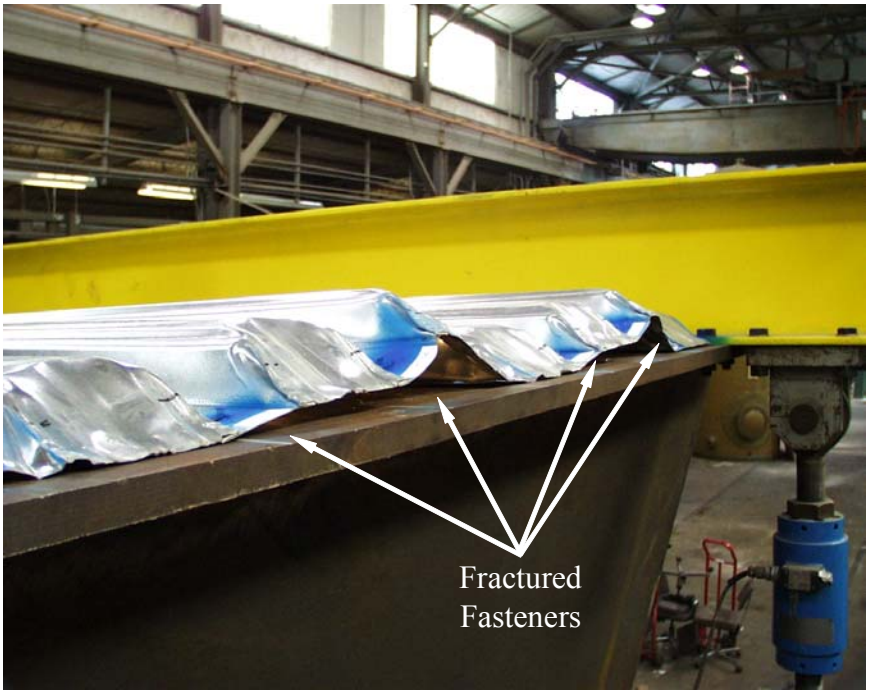

FIGURE 5.26 METAL DECK SHEETS BUCKLING AFTER END FASTENER FAILURES IN TEST M20-T3

5.2 BENDING TESTS

5.2.1 Bending Stiffness

The bending stiffness response for various bracing configurations is shown in Figure 5.27. Adjustments of the tip deflections were made using measured deflections at the end and interior supports. Corrections were determined assuming rigid body movement of the test specimen. The top-lateral bracing configurations used in the laboratory tests, caused no discernable change in bending stiffness from the unbraced case.

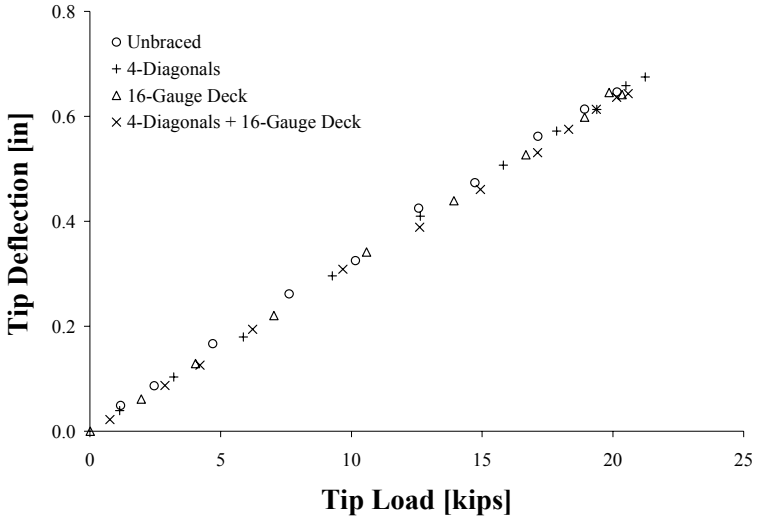

FIGURE 5.27 BENDING LOAD-DEFLECTION RESPONSE FOR VARIOUS BRACE CONFIGURATIONS

5.2.2 Brace Forces

The maximum top-lateral truss forces measured in the bending test series were considerably smaller in magnitude than those measured in the torsion tests. Typical brace force responses for the 2-diagonal and 4-diagonal truss configurations are shown in Figures 5.28 through 5.31. Theoretical predictions, shown as lines, were determined using expressions developed by Fan and Helwig (1999) as given in Section 2.3.2. Theoretical predictions were in fair agreement with measured values for both diagonal and strut forces. It should be noted that the magnitudes of the brace force were small in comparison to those generated in the torsion tests with maximum measured strains less than 50 microstrain, which correspond to approximately 1.5 ksi.

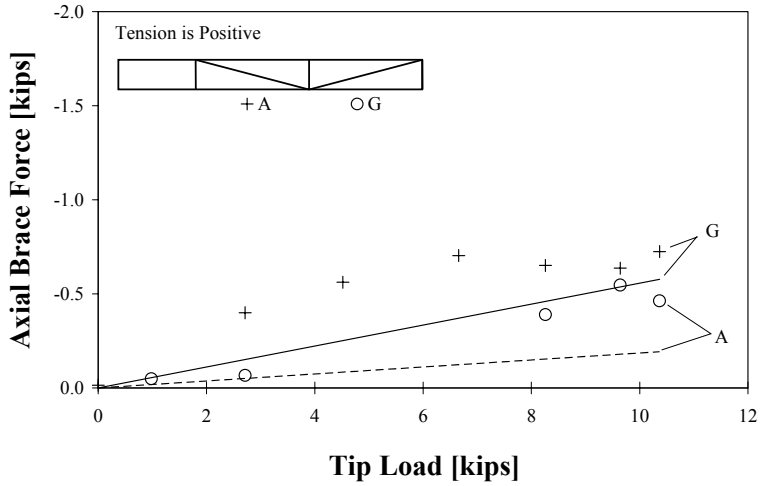

FIGURE 5.28 DIAGONAL BRACE FORCES, BENDING LOAD, 2-DIAGONALS

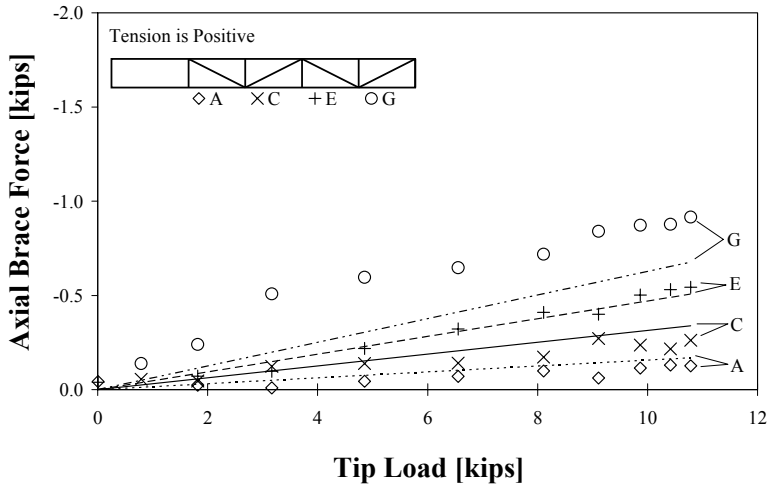

FIGURE 5.29 DIAGONAL BRACE FORCES, BENDING LOAD, 4-DIAGONALS

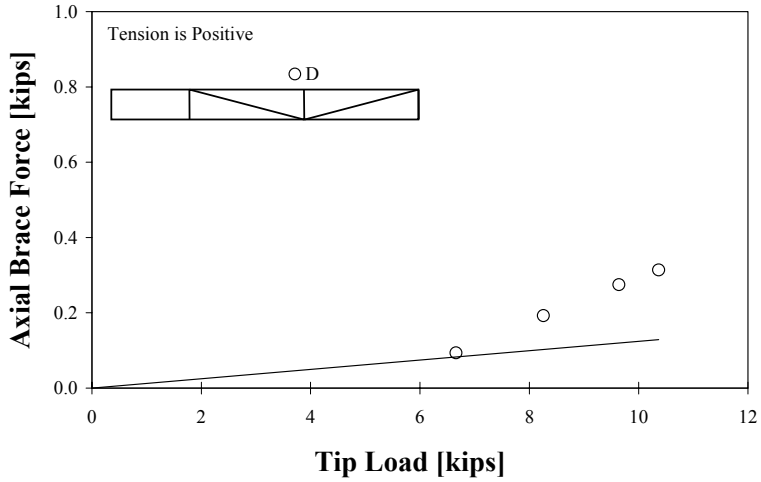

FIGURE 5.30 STRUT BRACE FORCES, BENDING LOAD, 4-DIAGONALS

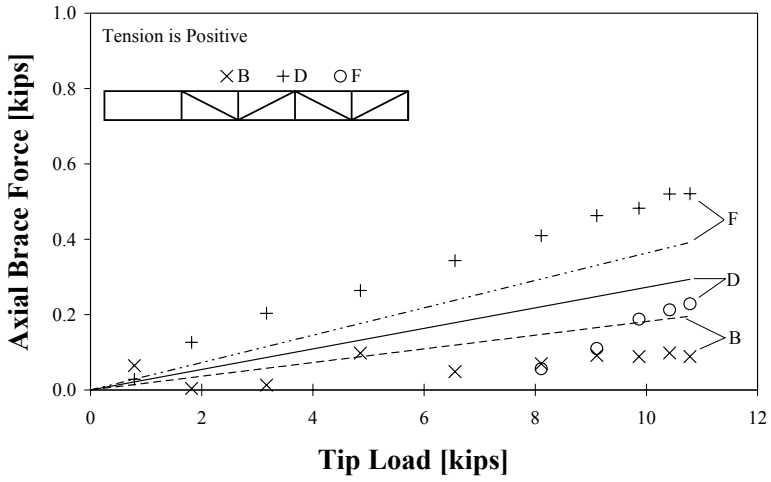

FIGURE 5.31 STRUT BRACE FORCES, BENDING LOAD, 4-DIAGONALS

CHAPTER 6
ANALYSIS OF LABORATORY RESULTS

6.1 FINITE-ELEMENT MODEL

A three-dimensional finite-element model was developed using the commercially available program ABAQUS to analyze the behavior of the full-scale trapezoidal steel box-girder test specimen and is shown in Figure 6.1. Structural elements were modeled using shell and truss elements. Four-node doubly-curved general purpose shell elements (S4) were used to model all of the girder plate elements. This included the top and bottom flanges, webs, web stiffeners, plate diaphragm, and permanent metal deck forms. Four-noded elements were chosen over the quadratic eight-noded elements used in the field test model (Chapter 3) because the laboratory test specimen geometry was straight. Three-node quadratic displacement truss elements (T2D3) were used to model the end K-diaphragm and top-lateral truss bracing.

The top-lateral truss elements were connected directly to the webs 3 in. below the top flange as shown in Figure 6.1a. Two shell elements were used to model the metal deck bracing at each section and were connected at the outer edge of the top flanges as shown in Figure 6.1b. The thicknesses of the deck elements were determined using the SDI shear stiffness as described in Section 2.2 and are listed in Table 5.2.

Support conditions were modeled with translational restraint in all directions at the intermediate and end support locations. These boundary conditions were imposed along a single line of nodes between the web stiffeners at each location. Concentrated forces placed at nodes were used to represent the bending and torsional forces applied in the laboratory tests and are illustrated in

Figure 6.1. Loads from the bending rams were applied to the bottom flange beneath the web stiffeners (Figure 6.1a) while loads from the torque rams were represented with equivalent concentrated forces at the center of the top flanges (Figure 6.1b).

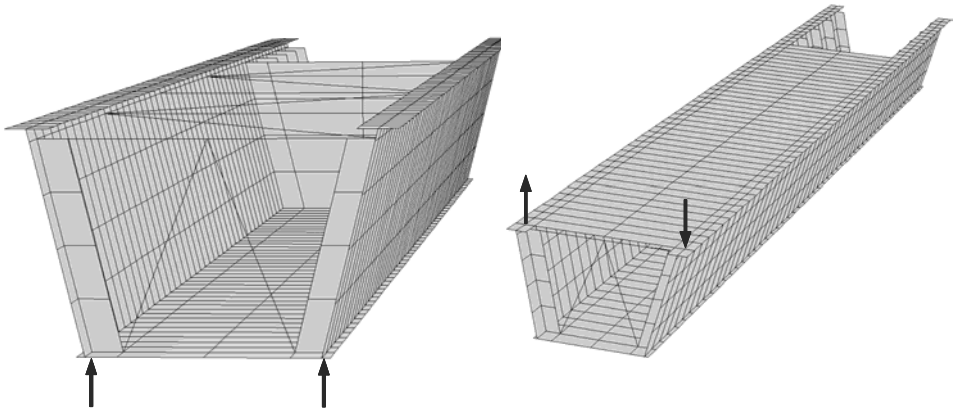

a) Truss b) Metal Decking

FIGURE 6.1 FINITE-ELEMENT MODELS FOR LABORATORY SPECIMEN WITH TOP-LATERAL BRACING

6.2 TORSIONAL STIFFNESS

For a cantilever beam with no warping restraint at the end support, the angle of twist is given by

$$\theta = \frac{TL}{GK_T} \tag{6.1}$$

where T is the applied torque, L is the member length, G is the shear modulus of elasticity, and K_T is the pure torsion constant for the cross-section. If warping is restrained fully at the support, the twist becomes

$$\theta = \frac{Ta}{GJ}\left[\frac{L}{a} - \tanh\frac{L}{a}\right] \tag{6.2}$$

where a is defined as

$$a = \sqrt{\frac{EI_w}{GK_T}} \tag{6.3}$$

The warping constant, I_w, of the cross-section can be quite cumbersome to calculate even for simple sections. A tabular finite-difference procedure developed by Heins (1975) to determine the warping constant is given in Appendix A. Rearranging Eqns. (6.1) and (6.2) in terms of a torsional stiffness gives

$$\frac{T}{\theta} = \frac{GK_T}{L} \tag{6.4}$$

$$\frac{T}{\theta} = \frac{GJ}{a}\left[\frac{L}{a} - \tanh\frac{L}{a}\right]^{-1} \tag{6.5}$$

Table 6.1 summarizes the average experimental torsional stiffness values. The lower- and upper-bound traditional hand method solutions were determined using Eqns. (6.4) and (6.5), respectively. Theoretical values for the 20-gauge deck with stiffening angles were not calculated, as there are no current methods to estimate the stiffness of these systems.

The experimental stiffness values were in moderate to fair agreement with theoretical predictions. Discrepancies seen in the metal-deck test configurations can be partly attributed to the difficulty in predicting fastener slip in the decking. This phenomenon has been observed in other tests involving metal decking and is discussed further in the following section (Blank, 1973; Currah, 1993). In addition, the torsional stiffness values are highly sensitive to the support movements and associated corrections. This can be seen in the torque-twist

response of the 4-diagonal test configuration (Figure 6.2), a test case where a large discrepancy between the experimental and theoretical torsional stiffness was seen. This sensitivity can also be seen in the rotations along the girder length as shown in Figure 5.5. This test case represents the most inaccurate case presented in Table 6.1. Examination of the torque-twist response curves and girder rotation plots for the other test configurations presented in Appendix A suggest the equivalent plate method coupled with the SDI deck stiffness can a reasonably predict the torsional behavior of a braced girder.

TABLE 6.1 THEORETICAL AND AVERAGE EXPERIMENTAL TORSIONAL STIFFNESS VALUES [KIP-IN/DEG]

Test Case	Hand Methods		ABAQUS	Experimental	$\frac{\text{Experimental}}{\text{ABAQUS}}$
	Lower	Upper			
U	11	288	170	180	1.06
2	1529	2023	1581	1588	1.00
4	2092	2645	2036	2496	1.23
M20	1055	1494	1347	1382	1.03
M20S	--	--	--	1547	--
M16	3035	3673	2502	2219	0.89
4M20	3323	3985	2914	3234	1.11
4M20S	--	--	--	3626	--
4M16	5165	5958	4295	4387	1.02

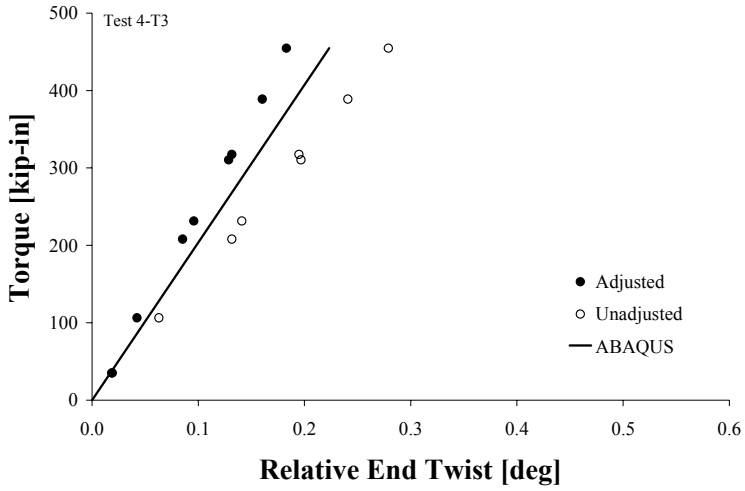

FIGURE 6.2 TORQUE-TWIST RESPONSE FOR GIRDER WITH 4-DIAGONALS AT MAXIMUM TEST LOAD

6.3 STRENGTH OF METAL DECKING

The shear strength of the metal decking used in the laboratory tests was estimated using the *Steel Deck Institute Diaphragm Design Manual 2nd Edition*. The SDI design strength of a diaphragm is based on three failure mechanisms. The first mode involves failure of fasteners within an edge panel (see Figure 6.3). The second mode involves failure of an interior panel at sheet-to-sheet or sidelap fasteners. The third involves failure of a corner fastener where the shears along the two orthogonal edges create a larger resultant force as illustrated in Figure 6.4. In testing bridge deck configurations, Currah (1993) found that strengths based on the third failure mode most closely predicted the actual measured strengths. The recommended equation to predict the shear strength is given by

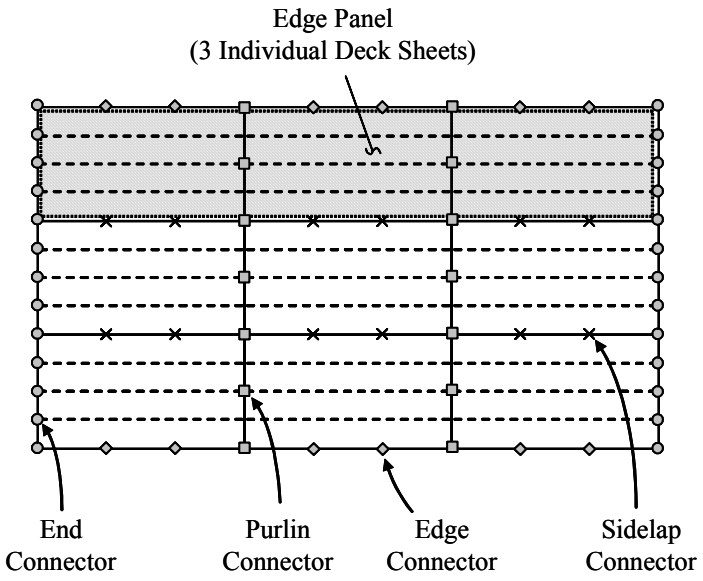

FIGURE 6.3 SCHEMATIC LAYOUT FOR DIAPHRAGM AND CONNECTORS

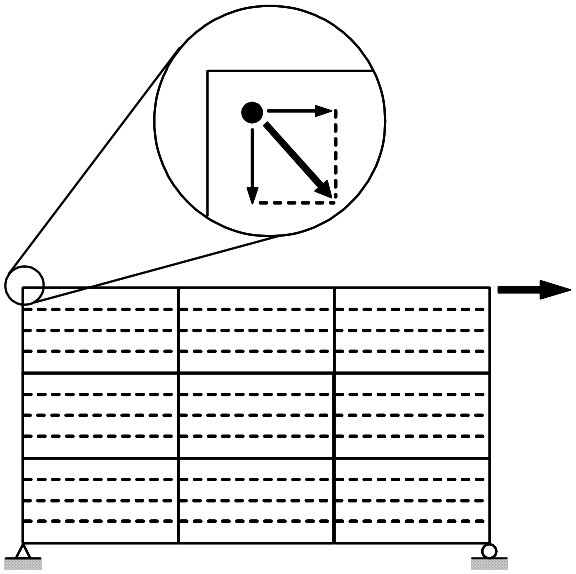

FIGURE 6.4 INCREASED RESULTANT FORCE FOR CORNER FASTENERS

$$S_n = Q_f \sqrt{\frac{1}{\left(\frac{L}{2A(\lambda-1)+B}\right)^2 + \frac{1}{N^2}}} \qquad \text{(SDI Eqn. 2.2-5*)}$$

where Q_f is the fastener strength, λ is a measure of a corrugation rib's tendency to deflect normal to the diaphragm plane (which relieves forces on corner fasteners). The variables *A, B,* and *N* define the fastener layout. The definitions for the variables in this equation are described in detail in Appendix B along with a numerical example. It should be noted that the nomenclature used by SDI refers to S_u as the predicted shear strength. In this research report, S_u will refer to the average applied shear loads while S_n will refer to the average shear strength or resistance.

SDI Eqn. (2.2-5*) as it appears above is an expanded form that only appears in the first edition of the SDI Manual. The simplified form given in the second edition assumes $\lambda = 1$. This assumption was judged to be invalid for bridge deck forms (Currah, 1993). The shear strengths of the decking used in the laboratory tests were calculated using SDI Eqn (2.2-5*) and are given in Table 6.2. Derivation of the resistance factor, ϕ, is described in Section 6.3.1.

The shear force generated in the decking of the laboratory tests was determined using Eqn. (2.13). Dividing the expression by the panel width, *b*, and rearranging gives the applied torque in terms average shear force in the decking.

$$T = 2A_o S_n \qquad (6.6)$$

where *T*, is the applied torque on the girder, A_o is the enclosed cross-sectional area, and S_n is the nominal average shear strength determined using SDI Eqn. (2.2-5*).

The torques corresponding to the proposed factored SDI strengths are plotted with the torque-twist curves for the 16- and 20-gauge metal-deck tests in

Figures 6.5 and 6.6. The proposed strengths correspond favorably with the upper limit of the initial linear response region. This would indicate that if the applied torques are below the proposed deck strength limit, the girder stiffness determined using the SDI shear stiffness can be expected.

TABLE 6.2 SDI METAL-DECK SHEAR STRENGTHS [KIPS/FT]

Decking	S_n	ϕS_n
20-Gauge	0.97	0.73
16-Gauge	1.58	1.19

$\phi = 0.75$

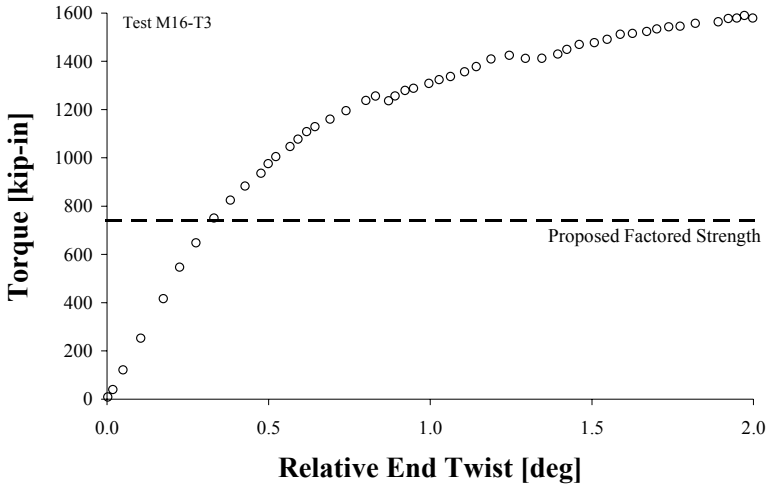

FIGURE 6.5 TORQUE-TWIST RESPONSE FOR 16-GAUGE DECK CONFIGURATION

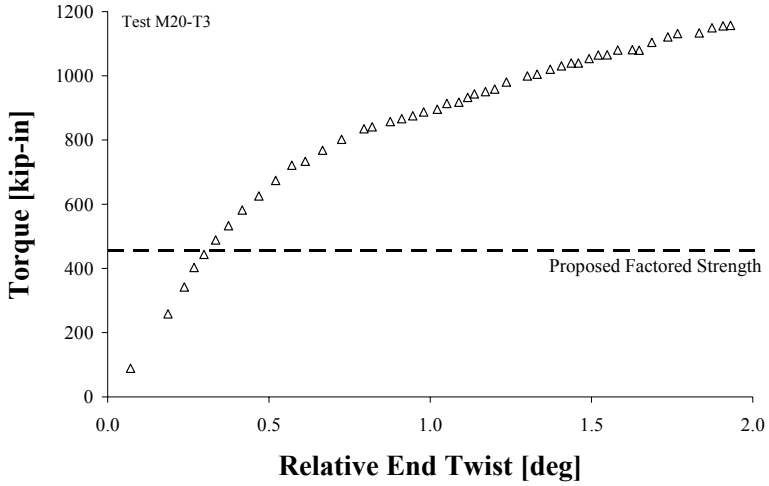

FIGURE 6.6 TORQUE-TWIST RESPONSE FOR 20-GAUGE DECK CONFIGURATION

6.3.1 Safety Factors

The factor of safety used in the SDI Manual combines both the load and resistance factors into one safety factor. Detailed derivations of the safety factors are documented in the first edition of the manual. The load factors are based on probabilistic techniques incorporating dead, sustained live, and maximum lifetime wind loading. For metal-deck utilized as construction bracing, the load factors are inherently present in the construction design loads that are prescribed by governing code provisions such as the *AASHTO LRFD Bridge Specification*. Therefore, the load factors contained within the SDI safety factor were removed to eliminate redundancy and excessive conservatism.

In load and resistance factor design, the reliability index, β, represents a comparative measure of the reliability of a structure or component. This index, which is discussed in detail by others (Ravindra and Galambos, 1978; Ellingwood

et al, 1982), can be used to determine a corresponding resistance factor, ϕ, by the following (AISC, 2000):

$$\phi = \left(R_m / R_n\right) e^{-0.55 \beta V_r} \tag{6.7}$$

where R_m is the mean resistance, R_n is the nominal resistance, and V_r is the coefficient of variation of the resistance. The resistance factor incorporated in the SDI safety factor was derived through calibration to numerous full-scale diaphragm and connection tests and considers variation in material yield stress, fabrication, and the ratio of measured test results to predicted strengths (Luttrell, 1981). These tests showed that mechanical fasteners had less variation in strength versus welded connections due to higher quality control. For diaphragms with mechanical fasteners, the ratio of R_m/R_n was equal to 1.09 with a coefficient of variation, V_r, equal to 0.170.

The β values inherent in the AISC LRFD specification are equal to 2.6 for members and 4.0 for connections. The larger β value for connections reflects the desire to have connections be stronger than the members they are connecting. For diaphragms with mechanical fasteners, the resistance factors obtained from Eqn (6.7) for β values equal to 4.0 and 2.6 were equal to 0.75 and 0.85, respectively.

Since the strength of metal-deck diaphragms is primarily controlled by failure at the connectors, a resistance factor of 0.75 is proposed for metal-deck lateral bracing systems used during the construction phase of box-girder bridges. Comparison of the design strengths using the proposed resistance factor compared favorably with experimental results as previously discussed. Additionally, for the six different bridge deck types tested by Currah (1993), design shear strengths calculated using the proposed resistance factor were all conservatively less than the actual measured strengths.

CHAPTER 7
DESIGN APPLICATION

This chapter presents a proposed design methodology for top-lateral bracing in trapezoidal steel box-girder bridge systems. The proposed design methods are based on satisfying both strength and stiffness criteria. Special design issues pertaining to metal-deck top-lateral bracing are examined. Numerical bracing design examples are presented in Appendix D.

7.1 OVERVIEW

Top-lateral bracing systems for box-girder bridge systems must satisfy both strength and stiffness criteria. These requirements vary depending on the type of top-lateral system that is used, what other types of bracing are present, and whether the bridge is curved or straight. The strength requirements are based on brace forces that are generated from four primary sources. These sources include girder torsional moments, girder bending moments, vertical loads on inclined webs, and lateral stability of the top flanges. Stiffness requirements are based on three criteria. These criteria are the control of girder rotations, the control of warping stresses, and providing lateral stability for the top flanges.

7.2 BRACING REQUIREMENTS FOR TOP-FLANGE LATERAL BUCKLING

For a lateral brace to be effective, it must have both sufficient strength and stiffness (Winter, 1960). Top-lateral truss and metal-deck bracing for box-girders can be classified as relative bracing systems because they prevent the relative lateral movement of adjacent brace points along the length of a compression member.

The bracing requirements for beams adopted by AISC were developed by Yura (1995) and are based on Winter's column bracing approach. Figure 7.1 shows the unbraced length of a column between relative brace points. The lateral brace with stiffness β_{lat} develops a brace force, F_{br}, which is related to the magnitude of the initial out-of-straightness of the column.

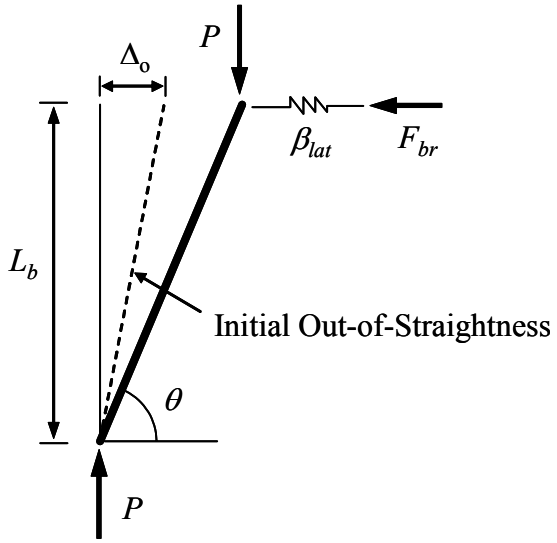

FIGURE 7.1 COLUMN BETWEEN RELATIVE BRACE POINTS

For a beam with n relative brace points, the required lateral brace stiffness and strength requirements are given by (AISC, 2001)

$$\beta_{lat} = \frac{4M_u C_d}{\phi L_b h_o} \tag{7.1}$$

$$F_{br} = 0.008 \frac{M_u C_d C_s}{h_o} \tag{7.2}$$

where M_u is the maximum factored moment, L_b is the unbraced length, h_o is the distance between flange centroids, ϕ is the resistance factor equal to 0.75.

C_d is a factor that equals 1.0 for single- and 2.0 for reverse-curvature bending. Reverse curvature bending results in both the top and bottom flanges being in compression. For I-girders, this significantly increases the lateral bracing requirements because both flanges can buckle laterally. This effect is not as pronounced in box-girders due to the relatively large lateral bending stiffness of the wide bottom flange, but can be conservatively accounted for with the previously defined C_d factor.

C_s is a factor that accounts for the increased brace force demands due to flange out-of-straightness. The brace force requirement in Eqn. (7.2) was developed assuming an initial out-of-straightness of 1/500 (0.002). Flange out-of-straightness values greater than the assumed value linearly increase the required brace forces.

In addition to fabrication imperfections, a shortening phenomenon can effectively increase the initial flange out-of-straightness, resulting in larger brace forces (Chen, 1999). Under compressive stresses, the top flanges of a box-girder shorten. This brace panel shortening permits lateral displacement of the brace point. Figure 7.2 shows the horizontal displacement, Δ_h, due to the shortening of the top flanges, Δ_s. Although this lateral translation increases the brace force requirements, it has no effect on the flange force or brace stiffness required to produce flange buckling between brace points. The shortening of one brace panel due to positive bending is given by

$$\Delta_s = \frac{M}{ES_{top}} s \tag{7.3}$$

where M is taken as the moment at the center of the brace panel, E is the modulus of elasticity of steel, S_{top} is the section modulus for the top flange, and s is the brace panel length. The top-lateral bracing is ignored when determining the

section modulus as it generally has a negligible effect on the large bending moment of inertia of typical box-girders. Ignoring the top-lateral bracing also provides a conservative estimate of the shortening. The corresponding horizontal displacement due to shortening, normalized by the brace panel length is

$$\frac{\Delta_h}{s} = \frac{M}{ES_{top}} \frac{s}{b_{top}} \tag{7.4}$$

The resulting out-of-straightness factor is

$$C_s = \frac{\frac{\Delta_o}{s} + \frac{\Delta_h}{s}}{0.002} \tag{7.5}$$

where Δ_h/s is the additional out-of-straightness due to shortening and Δ_o/s is the actual flange out-of-straightness.

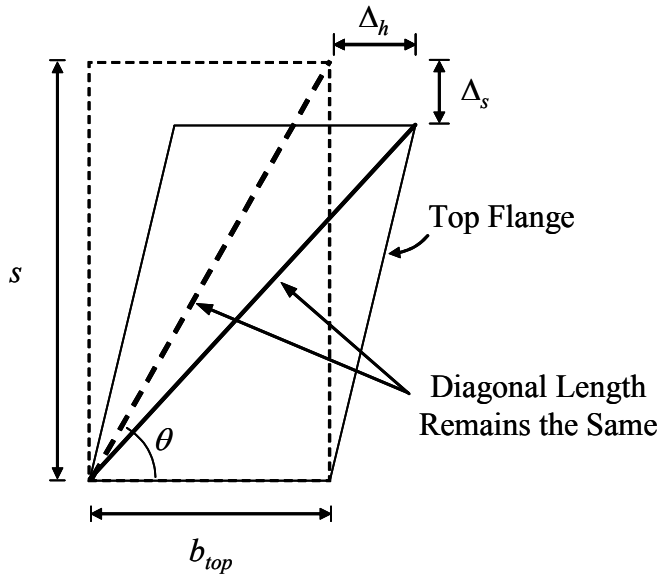

FIGURE 7.2 LATERAL DISPLACEMENTS DUE TO BRACE PANEL SHORTENING

7.2.1 Truss Systems

The stiffness and strength requirements given by Eqns. (7.1) and (7.2) are for a perpendicular lateral brace. Conversion to a diagonal truss member can be made using the cosine function. For the member shown in Figure 7.1, the equivalent perpendicular brace stiffness is equal to the axial member stiffness multiplied by $\cos^2\theta$. The axial brace force is the value from Eqn. (7.2) divided by the $\cos\theta$.

7.2.2 Metal-Deck Systems

For metal-deck systems, the stiffness and strength requirements can be obtained by considering an arbitrary braced flange length as shown in Figure 7.3. The effective shear stiffness, G', of the diaphragm panel is equal to

$$G' = \frac{V/b}{\Delta/L_b} \tag{7.6}$$

where b is the diaphragm panel length. Expressing the lateral brace stiffness in terms of the effective shear stiffness, G', results in

$$\beta_{lat} = \frac{V}{\Delta} = \frac{G'b}{L_b} \tag{7.7}$$

Substituting the required lateral brace stiffness defined in Eqn. (7.1) and rearranging gives

$$G'_u = \frac{4M_u C_d}{\phi\, b\, h_o} \tag{7.8}$$

Eqn. (7.8) represents the required effective shear stiffness of metal-decking used to continuously brace the two top flanges of a box-girder. The continuous nature of the deck bracing results in a required effective shear stiffness that is

independent of the braced length. In addition, an advantage of metal-deck systems over truss systems is that they are not susceptible to the effects of shortening due to their "accordion-like" profile. Therefore, for metal-deck systems, the Δ_h/s term in Eqn. (7.5) can be omitted.

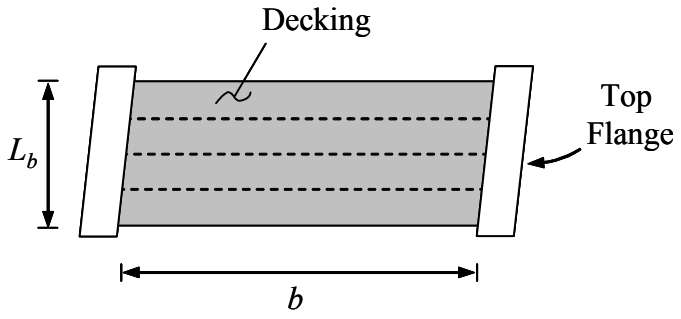

a) Arbitrary Length of Top Flanges

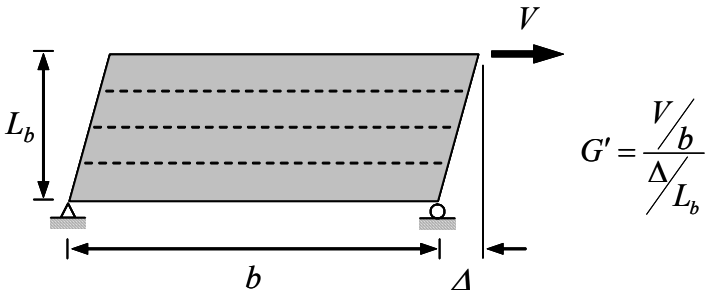

b) Effective Shear Stiffness

FIGURE 7.3 RELATIVE METAL-DECK BRACING FOR TOP-FLANGES OF BOX GIRDER

The shear strength requirement for the metal-deck bracing is obtained from Eqn. (7.2).

$$S_u = \frac{F_{br}}{b} = 0.008 \frac{M_u C_d C_s}{b\, h_o} \tag{7.9}$$

7.3 BRACE STRENGTH REQUIREMENTS

Brace forces in top-lateral bracing systems of steel box-girders originate from four primary sources:

1.) Girder torsional moments

2.) Girder bending moments

3.) Vertical flange loads on inclined webs

4.) Lateral-buckling forces of the top flanges

Design of top-lateral bracing must take into consideration each of these potential load conditions.

7.3.1 Girder Torsional Moments

Torsional moments on the girder create shear flow in the quasi-closed cross section, which generate forces in top-lateral bracing systems as shown in Figure 7.4. Results from the laboratory test program have demonstrated that application of the equivalent plate approximation produces reasonably accurate brace force predictions. The magnitude of the brace forces can be determined by calculating the shear force on the brace panel using Eqn. 2.13. For metal-deck systems, the calculated panel shear force can be converted to an average shear by simply dividing by the length of the metal-deck panels. For truss systems, individual member forces can be determined by resolving the panel shear force and applying basic truss analysis techniques. These truss forces are independent of the member sizes and depend only on the truss-configuration and brace panel geometry.

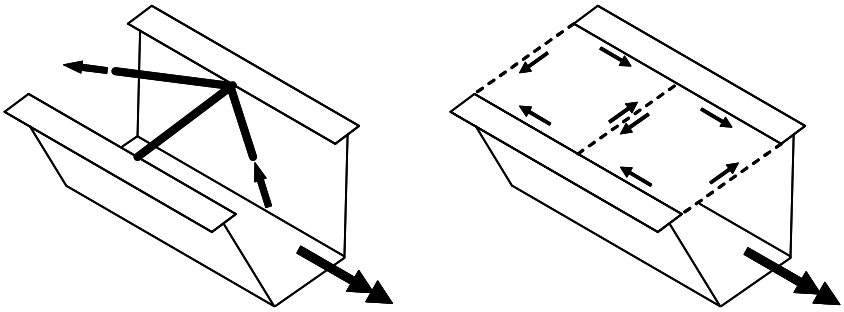

a) Truss b) Metal Deck

FIGURE 7.4 BRACE FORCES DUE TO GIRDER TORSIONAL MOMENTS

7.3.2 Girder Bending Moments

The brace forces introduced by box-girder bending are the direct result of compatibility between the bracing and the top flanges. Top-lateral bracing attached to or near the top flanges attracts compressive forces under positive bending moments as shown in Figure 7.5. These forces increase with both increasing member size and brace panel length (angle between diagonals and top flange decreases). These forces can be quite significant and are often times equal to or greater than the forces generated by torsion. These bending induced brace forces can be calculated using expressions developed by Fan and Helwig (1999). For convenience, these formulae have been reproduced in Section 2.3.2.

One advantage of metal-deck bracing systems is that they do not develop the bending induced forces that occur in truss systems. This is because the in-plane stiffness of the deck panels transverse to the corrugation ribs is extremely small. Therefore, strength design of metal-deck top-lateral bracing systems need not consider forces induced by vertical bending of the box-girder.

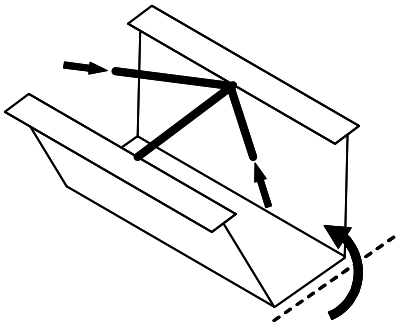

FIGURE 7.5 BRACE FORCES DUE TO VERTICAL BENDING OF GIRDER

7.3.3 Horizontal Force Components from Vertical Flange Loads

The vertical construction loads acting on the top flanges create lateral force components due to the inclined webs as shown in Figure 7.6. Bracing is necessary to resist these forces and control distortional and lateral flange stresses. Both top laterals and internal diaphragms can carry these force components. Others have also demonstrated that full-height web stiffeners attached to the bottom flanges can also be effective (Branco and Green, 1984). If the designer has chosen to have the top-lateral bracing system carry these force components, then their contribution should be included in the strength design. The magnitude of these forces is related to the web inclination as shown in Figure 7.6. For truss systems, the member forces will vary depending on truss arrangement. Fan and Helwig (1999) conducted analytical studies on both single-diagonal and X-type truss systems and found that the brace forces due to the horizontal components tended to be small compared to those generated by bending and torsion. Therefore, it was recommended that the struts be designed to carry the entire lateral force component with the diagonal forces remaining unchanged. These brace force formulations can be found in Section 2.3.2.

For metal-deck systems, in the absence of internal diaphragms, the strength design must account for these horizontal force components. Further discussion of

the effects of these forces on the predicted SDI shear strength is given in Section 7.5.3.

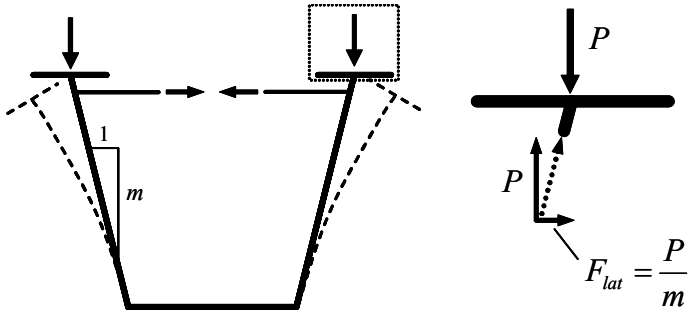

FIGURE 7.6 BRACE FORCES DUE TO HORIZONTAL COMPONENT OF VERTICAL FLANGE LOAD ON INCLINED WEB

7.3.4 Lateral Stability Requirements for Top Flanges

Lateral instability of the top flanges in compression regions can be handled using top-lateral systems and/or internal diaphragms. Both systems are effective at preventing the lateral movement of the top flanges. Like the horizontal force components, if the designer has elected to use the top-lateral bracing to provide the lateral stability for the top flanges then the force requirements outlined in Section 7.2 should be accounted for in the strength design. These brace forces, shown in Figure 7.7, can be either tensile or compressive, depending on the direction the flange wants to buckle. Unlike the brace forces generated by bending and torsion, which can be additive or subtractive with one another, the brace forces from lateral stability will always increase the magnitude of the design brace force.

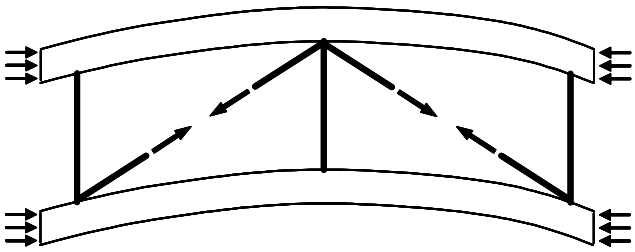

FIGURE 7.7 BRACE FORCES ASSOCIATED WITH LATERAL FLANGE BUCKLING

7.3.5 Design Brace Forces

The comprehensive strength design for top-lateral bracing systems must account for the four potential force components previously described. For metal-deck systems, the bending induced load effect can be neglected.

When using superposition of the individual components to obtain the design brace forces, care should be taken to maintain proper sign conventions. For example, for a Warren single-diagonal brace geometry, torsional moments on the girder cause adjacent diagonals to alternate between tension and compression. Vertical bending of the girder, however, causes compression in all the diagonals in positive moment regions. Brace forces from lateral stability requirements will always increase the magnitude of the resultant brace force from torsion and bending effects. The design forces for straight girders differ from curved girders only in the fact that the torsional force components are not present.

7.4 BRACE STIFFNESS REQUIREMENTS

The brace stiffness requirements for top-lateral bracing systems are based on satisfying three criteria:

1.) Controlling girder rotations

2.) Controlling warping stresses

3.) Preventing lateral buckling of the top flanges

Adequate bracing design must satisfy the criterion with the greatest lateral-brace stiffness requirement.

7.4.1 Controlling Girder Rotations

In curved steel box-girder bridge systems, the large torsional moments observed during casting of the bridge deck can cause bridge girders to undergo significant rotations. In multi-girder bridges, this results in differential rotations between adjacent girders, as shown in Figure 7.8. These misalignments in the superelevation pose both construction difficulties and roadway rideability problems. Controlling these rotations can be accomplished by either providing external diaphragms to maintain alignment between adjacent girders or increasing the torsional stiffness of the girders themselves. Memberg (2002) has developed recommendations for when external diaphragms may be necessary as well as selection of appropriate external diaphragm spacings.

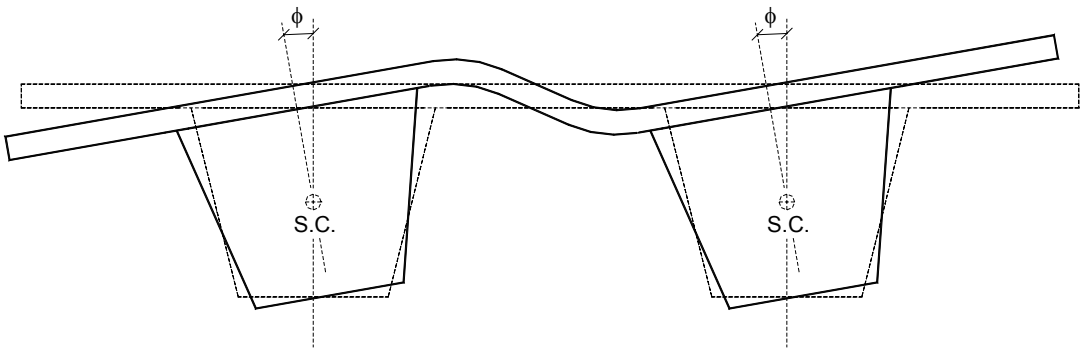

FIGURE 7.8 DIFFERENTIAL GIRDER ROTATIONS CAUSING SUPERELEVATION MISALIGNMENT (MEMBER, 2002)

If the designer elects to eliminate the use of external diaphragms, then the top-lateral bracing system provides the easiest means to control the girder torsional stiffness. To design the top-lateral system, there must be a criterion for

the allowable differential rotations between girders. Unfortunately, no uniform criterion exists. One suggestion has been to limit the vertical displacement at the outer tips of the top flanges to ¼ in. and was based on the engineering judgement and experience of a senior bridge designer (Memberg, 2002). Since the development of criteria for differential rotation limit is beyond the scope of this research endeavor, the design methods presented herein will be based on a rotation limit that has already been established and the assumption that no external diaphragms will be used.

For quasi-closed box-girders, the thickness of the equivalent plate representing the top-lateral bracing is the dominant factor controlling the torsional stiffness. In design, the bridge span, curvature, and cross-sectional dimensions will generally be established before the bracing system is designed. Thus, the primary property affecting the torsional stiffness is the pure torsion constant, K_T, which is almost directly proportional to the equivalent plate thickness representing the top-lateral bracing. Determination of the required equivalent plate thickness is obtained by substituting the plate dimensions of a quasi-closed trapezoidal box girder into Eqn. (2.5). Solving for the required equivalent plate thickness gives

$$\left(t_{eq}\right)_{req'd} = b_{eq}\left[\frac{4A_o^2}{K_T} - 2\frac{b_w}{t_w} - \frac{b_{bf}}{t_{bf}}\right]^{-1} \tag{7.10}$$

where K_T is the pure torsion constant desired, A_o is the enclosed area, and b and t are the respective width and thicknesses of the equivalent plate (*eq*), webs (*w*), and bottom flange (*bf*).

For truss systems, member sizes can be selected to obtain the required equivalent thickness in Eqn. (7.10). The equivalent thickness for a single-

diagonal truss configuration is defined by Eqn. (2.9). Formulations for other truss configurations are presented elsewhere (Heins, 1973).

7.4.2 Controlling Warping Stresses

Top-lateral bracing systems not only increase the torsional stiffness of the girder, but can also be used to control warping stresses. Since the determination of all the stresses in a curved box-girder bridge under torsion and bending is difficult, it is advantageous to determine when it is necessary to calculate both the pure and warping torsional stresses. A study by Heins (1978) was conducted on various curved box-girder geometries. Results indicated that for box-sections with width-to-depth ratios between 1 and 3, the ratio of the normal bending and warping normal stresses was less than 10% if the top-lateral equivalent plate thickness was greater than 0.050 in. Therefore, if this stiffness criterion is satisfied, it can free the designer from having to calculate secondary warping stresses.

7.4.3 Lateral Stability Requirements for Top Flanges

As discussed in Section 7.3.4, if the designer has elected to use the top-lateral system to stabilize the top flanges, then the bracing must provide the stiffness required in Section 7.2.

7.4.4 Design Brace Stiffness

Adequate design of top-lateral systems for stiffness should satisfy all of those criteria that the designer deems applicable. For example, a designer may elect to use external diaphragms to control differential rotations and use internal diaphragms to stabilize the top flanges. In this case, the stiffness requirement may only be based on satisfying the warping stress criterion. In cases where multiple criteria are applicable, the bracing design should satisfy the one with the greatest stiffness requirement.

7.5 DESIGN ISSUES FOR METAL-DECK SYSTEMS

7.5.1 Additional Load Effects

The controlling factor for the shear strength of metal deck diaphragms is the strength of the connection. For both screw and pin-driven fasteners, the connector strength is primarily controlled by bearing of the deck material against the fasteners and not the shear strength of the actual fasteners themselves. For metal deck used as top-lateral bracing, the forces generated at the connectors originate from three primary sources:

1) In-plane shear induced by torsion of the girder

2) Out-of-plane loads on the deck panels

3) Horizontal force components due to vertical loads on inclined webs.

Torsion of the girder induces shear flow in the quasi-closed cross section, effectively subjecting the deck panels to pure shear as illustrated in Figure 7.4b. The maximum shear that can be applied is controlled by the resultant force on the corner fasteners and is the basis for the proposed design shear strength equation listed in Chapter 6 (SDI Eqn. 2.2-5*). This shear strength equation, however, only accounts for fastener forces due to pure shear on the diaphragm. Consequently, connector forces induced by other load effects were investigated to determine their significance.

Metal-deck panels placed between girder flanges are fastened at both ends before casting of the concrete deck. The out-of-plane loads from the wet concrete introduce additional forces as a result of the end restraint as shown in Figure 7.9. The magnitude of these forces was investigated to establish their significance relative to typical connector strengths. A second-order analysis was conducted on a pin-pin beam element representing a portion of the deck width. A uniform load corresponding to an 8 in. thick slab at 150 lb/ft^3 was applied. Negligible section

area and moment of inertia were used to provide a conservative estimate. For the bridge deck used in bridge Connect K of the field studies, the deck span was 94 in. and the resulting horizontal fastener loads were 150 lbs. per fastener. This corresponded to approximately 5% of the connector strength associated with the 16-gauge deck and 8% for 20-gauge deck. The significance of these connector forces is minimal for two reasons. First, the forces are self-relieving through bearing deformations at the fasteners. Secondly, the experimental shear strength tests conducted on various bridge decks by Currah (1993) included an 80 psf. out-of-plane load, which simulated a 6 in. concrete slab. Since the resulting experimental shear strengths correlated well with the proposed SDI predictions, it is reasonable to neglect the effects of out-of-plane deck loads.

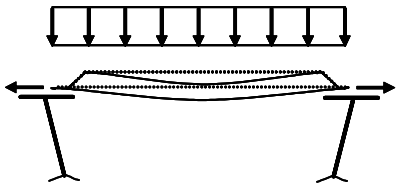

FIGURE 7.9 CONNECTOR FORCES DUE TO OUT-OF-PLANE DECK LOADS

For box girders with inclined webs, the vertical loads applied to the top flanges create outward horizontal force components as described in Section 7.3.3. Metal-deck bracing used to handle these forces have added connector force demands beyond those created by pure shear on the diaphragm panel. To place perspective on the magnitude of these forces relative to typical connector strengths, the lateral force component was calculated for bridge Connect K of the field studies. The twin-girder bridge had a typical 4:1 web slope (the maximum currently permitted by AASHTO), an 8 in. concrete slab, and a total roadway width of 30 ft. The force per fastener due to the horizontal force components was

approximately 100 lbs., less than 4% of the connector strength for the 16-gauge decking.

7.5.2 Modified Design Shear Strength

The metal-deck shear strength equation based on SDI Eqn. (2.2-5*) can be modified to account for additional connector forces caused by loadings other than pure shear on the diaphragm. The modified equation accounts for additional connector forces by reducing the connector strength, Q_f, and is given by

$$S_n = \left(Q_f - Q_2\right)\sqrt{\frac{1}{\left(\frac{L}{2A(\lambda-1)+B}\right)^2 + \frac{1}{N^2}}} \tag{7.11}$$

where Q_2 is the force per end connector caused by loads other than pure shear on the diaphragm. Eqn. (7.11) conservatively assumes Q_2 to act in the direction of the resultant force, Q_r, which greatly simplifies the modified formulations. Detailed discussion and derivation of Eqn. (7.11) can be found in Appendix B.

7.5.3 Factors Affecting Deck Strength and Stiffness

In order to better identify the applications and limitations of metal-deck bracing, it is helpful to examine the factors affecting and the limits of its strength and stiffness. The primary factors governing these properties are the gauge thickness of the base material and the fastener layout. Table 7.1 summarizes the effect of these parameters on the strength and stiffness of the decking used in the laboratory experiments. Strength values were calculated using the proposed SDI procedures outlined in Appendix B.

TABLE 7.1 EFFECT OF GAUGE THICKNESS AND FASTENER LAYOUT ON DECK SHEAR STRENGTH AND STIFFNESS

Case	Gauge	Fastener Spacing		S_n [kips/ft]	% Diff	G' [kips/in]	% Diff
		End	Stitch				
1	16	Every Valley	18 in.	1.58	--	124.8	--
2	16	Every Valley	none	0.72	-55%	118.6	-5%
3	16	Every Valley	6 in.	2.93	85%	127.3	2%
4	20	Every Valley	18 in.	0.97	-39%	53.2	-57%
5	14	Every Valley	18 in.	1.93	22%	191.8	54%
6	16	Every Other	18 in.	1.33	-16%	21.4	-83%
7	16	Every Valley (2@corners)	18 in.	2.31	46%	126.2	1%
8	16	Two Per Valley	18 in.	2.54	61%	126.6	1%

Case 1 represents the 16-gauge configuration used in the laboratory tests. It can be seen from cases 2 and 3 that the spacing of stitch fasteners between sheets has a dramatic effect on the shear strength, but very little effect on the stiffness. Similarly, increasing the number of end fasteners beyond a fully-fastened condition (1 in every valley) can produce significant increases in strength but does not appreciably affect the stiffness (cases 7 and 8). Reducing the number of end fasteners to one every other valley (case 6) results in a severe stiffness reductions with only a minor strength decreases. Changing the thickness of the gauge material generally affects the stiffness to a greater degree than strength (cases 4 and 5). Although significant increases in strength and stiffness can also be attained by using a thicker gauge, it is limited by what bridge deck manufacturers produce. Currently, 16-gauge is the thickest commonly available bridge deck produced by most manufacturers. In contrast, increasing the number of fasteners

is a fairly easy way to satisfy design requirements. These effects were observed in the experimental tests conducted by Currah (1993) and resulted in the following recommendations:

- At least one end fastener shall be placed in every valley
- Sidelap fastener spacing shall not exceed 18 in.

7.5.4 Combined Truss-Deck Configurations

Results from the field and laboratory test programs have indicated that when top-lateral truss and metal-deck systems are used in conjunction, the torsional stiffness of the system can be reasonably predicted using a combined equivalent top-plate thickness equal to the sum of the individual truss and deck equivalent thicknesses. Therefore, the shear stiffness of a combined system can be taken as the algebraic sum of the individual shear stiffnesses. This combined shear stiffness is then used to satisfy the bracing requirements outlined in Section 7.4.

The distribution of forces in a combined truss-deck bracing system during initial loading is proportional to the relative stiffness of each system. As the brace forces increase, the force in the metal-deck bracing will approach and exceed its shear strength. The ductile behavior of metal decking, which was observed in the laboratory tests and by others (Currah 1993; Luttrell, 1981) allows for force redistribution. This is generally true since the strength of truss systems tends to be much greater than the strength of metal-deck systems. Therefore, as long as the deck strength is less than that of the truss bracing, the ultimate strength of the combined system can be taken as the algebraic sum of the individual strengths.

7.5.5 Limitations & Design Recommendations

The laboratory test results have demonstrated that permanent metal deck forms can substantially increase the torsional stiffness of a trapezoidal box-girder. In comparison to truss systems, however, the relatively low shear strength of the

metal-decking limits its applicability as stand-alone bracing system in curved bridge applications where torsional loads produce large brace forces. For even moderately curved bridges, the shear forces induced by torsion can be considerably larger than the shear strength that a heavy-gauge metal-deck system can provide. For example, the 16-gauge deck configuration for case 3 in Table 7.1 has an factored shear strength of 2.07 kips/ft. This shear strength utilizes a fully-fastened configuration with closely spaced sidelap fasteners and is near the upper limit of what deck-systems can achieve. By comparision, the maximum torsional shear forces in a 150 ft. simply-supported single girder with a radius of curvature of 1000 ft and cross-sectional dimensions similar to the laboratory specimen due to only the dead weight of the steel is equal to 1.88 kips/ft. Additional loads due to a 15 ft. wide 8 in. concrete slab (not staged) would increase the maximum brace force to 4.08 kips/ft.

7.6 DESIGN EXAMPLES

Two numerical design examples were conducted to illustrate the design recommendations presented in this Chapter. The bracing design examples include the design of a top-lateral truss system for a curved girder and a metal-deck bracing system for a straight girder. Detailed calculations can be found in Appendix D.

The cross-sectional properties of the girders used in the design examples were those of the bridge connect that the laboratory test specimen was based on. The bridge under consideration was a 150 ft. single-span simply-supported twin box-girder bridge with a 30 ft. wide roadway and an 8 in. thick concrete deck.

The radius of curvature for the curved girder example was equal to 450 ft. In this example, the top-lateral brace forces were primarily due to torsion of the girder. Top-lateral forces from torsion, bending, and lateral stability requirements

respectively accounted for approximately 66%, 15%, and 19% of the total compressive design force. In the design example presented, the top-lateral truss bracing was specified to handle the forces associated with top-flange lateral stability. Internal diaphragms, which would likely be present for fabrication and to control cross-section distortion, could have been specified to handle these forces. The 20% decrease in the design compressive force, however, would have only changed the brace member selected by one size (WT10.5x46.5 vs. WT10.5x55.5).

An alternate brace geometry was considered to illustrate the increased brace force demands when fewer braces are used. Using only five diagonal braces versus nine increased the design compressive brace force by over 40%. This increase is caused by the inefficiency of a sharply inclined diagonal brace in handling the panel shears from torsion. In this case, the proportion of the top-lateral force due to torsion increased to over 85% of the design force.

A metal-deck bracing system was not feasible as a stand-alone system in the curved girder example due to the large torsional forces present. The largest design average shear force was equal to 16 kips/ft. By comparison, the strongest metal-deck configuration listed in Table 7.1 (case 3) had a factored strength of only 2.2 kips/ft., less than 15% of the design force.

For the straight-girder design, a metal-deck top-lateral bracing system alone was capable of providing adequate lateral bracing. Since metal-deck systems do not attract significant forces from bending, only the strength and stiffness requirements due to lateral-stability of the top flange governed. Additional strength and stiffness requirements from torsion due to unbalanced construction loads were not considered in the design example and should be investigated for their significance.

CHAPTER 8
SUMMARY AND CONCLUSIONS

The primary objectives of this research were to develop a design methodology for top-lateral bracing systems in steel box-girder bridge systems and evaluate alternative bracing methods such as permanent metal deck forms. This objective was achieved through a series of field and laboratory experiments.

8.1 FIELD EXPERIMENTS

The field experiments were conducted on a trapezoidal steel box-girder bridge during construction of a highway interchange. Loading was applied to the bare steel superstructure using a construction crane. Top-lateral brace forces were measured and were reasonably predicted by the finite-element model. Discrepancies between the experimental results and analytical predictions were associated with the distribution of the top-lateral forces of between the inner and outer bridge girders. This discrepancy was partially due to the modeling of the external diaphragms connecting the adjacent girders. Tests involving the use of permanent metal-deck forms as lateral bracing provided evidence to warrant further investigations in a laboratory setting.

8.2 LABORATORY EXPERIMENTS

The subsequent laboratory experiments were conducted on a 54 ft. long 54 in. deep straight trapezoidal steel box-girder specimen. Pure torsion and bending tests were conducted with various top-lateral bracing configurations. A variety of internal bracing configurations were tested using a traditional single-diagonal top-lateral truss, permanent metal-deck forms, and an internal K-diaphragm. Test

results indicated that the use of an internal K-diaphragm had no discernable influence on the torsional stiffness of the girder. The permanent metal-deck forms used as lateral bracing produced significant torsional stiffness increases, ranging between 8 and 12 times that of the unbraced girder. The magnitude of these increases was similar to those produced by the truss configurations used, which exhibited stiffness increases between 9 and 14 times. When truss and metal-deck systems were used in combination, the resulting girder behavior was commensurate with the superposition of the two bracing systems, producing stiffness increases between 18 and 24 times.

Comparisons between experimental and theoretical torsional stiffnesses were generally within 10% and differed by at the most by 23%. These discrepancies were largely due to the sensitivity of the torsional stiffness to end support movements and the associated displacement corrections that were made.

Brace forces measured in the top-lateral truss bracing under torsional loads were well predicted using existing methods that utilize the equivalent-plate approximation. Truss forces measured in combined truss and metal-deck configurations were proportional to the relative equivalent plate thickness of the two individual systems. Truss forces measured under bending loads were in moderate to fair agreement with expressions developed by Fan and Helwig (1999). These discrepancies, however, were due in part to the small magnitude of forces being measured in the bending tests.

Overall, the laboratory test results indicated that the use of the equivalent flat-plate approximation to model both the top-lateral truss and metal-deck bracing systems appears both valid and reasonable. For metal-deck systems, the equivalent plate thickness was determined using the effective shear stiffness predicted by the *Steel Deck Institute Diaphragm Design Manual*. In addition,

proposed shear strength formulations based on the SDI Manual correlated well with the response of the girder with metal-deck bracing.

8.3 BRACING DESIGN GUIDELINES

The bracing design guidelines presented in Chapter 7 were developed from the field and laboratory studies and are based on satisfying a dual strength and stiffness criteria. These requirements vary depending on the type of top-lateral system that is used, what other types of bracing are present, and whether the bridge is curved or straight. The strength requirements are based on brace forces that are generated from four primary sources. These sources include girder torsional moments, girder bending moments, vertical loads on inclined webs, and lateral buckling of the top flanges. Stiffness requirements are based on three criteria. These criteria include control of girder rotations, control of warping stresses, and lateral stability of the top flanges. The proposed design guidelines provide a systematic approach for establishing the individual factors contributing to the strength and stiffness requirements.

For truss bracing systems, brace forces caused by girder bending moments can be significant and in some instances, can be greater in magnitude than those caused by torsion. These bending induced forces increase with increasing member size and brace inclination. In addition, a shortening phenomenon associated with positive bending regions further increase brace force demands.

Metal-deck bracing, on the other hand, does not attract significant forces from bending and is not susceptible to the effects of shortening due to its "accordion-like" profile. Although metal-deck systems can substantially increase the torsional stiffness of a box-girder, the relatively low shear strength for even the most robust metal-deck systems limits its use as a stand-alone bracing system in curved bridge applications where torsion induced forces are high.

8.4 FUTURE RESEARCH

The design and behavior of trapezoidal steel box-girder bridge systems have several areas that require further investigation. Differential girder rotations between adjacent girders can create construction difficulties as well as rideability issues. Although efforts have been made to develop design guidelines for the use of external diaphragms to control these rotations, there exists no uniform criterion for acceptable differential rotations.

Direct attachment of metal-deck sheets to the top flanges provides the greatest potential stiffness for metal-deck bracing systems. Investigation of the use of shear studs fired directly through decking may provide an economical alternative to the use of powder actuated fasteners. Strength, fatigue, and quality control issues are some of the issues that still need to be addressed.

Recent research on the early stiffness of concrete by Topkaya (2002) has demonstrated that significant composite action develops at very early concrete ages. This early stiffness significantly affects the brace force demands during staged construction. Further research efforts are necessary to incorporate the benefits of early concrete stiffness and staged pouring into the proposed bracing design guidelines.

APPENDIX A
TEST SPECIMEN PROPERTIES

A.1 TORSIONAL PROPERTIES

A.1.1 Shear Center

The location of the shear center and the warping constant was determined using a finite difference approach presented by Heins (1975) and was derived for use with open sections. For pseudo-closed cross-sections, the shear center is nearly coincident with that of the open section. The cross-sectional dimensions used in the analysis utilize a simplified cross-section, shown in Figure A.1, in which the small area of the bottom flange outside of the webs was ignored. The endpoints of the flanges and intersection points where the webs and flanges meet correspond to the centerline of the flanges. The arrows next to each element define the element's orientation and flow direction, which should not be confused with the actual shear flow. These flow directions are used to maintain proper signs during calculations. The flow direction, which travels from points *i* to *j*, can be selected arbitrarily and does not necessarily correspond to the direction of shear flow. For convenience, a continuous flow loop A-B-C-D-E-F was chosen.

The coordinates of the shear center relative to the centroid of the cross-section are given by

$$x_o = \frac{I_{xy} I_{wx} - I_y I_{wy}}{I_{xy}^2 - I_x I_y} \tag{A.1}$$

$$y_o = \frac{I_x I_{wx} - I_{xy} I_{wy}}{I_{xy}^2 - I_x I_y} \tag{A.2}$$

where I_x and I_y are the moments of inertia, I_{xy} is the product of inertia and

$$I_{wx} = \frac{1}{3}\sum(w_i x_i + w_j x_j)t_{ij}L_{ij} + \frac{1}{6}\sum(w_i x_j + w_j x_i)t_{ij}L_{ij} \tag{A.3}$$

$$I_{wx} = \frac{1}{3}\sum(w_i y_i + w_j y_j)t_{ij}L_{ij} + \frac{1}{6}\sum(w_i y_j + w_j y_i)t_{ij}L_{ij} \tag{A.4}$$

For sections that have one axis of symmetry, I_{xy} is equal to zero. As a result, the the shear center coordinates for the trapezoidal section simplify to

$$x_o = 0 \tag{A.5}$$

$$y_o = -\frac{I_{wx}}{I_y} \tag{A.6}$$

Thus, the only values necessary to determine the shear center are I_{wx} and I_y. Table A.1 presents the finite difference solution using a tabular format. Columns (2) and (3) list the coordinates of each endpoint relative to the centroid of the cross section. Columns (4) and (5) list the thickness and length of each element, respectively. The moment of inertia about the y-axis can be calculated using

$$I_y = \frac{(x_i^2 + x_i x_j + x_j^2)t_{ij}L_{ij}}{3} \tag{A.7}$$

More common hand methods can be used to determine the moment of inertia, but the usage of the tabular format for the finite difference approach allows for easy implementation.

The value ρ_{ij} listed in column (7) refers to the perpendicular distance between the centroid of the cross-section and the long axis of each element. The sign of ρ_{ij} is defined as positive if the centroid resides on the left-hand side of the

element's flow vector. Therefore, elements A-B and E-F are the only two elements with negative ρ_{ij} values. The value for ρ_{ij} for each of the web elements is

$$\rho_{BC} = \rho_{DE} = \frac{4}{\sqrt{17}}\left(\frac{b_{bf}}{2} + \frac{y_{na}}{4}\right) \tag{A.8}$$

The w_{ij} within each element is computed as the product $\rho_{ij}\, w_{ij}$ and is listed in column (8). The value of the parameter w is given by

$$w_j = w_i + \rho_{ij} L_{ij} \tag{A.9}$$

where the direction of flow is from point i to j. The w values listed in column (9) were calculated by first assuming a reference point at A equal to zero. The value of w at point B was then determined based on the assumed value at A using Eqn. (A.9) and knowing the flow direction. The calculation is then repeated for subsequent points as indicated by the arrows in Table A.1. The calculation for point G requires subtraction of w_{GB} because of the defined flow direction. I_{wx} is then calculated from Eqn. (A.3) using the sum of columns (10) and (11). The y-coordinate for the shear center was then calculated using Eqn. (A.6) and was equal to –43.6 in. The negative sign indicates the shear center resides below the centroid at a distance of 24.4 in. below the bottom flange.

It should be noted that only the relative difference of the w values is important. Thus, the choice and value of the reference point can be arbitrary, though the choice of zero is most convenient. In addition, the w values are not affected by the choice of flow directions. Selecting an opposite flow direction reverses both the sign of ρ_{ij} as well as the positions of points i and j in Eqn. (A.6), yielding the same result for w.

A.1.2 Warping Constant

The warping constant, I_w, is determined using a similar tabular method and is summarized in Table A.2. The value ρ_o refers to the perpendicular distance between the shear center and the long axis of each element. The term w_o is calculated in the same manner as w in the shear center calculations and is given by

$$w_{o_j} = w_{o_i} + \rho_{o_{ij}} L_{ij} \tag{A.10}$$

The sign of ρ_o is similarly positive if the shear center resides on the left-hand side of the element's flow vector. In this case, elements A-B, C-D, and E-F have negative ρ_o values. The value of ρ_o for the webs is given by

$$\rho_{o_{BC}} = \rho_{o_{DE}} = \frac{4}{\sqrt{17}}\left(\frac{b_{bf}}{2} - \frac{y_{sc}}{4}\right) \tag{A.11}$$

The normalized warping at each point is listed in column (9) and is defined as

$$W_{n_i} = \frac{\sum (w_{o_i} + w_{o_j})\, t_{ij} L_{ij}}{2A} - w_{o_i} \tag{A.12}$$

where A is the total area of all the individual elements and is given by $A = \Sigma t_{ij} L_{ij}$. The sum of column (10) is used to calculate the warping constant, which is given by

$$I_w = \frac{\sum \left(W_{n_i}^2 + W_{n_i} W_{n_j} + W_{n_j}^2\right) t_{ij} L_{ij}}{3} \tag{A.13}$$

A.1.3 Sample calculations for shear center

$$I_y = \frac{1}{3}\sum (x_i^2 + x_i x_j + x_j^2) t_{ij} L_{ij} = \frac{300875}{3} = 100292 \text{ in}^4$$

$$w_B = w_G + \rho_{BG} L_{BG} \rightarrow w_G = -184 - (184) = -369 \text{ in}^2$$

$$I_{wx} = \frac{1}{3}\sum (w_i x_i + w_j x_j) t_{ij} L_{ij} + \frac{1}{6}\sum (w_i x_j + w_j x_i) t_{ij} L_{ij}$$

$$= \frac{10009829}{3} + \frac{5741294}{6} = 4293492 \text{ in}^5$$

$$y_o = -\frac{I_{wx}}{I_y} = -\frac{4293492}{100292} = -42.81 \text{ in}$$

$$y_{sc} = y_{na} + y_o = 18.74 - 42.81 = -24.07 \text{ in below bottom flange}$$

A.1.4 Sample calculations for warping properties

$$A = \sum t_{ij} L_{ij} = 118.5 \text{ in}^2$$

$$w_{o_F} = w_{o_E} + \rho_{o_{EF}} L_{EF} = 635 + (-405) = 230 \text{ in}^2$$

$$W_{n_B} = \frac{\sum \left(w_{o_i} + w_{o_j} \right) t_{ij} L_{ij}}{2A} - w_{o_B} = \frac{27312}{2(118.5)} - (-405) = 520 \text{ in}^4$$

$$I_w = \frac{\sum \left(W_{n_i}^2 + W_{n_i} W_{n_j} + W_{n_j}^2 \right) t_{ij} L_{ij}}{3} = \frac{61973906}{3} = 2.07 \times 10^7 \text{ in}^6$$

TABLE A.1 SHEAR CENTER PROPERTIES

(1)	(2)	(3)	(4)	(5)	(6)	(7)	(8)	(9)	(10)	(11)
Point	***X***	***Y***	t_{ij}	L_{ij}	$(x_i^2+x_ix_j+x_j^2)t_{ij}L_{ij}$	ρ_{ij}	$w_{ij}=\rho_{ij}\,L_{ij}$	***w***	$(w_ix_i+w_jx_j)\,t_{ij}L_{ij}$	$(w_ix_j+w_jx_j)\,t_{ij}L_{ij}$
A	-46.8	35.9						0		
			1	5	29402	-36.9	-184		38465	43072
B	-41.8	35.9						-184		
			0.375	56.7	78577	31.8	1803		-800198	-1327333
C	-28.0	-19.1						1619		
			1	56	43904	19.1	1072		1681255	-1681255
D	28.0	-19.1						2691		
			0.375	56.7	78577	31.8	1803		5591321	5064185
E	41.8	35.9						4495		
			1	5	29402	-36.9	-184		1945746	1950353
F	46.8	35.9						4310		
G	-36.8	35.9						-369		
			1	5	23140	36.9	184		106183	110789
B	-41.8	35.9						-184		
E	41.8	35.9						4495		
			1	5	23140	36.9	184		1797952	1802558
H	36.8	35.9						4679		
Sum					306143				10360724	5962370

TABLE A.2 WARPING PROPERTIES

(1) *Point*	(2) t_{ij}	(3) ρ_o	(4) L_{ij}	(5) $\rho_o L_{ij}$	(6) w_o	(7) $t_{ij}L_{ij}$	(8) $(w_{o_i} + w_{o_j})\, t_{ij} L_{ij}$	(9) W_n	(10) $\left(W_{n_i}^2 + W_{n_i} W_{n_j} + W_{n_j}^2\right) t_{ij} L_{ij}$
A					0			115	
	1	-80.9	5	-405		5.0	-2023		1717325
B					-405			520	
	0.375	21.2	56.7	1204		21.3	8391		8135267
C					799			-684	
	1	-24.4	56	-1368		56.0	12905		26211065
D					-569			684	
	0.375	21.2	56.7	1204		21.3	1407		8135267
E					635			-520	
	1	-80.9	5	-405		5.0	4328		1717325
F					230			-115	
G					-809			925	
	1	80.9	5	405		5.0	-6070		8028829
B					-405			520	
E					635			-520	
	1	80.9	5	405		5.0	8374		8028829
H					1040			-925	
Sum						118.5	27312		61973906

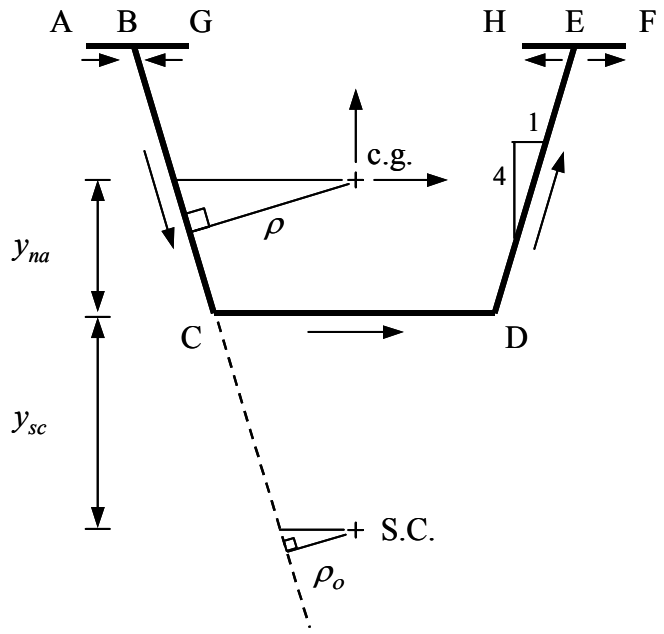

FIGURE A.1 SECTION GEOMETRY AND FLOW DIRECTIONS

A.2 TOP FLANGE IMPERFECTIONS

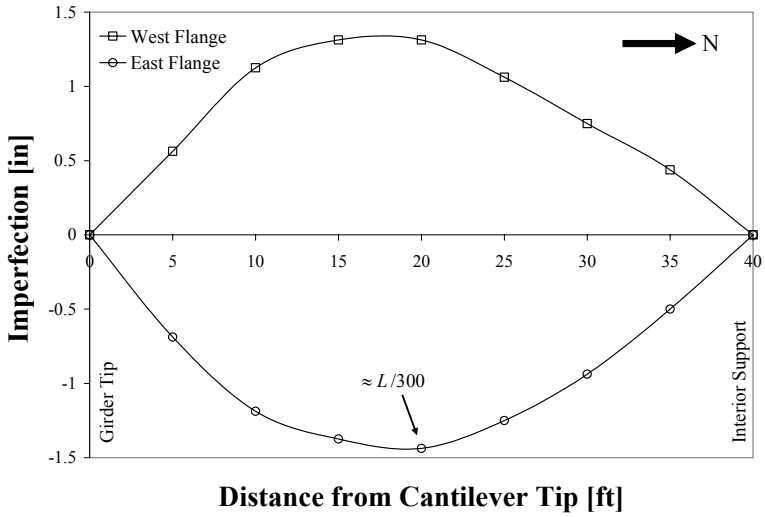

FIGURE A.2 INITIAL OUT-OF-STRAIGHTNESS OF TOP FLANGES

APPENDIX B
METAL DECK PROPERTIES

B.1 MEASURED CROSS-SECTIONAL DIMENSIONS OF DECKING

The bridge deck forms used in the field and laboratory tests had small stiffening ribs formed into each corrugation during the rolling process. The actual measured dimensions are shown in Figure B.1. These dimensions were identical for all material gauge thicknesses used in both the field and laboratory tests.

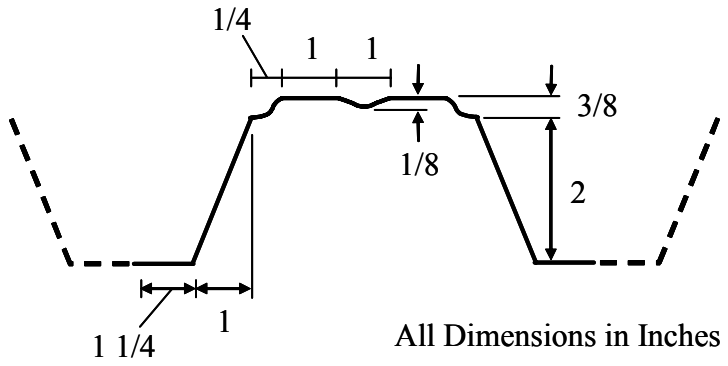

FIGURE B.1 MEASURED DIMENSIONS FOR ONE CORRUGATION

B.2 SHEAR STIFFNESS OF DECKING USING SDI MANUAL

The determination of the shear stiffness of permanent metal deck forms used as bracing in trapezoidal steel box-girder bridges is based on procedures from the *Steel Deck Institute Diaphragm Design Manual*. The shear stiffness obtained is used to determine the thickness of an equivalent flat steel plate.

B.2.1 Effective Shear Modulus

The effective shear stiffness, G', of a permanent metal deck form is defined by Eqn. (3.3-3) of the *Steel Deck Institute Diaphragm Design Manual 2nd Edition*.

$$G' = \frac{Et}{2.6\left(\frac{s}{d}\right) + \phi D_n + C} \qquad \text{(SDI Eqn. 3.3-3)}$$

where

E = Modulus of elasticity of steel = 29000 ksi

t = Base metal thickness of decking, in.

s = Flattened width of one rib, in.

d = Corrugation pitch, in.

ϕ = Reduction factor for multiple deck spans (1.0 for simple spans)

D_n = Warping constant

C = Connection slip parameter

B.2.2 Connector slip parameter

Eqn. (3.3-1) in the SDI Manual (2nd Edition) represents a simplified connector slip parameter. This simplified equation assumes that the number of intermediate edge connectors, n_e, equals the number of sidelap fasteners, n_s. For deck forms used as lateral bracing in box-girder bridges, there are no intermediate edge connectors. Consequently, the more exact equation for C, which appears on page 29 of the first edition of the SDI manual, is more appropriate (Currah, 1993).

$$C = \frac{2EtL}{a} S_f \left(\frac{n_{sh} - 1}{2\alpha_1 + n_p \alpha_2 + 2n_s \dfrac{S_f}{S_s}} + \frac{1}{2\alpha_1 + n_p \alpha_2 + n_e} \right) \qquad \text{(B.1)}$$

where

L = Overall diaphragm panel length, ft.

a = Overall diaphragm panel width, in.

n_{sh} = Number of individual deck sheets in panel width a

n_s = Number of sidelap fasteners in length L per sidelap

n_p = Number of purlins (zero for all tests)

n_e = Number of edge connectors (zero for all tests)

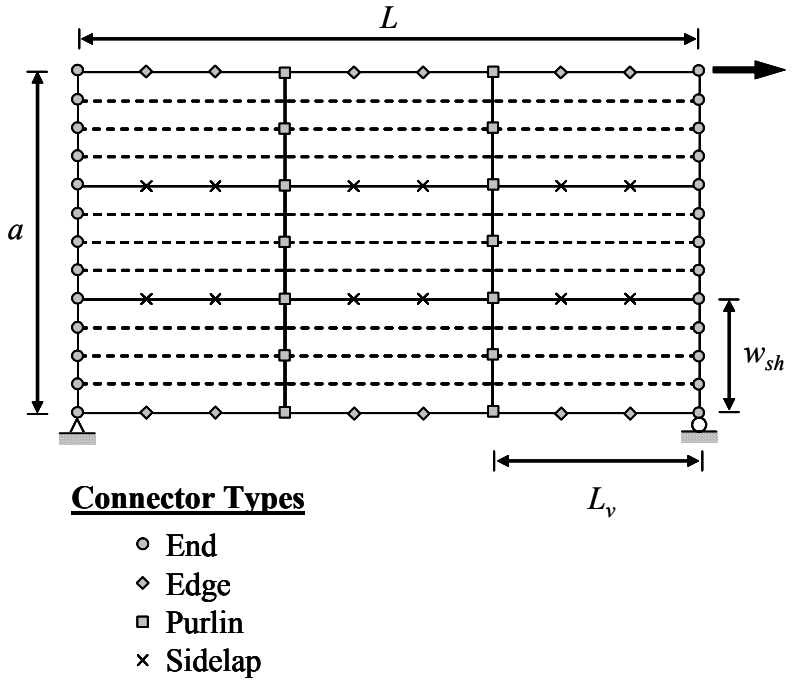

FIGURE B.2 SCHEMATIC LAYOUT FOR DIAPHRAGM

α_1 and α_2 are end distribution factors for the fasteners at the ends and interior purlins, respectively, (see Figure B.3) and are defined by

$$\alpha = \sum \frac{x_e}{w_{sh}} \tag{B.2}$$

where

x_e = Distance from the centerline of an individual deck sheet to each end fastener, in.

w_{sh} = Width of individual deck sheet, in.

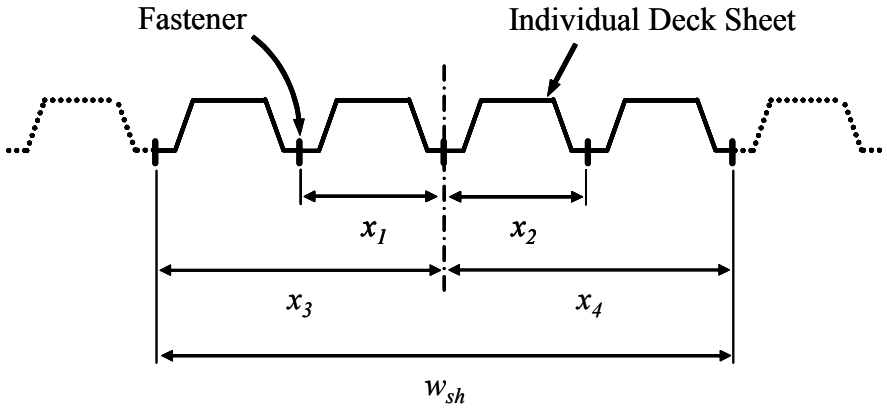

FIGURE B.3 DISTANCES FOR FASTENER DISTRIBUTION FACTOR

The structural connector flexibility, S_f, and sidelap connector flexibility, S_s, are defined in Section 4 of the 2nd edition of the SDI Manual. The structural connectors used in the laboratory tests were Hilti ENP2-21-L15 powder actuated fasteners and are defined by

$$S_f = \frac{1.25 \times 10^{-3}}{\sqrt{t}} \tag{SDI Eqn. 4.6-4}$$

The sidelap fasteners used in the laboratory tests were No. 14 Buildex TEKS screws are defined by

$$S_s = \frac{3 \times 10^{-3}}{\sqrt{t}} \qquad \text{(SDI Eqn. 4.5.1-2)}$$

For sidelap fasteners that are attached to heavier substrate material, as was in case for fasteners attached to the stiffening angles in test M20S, the connector flexibility is reduced and is defined by

$$S_s = \frac{1.3 \times 10^{-3}}{\sqrt{t}} \qquad \text{(SDI Eqn. 4.5.1-1)}$$

B.2.3 Warping Constant

The warping constant is defined as

$$D_n = \frac{D}{12L} \qquad \text{(SDI Eqn. 3.3-2)}$$

where the value of D is defined in Appendix IV of the 2nd edition of the SDI Manual. The D-value is dependent on the end fastener arrangement chosen. For deck bracing systems, it is recommended that fasteners be placed in every corrugation valley as dramatic increases in diaphragm stiffness can be achieved at relatively little expense (Currah, 1993). Therefore, equations for the fully-fastened configuration (fastener in each corrugation valley), designated *DW1*, will be reproduced. The symbols in the following equations refer to dimensions defined in Figure B.4 and are only applicable to the determination of the D-Value.

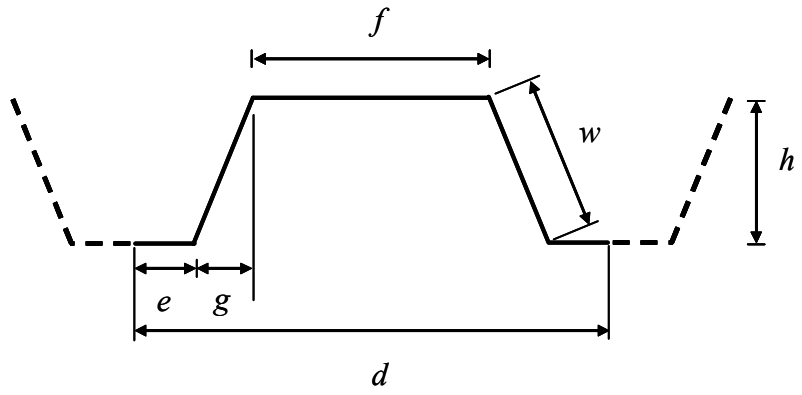

FIGURE B.4 PROFLIE DIMENSIONS FOR ONE CORRUGATION

D-Value Equations:

$$WT = 4f^2(f + w)$$

$$PW = \frac{1}{t^{1.5}}$$

$$V = 2(e + w) + f$$

$$D1 = \frac{1}{3}h^2(2w + 3f)$$

$$D2 = \frac{D1}{2}$$

$$D3 = \frac{1}{12}\frac{h^2}{d^2}\left[V\left(4e^2 - 2ef + f^2\right) + d^2\left(3f + 2w\right)\right]$$

$$C1 = \frac{1}{\left(D3 - \frac{D2}{2}\right)}$$

$$D4(1) = 24\frac{f}{C1}\left(\frac{C1}{WT}\right)^{0.25} = G4(1)$$

$$DW1 = G4(1)\left(\frac{f}{d}\right)PW$$

where *DW1* is the value used for the variable *D* in SDI Eqn. (3.3-2) and corresponds to a fully-fastened configuration.

B.2.4 Sample Calculation for Deck Shear Stiffness

For the 16-gauge metal deck used in the laboratory tests:

Deck Dimensions

t = 0.0598 in. $\quad h = 2.5$ in.

d = 8 in. $\quad f = 4$ in.

e = 1.25 in. $\quad w = \sqrt{h^2 + g^2} = 2.7$ in

g = 1.0 in. $\quad s = 2e + 2w + f = 11.9$ in

Connector Slip Parameter

L = 87 in. = 7.25 ft.

a = (15 sheets)(32 in/sheet) = 480 in.

n_{sh} = 15

n_s = 4

w_{sh} = 32 in.

n_p = 0

α_2 = 0

n_e = 0

t = 0.0598 in.

s = 11.9 in.

w_{sh} = 32 in.

$$S_f = \frac{1.25\times10^{-3}}{\sqrt{t}} = \frac{1.25\times10^{-3}}{\sqrt{0.0598}} = 0.0051$$

$$S_s = \frac{1.3\times10^{-3}}{\sqrt{t}} = \frac{1.3\times10^{-3}}{\sqrt{0.0598}} = 0.0053$$

$$C = \frac{2EtL}{a} S_f \left(\frac{n_{sh} - 1}{2\alpha_1 + n_p \alpha_2 + 2n_s \frac{S_f}{S_s}} + \frac{1}{2\alpha_1 + n_p \alpha_2 + n_e} \right)$$

$$= \frac{2(29000)(0.0598)(7.25)}{480} (0.0051) \left(\frac{15}{2(1.5) + 0 + 2(4) \frac{0.0051}{0.0053}} + \frac{1}{2(1.5) + 0 + 0} \right)$$

$$= 0.44$$

Warping Factor & D-Value

$$WT = 4(4)^2 (4 + 2.69) = 428$$

$$PW = \frac{1}{(0.0598)^{1.5}} = 68.4$$

$$V = 2(1.25 + 2.69) + 4 = 11.89$$

$$D1 = \frac{1}{3}(2.5)^2 \left[2(2.69) + 3(4) = 36.2 \right]$$

$$D2 = \frac{36.2}{2} = 18.1$$

$$D3 = \frac{1}{12} \frac{(2.5)^2}{(8)^2} \left\{ 11.89 \left[4(1.25)^2 - 2(1.25)(4) + (4)^2 \right] + (8)^2 \left[3(4) + 2(2.69) \right] \right\}$$

$$= 10.24$$

$$C1 = \frac{1}{\left(10.24 - \frac{18.1}{2} \right)} = 0.84$$

$$D4(1) = 24 \frac{4}{0.84} \left(\frac{0.84}{428} \right)^{0.25} = G4(1) = 24.0$$

$$DW1 = 24.0 \left(\frac{4}{8} \right) 68.4 = 819$$

$$D_n = \frac{819}{12(7.25)} = 9.4$$

Effective Shear Modulus

$$G' = \frac{(29000)(0.0598)}{2.6\left(\frac{11.9}{8}\right) + (1.0)(9.4) + 0.44} = 126.4 \text{ kips/in}$$

Equivalent Plate Thickness

$$\boxed{t_{eq} = \frac{126.4 \text{ kips/in.}}{11000 \text{ ksi}} = 0.01149 \text{ in.}}$$

TABLE B.1 EQUIVALENT PLATE THICKNESSES FOR METAL DECKING

Decking	t_{eq} [in]
16-Gauge Field Test	0.01168
20-Gauge Lab Test	0.00387
16-Gauge Lab Test	0.01149

B.3 SHEAR STRENGTH OF DECKING USING SDI MANUAL

The shear strength formulations presented herein are based on the strength formulations from the *Steel Deck Institute Diaphragm Design Manual, 2nd Edition*. These formulations are modified for the specific diaphragm arrangements of bridge deck form used in trapezoidal steel box-girder bridges. Detailed derivations of the original formulations can be found in the SDI Manual and are not derived herein. In the SDI Manual the variable S_u is used to describe the average shear strength of the decking. In this research report, S_u will be replaced with S_n, the nominal average shear strength of the decking, while S_u will refer to the required average shear strength as described in Chapter 7.

B.3.1 Shear Strength Equations

The shear strength of bridge deck diaphragms is controlled by failure at a corner fastener. This failure mechanism is "End Member" failure mechanism (mode 3) outlined in the SDI Manual and is pictured in Figure B.5.

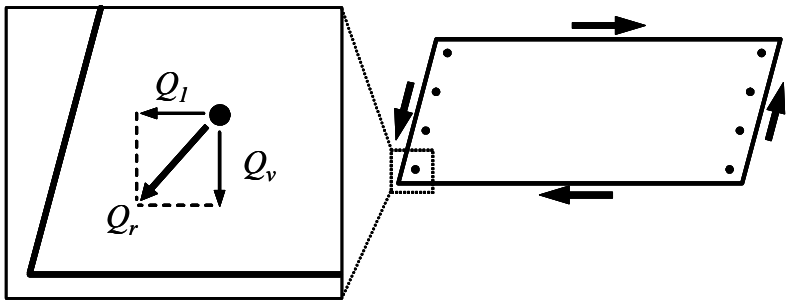

FIGURE B.5 RESULTANT FORCE AT CORNER FASTENER

Determination of the deck shear strength begins with setting the connector strength, Q_f, equal to the resultant corner force

$$Q_f = \sqrt{Q_1^2 + Q_v^2} \tag{B.3}$$

The force per fastener along the edge of a panel, Q_v, is given by

$$Q_V = \frac{S_n}{N} \tag{B.4}$$

where S_u is the average panel shear (kips/ft) and N is the number of end fasteners per ft. The value of the force component Q_1 is given by

$$Q_1 = \frac{S_n L}{2A(\lambda - 1) + B} \tag{B.5}$$

where

A = 2 for double-edge fasteners, 1 for single-edge fasteners

$$B = n_s \alpha_s + \frac{1}{w_{sh}^2}\left(2n_p \sum x_p^2 + 4\sum x_e^2\right)$$

$$\lambda = 1 - \frac{hL_v}{240\sqrt{t}}$$

$$\alpha_s = \frac{Q_s}{Q_f}$$

x_p = Same as x_e but at purlins (not applicable since no purlins used)

and L, α_1, α_2, n_s, n_p, n_e, x_e, and w_{sh}, have been previously defined in Section B.2 with the shear stiffness calculations. Substituting Eqns. (B.4) and (B.5) into Eqn. (B.3) yields

$$S_n = Q_f \sqrt{\frac{1}{\left(\frac{L}{2A(\lambda - 1) + B}\right)^2 + \frac{1}{N^2}}} \qquad \text{(SDI Eqn. 2.2-5*)}$$

where

Q_f = 61.1t(1-4t) for Hilti ENP2-21-L15 (SDI Eqn. 4.6-3)

Q_s = 28.4t for #14 screws

L_v = Purlin spacing = L for all cases

The expression for S_n in Eqn. (2.2-5*) is the expanded form of SDI Eqn. (2.2-5), which assumes the parameter $\lambda = 1$. The expanded form of this equation is more appropriate for determining the shear strength of steel bridge deck forms and only appears in the first edition of the SDI Manual (Currah, 1993).

The shear strength given by SDI Eqn. (2.2-5*) is based only on the connector forces induced by pure shear on the diaphragm. The shear strength formulation can be modified to account for additional connector forces by reducing the connector strength, Q_f. Connector forces from secondary sources, such as those described in Chapter 7, will generally act along the length of the panel (direction of Q_1) and will be additive to the shear induced force Q_1 at two corners. The modified shear strength equation is given by

$$S_n = \left(Q_f - Q_2\right)\sqrt{\frac{1}{\left(\frac{L}{2A(\lambda-1)+B}\right)^2 + \frac{1}{N^2}}} \qquad \text{(B.6)}$$

where Q_2 is the force per connector due to load effects other than pure shear on the diaphragm. Eqn. (B.6) conservatively assumes Q_2 to act in the direction of the resultant force. This assumption greatly simplifies the strength equation because accounting for the true direction Q_2 to acts results in a second-order non-linear equation for S_n. Accounting for the true direction of additional connector forces would have resulted in a second-order non-linear equation for S_n. Such accuracy is not warranted for the generally small magnitudes of Q_2 forces.

B.3.2 Sample Calculation for Deck Shear Strength

For the 16-gauge metal deck used in the laboratory tests:

For λ

$L = L_v = 87$ in. = 7.25 ft.

$h = 2.5$ in.

$t = 0.0598$ in.

$$\lambda = 1 - \frac{(2.5)(7.25)}{240\sqrt{0.0598}} = 0.69$$

For B

$Q_f = 61.1(0.0598)[1\text{-}4(0.0598)] = 2.78$ kips $\qquad n_s = 4$

$Q_s = 28.5(0.0598) = 1.7$ kips $\qquad n_p = 0$

$\alpha_s = \frac{1.7}{2.78} = 0.61$ $\qquad w_{sh} = 32$ in.

$$\sum x_e^2 = 2(8^2) + 2(16^2) = 640 \text{ in}^2$$

$$B = (4)(0.61) + \frac{1}{(32)^2}\left[0 + 4(640)\right] = 4.95$$

For S_u

$A = 1$ for single edge fastener

$$N = \frac{5 \text{ fasteners}}{32 \text{ in.}}\left(\frac{12 \text{ in.}}{\text{ft.}}\right) = 1.875 \text{ fasteners/ft.}$$

$$S_n = (2.78)\sqrt{\frac{1}{\left(\frac{7.25}{2(1)(0.69-1)+4.95}\right)^2 + \frac{1}{(1.875)^2}}} = 1.58 \text{ kips/ft.}$$

The unfactored shear strengths, S_n, for each metal deck test are given in Table B.2. The value of the resistance factor, ϕ, is equal to 0.75.

TABLE B.2 SDI METAL DECK SHEAR STRENGTHS [KIPS/FT]

Decking	S_n	ϕS_n
16-Gauge Field Test	0.85	0.64
20-Gauge Lab Test	0.97	0.73
16-Gauge Lab Test	1.58	1.19

APPENDIX C
ADDITIONAL TEST RESULTS

C.1 ADDITIONAL TORQUE-TWIST RESPONSES COMPARING END SUPPORT ADJUSTMENTS

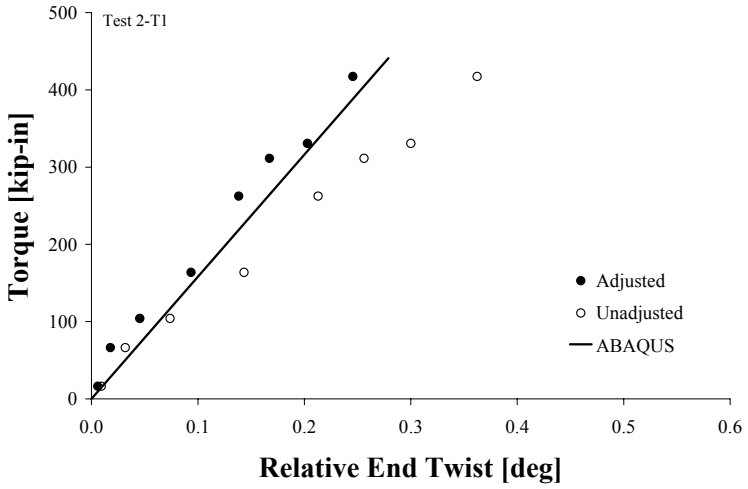

FIGURE C.1 TORQUE-TWIST RESPONSE FOR GIRDER WITH 2-DIAGONALS AT MAXIMUM TEST LOAD

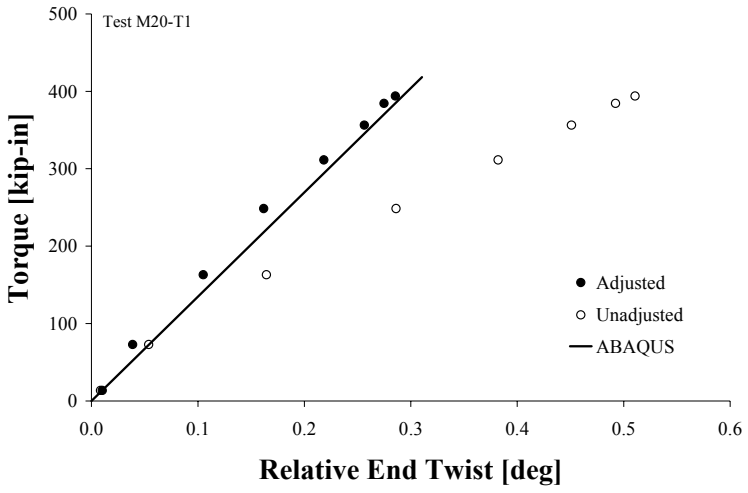

FIGURE C.2 TORQUE-TWIST RESPONSE FOR GIRDER WITH 20-GAUGE DECK AT MAXIMUM TEST LOAD

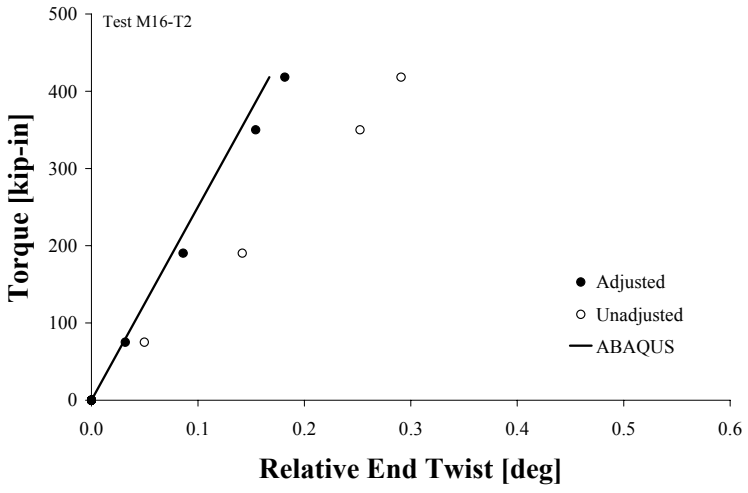

FIGURE C.3 TORQUE-TWIST RESPONSE FOR GIRDER WITH 16-GAUGE DECK AT MAXIMUM TEST LOAD

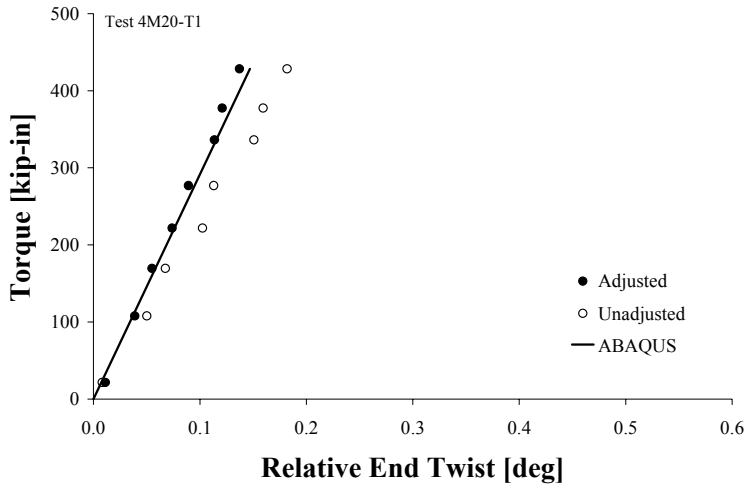

FIGURE C.4 TORQUE-TWIST RESPONSE FOR GIRDER WITH 4-DIAGONALS AND 20-GAUGE DECK AT MAXIMUM TEST LOAD

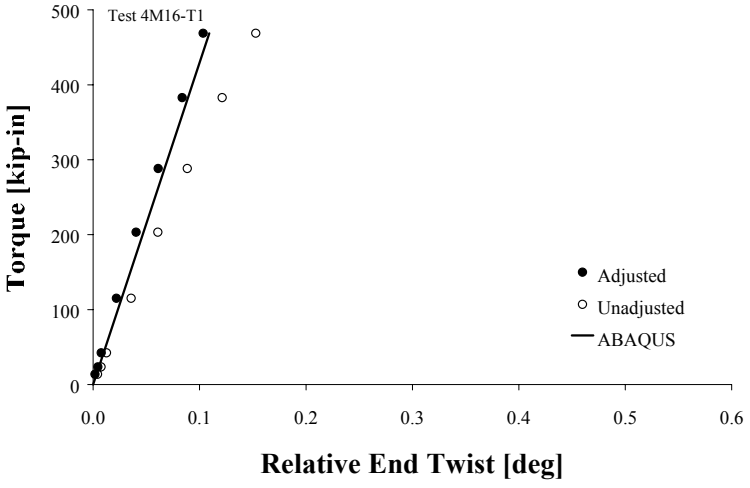

FIGURE C.5 TORQUE-TWIST RESPONSE FOR GIRDER WITH 4-DIAGONALS AND 16-GAUGE DECK AT MAXIMUM TEST LOAD

C.2 ADDITIONAL PLOTS OF ROTATION ALONG GIRDER LENGTH COMPARING END SUPPORT ADJUSTMENTS

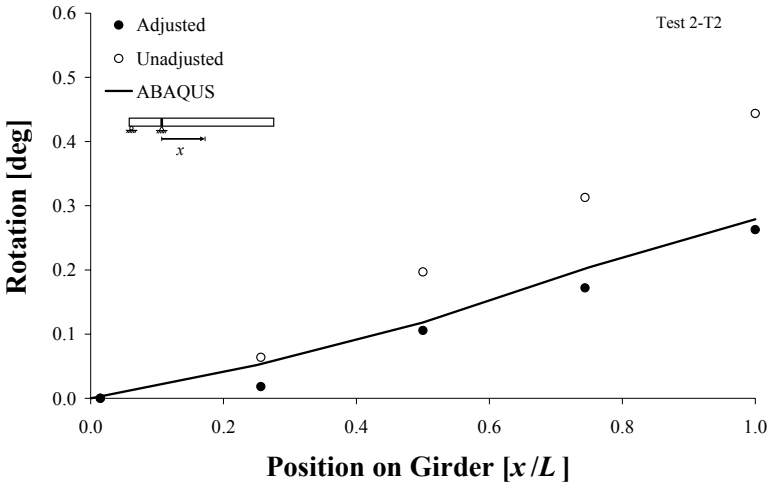

FIGURE C.6 ROTATIONS ALONG GIRDER LENGTH , 2-DIAGONALS AT MAXIMUM TEST LOAD

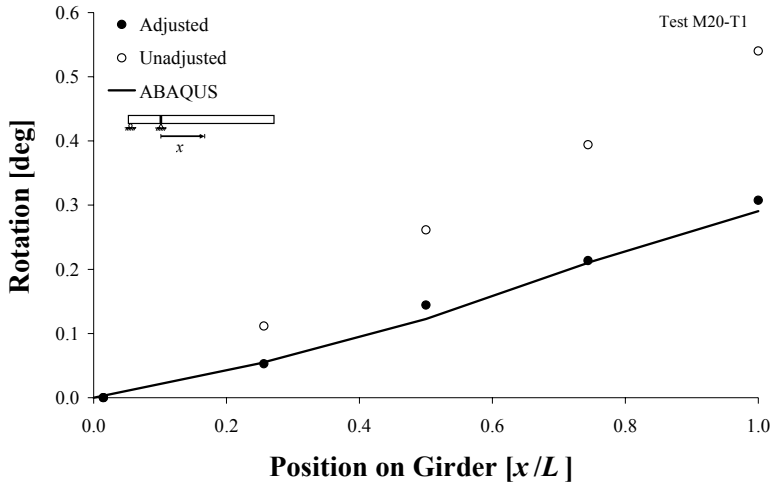

FIGURE C.7 ROTATIONS ALONG GIRDER LENGTH, 20-GAUGE DECK AT MAXIMUM TEST LOAD

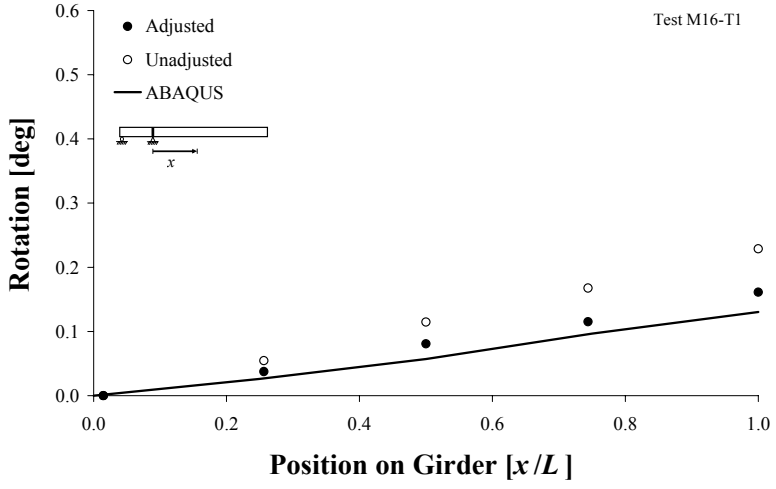

FIGURE C.8 ROTATIONS ALONG GIRDER LENGTH, 16-GAUGE DECK AT MAXIMUM TEST LOAD

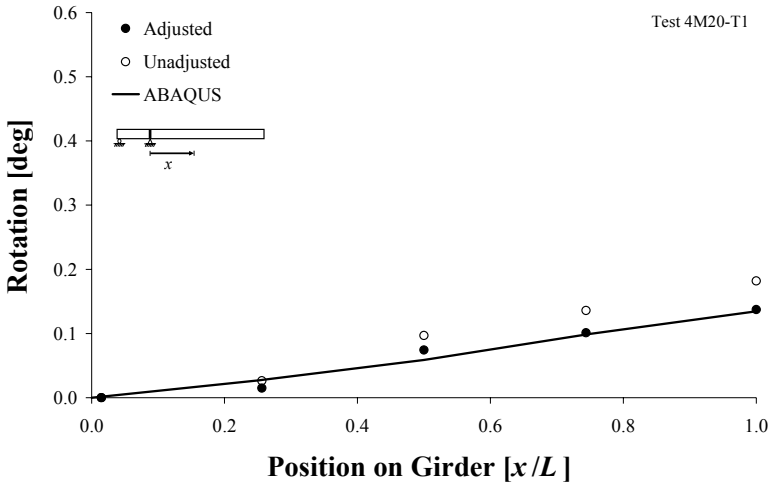

FIGURE C.9 ROTATIONS ALONG GIRDER LENGTH, 4- DIAGONALS WITH 20-GAUGE DECK AT MAXIMUM TEST LOAD

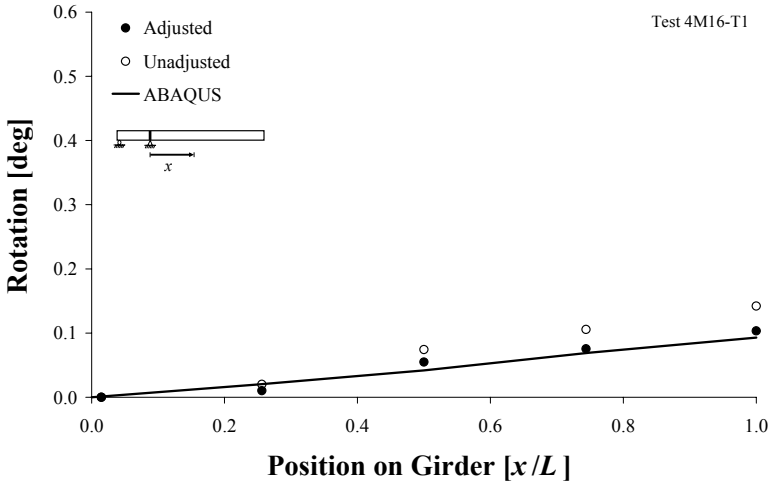

FIGURE C.10 ROTATIONS ALONG GIRDER LENGTH, 4- DIAGONALS WITH 16-GAUGE DECK AT MAXIMUM TEST LOAD

APPENDIX D
DESIGN EXAMPLES

The following design examples will illustrate the bracing design methodologies and requirements outlined in Chapter 7. The bracing design examples include design of a top-lateral truss system for a curved girder and a metal-deck bracing system for a straight girder.

D.1 CURVED GIRDER

D.1.1 Bridge Properties

Design a top-lateral truss bracing system for the single span simply-supported twin box-girder bridge. The concrete roadway is 30 ft. wide and 8 in. thick. The following design example will be based on the outer girder, which has an arc span of 150 ft. and a radius of curvature of 450 ft. The cross-sectional dimensions and properties of the girder are shown in Figure D.1.

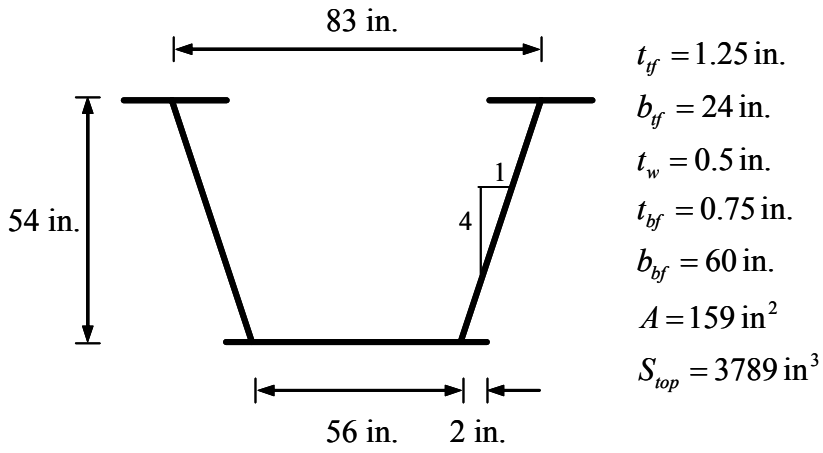

FIGURE D.1 CURVED GIRDER PROPERTIES

D.1.2 Loading

Steel Girder: (add 10% for wt. of all bracing)

$$(159\,\text{in}^2)(3.4\,\text{lb/ft/in}^2)(1.1)/1000 = 0.6\,\text{klf}$$

Concrete Slab: $$(15)\left(\frac{8}{12}\right)(0.150\,\text{kips/ft}^3) = 1.5\,\text{klf}$$

Use construction load factor = 1.3

$$M_{\max} = (1.3)\frac{(2.1\,\text{klf})(150\,\text{ft})^2}{8} = 7680\,\text{k - ft} = 92{,}160\,\text{k - in}$$

D.1.3 Trial Brace Spacing

Initial brace spacing will be based on an unbraced length which yields a lateral-torsional buckling moment greater than M_{max}. Determine buckling moment from AASHTO Eqn. (6.10.4.2.6a-1) and consider a half–girder model.

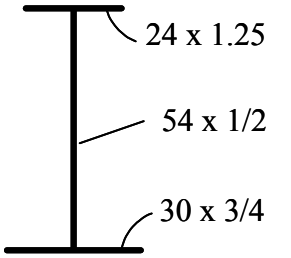

$$J = \frac{1}{3}\left[24(1.25)^3 + 54(0.5)^3 + 30(0.75)^3\right] = 22\,\text{in}^4$$

$$I_{yc} = \frac{1}{12}(1.25)(24)^3 = 1440\,\text{in}^4$$

FIGURE D.2 HALF-GIRDER PROPERTIES

Buckling load for trapezoidal girder is twice that of the half-girder.

$$2M_{cr} = 2\,\pi\,E\left(\frac{I_{yc}}{L_b}\right)\sqrt{0.772\frac{J}{I_{yc}} + 9.87\left(\frac{d}{L_b}\right)^2}$$

at L_b = 50 ft., $2M_{cr}$ = 11041 k-ft > M_y. Brace spacing not governed by LTB. Select trial spacing so brace angle, θ > 20 deg. Select 9 brace panels at a spacing

of s = 200 in., θ = 22.5 deg. Use a single-diagonal truss configuration with first brace panel oriented in tension. Brace members shall be WT sections with flange bolted to the bottom face of top flanges.

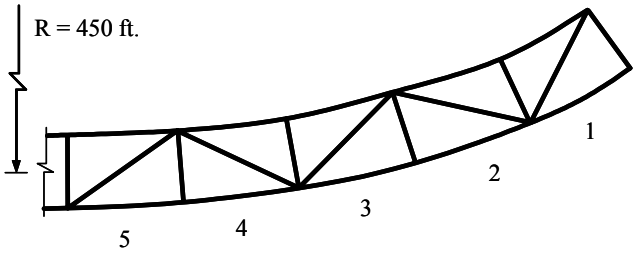

FIGURE D.3 SINGLE-DIAGONAL TRUSS BRACE LAYOUT

D.1.4 Strength Requirements

Table D.1 summarizes the girder torques, moments, and respective diagonal brace forces. The girder torques were determined using the M/R-method developed by Tung and Fountain (1970) at the center of each brace panel. Example calculations for the diagonal brace forces due to torsion and bending are given below.

TABLE D.1 SUMMARY OF GIRDER AND DIAGONAL BRACE FORCES

Panel	Position [ft]	T [k-ft]	M [k-ft]	D_{tor} [kips]	D_{bend} [kips]
1	8.33	836	1608	289	-23
2	25.00	725	4256	-251	-60
3	41.67	530	6147	184	-86
4	58.33	279	7282	-97	-102
5	75.00	0	7660	0	-108

The enclosed area, A_o should be calculated based on the centerline of the top-lateral bracing and other plate centerlines. Since bracing will be attached to the bottom of the top flange, assume enclosed height = 54 in.

$$A_o = (54)\left(\frac{83+60}{2}\right) = 3753\,\text{in}^2$$

Subsequent example calculations are for brace panel 2. Negative values indicates compression.

Brace force due to torsion is given by Eqn. (2.14)

$$D_{tor} = \frac{Td}{2A_o} = \frac{(-725)(12)(216.5)}{2(3753)} = -251\,\text{kips}$$

Brace forces due to bending are calculated from Eqn. (2.15) and requires initial brace sizes. Since larger brace areas result in larger design forces, select initial member sizes to produce conservative initial design force. Select diagonal and strut area equal to area of top flange.

$$A_d = A_s = A_f = 30\,\text{in}^2$$

$$K_1 = \frac{d}{A_d} + \frac{b^3}{A_s d^2} + \frac{s^3 b^2}{2b_f^3 t_f d^2} = \frac{216.5}{30} + \frac{83^2}{2(24)^3(1.25)(216.5)^2} = 41.6\,\text{in}^{-1}$$

$$f_{xtop} = \frac{M}{S_{top}} = \frac{(4265)(12)}{3789} = 13.5\,\text{ksi}$$

$$D_{bend} = \frac{(13.5)(200)^2}{(41.6)(216.5)} = -60\,\text{kips}$$

Brace force due to lateral stability requirements from Eqn. (7.2). For no reverse curvature bending C_d = 1.0. Assume actual flange out-of-straightness is less than 0.002, use 0.002. Find force amplification due to shortening.

$$\frac{\Delta_h}{s} = \frac{M_u}{ES_{top}} \frac{s}{b_{top}} = \frac{(7680)(12)}{(29{,}000)(3789)} \frac{(200)}{(83)} = 0.002$$

$$C_s = \frac{0.002 + 0.002}{0.002} = 2.0$$

$$F_{br} = 0.008 \frac{M_u C_d C_s}{h_o} = 0.008 \frac{(7680)(12)(1.0)(2.0)}{54} = 27.3 \text{ kips}$$

Resolve horizontal brace force into diagonal

$$D_{LTB} = F_{br} \left(\frac{d}{b_{top}} \right) = 27.3 \left(\frac{200}{83} \right) = 71 \text{ kips}$$

Diagonal brace forces for lateral stability will increase magnitude of largest tension and compression forces. Design brace forces are

$$P_u = D_{tor} + D_{bend} \pm D_{LTB}$$
$$= -251 - 60 - 71 = -382 \text{ kips (compression)}$$
$$= +289 - 23 + 71 = 338 \text{ kips (tension)}$$

Design for compression as beam-column using AISC LRFD (2001).

$$L_b = 216.5 \text{ in.} \approx 18 \text{ ft.}$$
$$\text{k} = 1.0$$
$$P_u = 382 \text{ kips}$$

Beam-column interaction for WT's (AISC H1-1a)

$$\frac{P_u}{\phi P_n} + \frac{8}{9} \left(\frac{M_u}{\phi M_n} \right) \leq 1.0 \text{ for } P_u \geq 0.2 \phi P_n$$

Select initial size using column tables. Try WT10.5x55.5

$$\phi P_n = 453 \text{ kips}$$

$$A = 16.3 \text{ in}^2$$

$$y = 2.23 \text{ in.}$$

$$e = 2.23 + \frac{1.25}{2} = 2.86 \text{ in.}$$

$d = 10.76 \text{ in.}$

$I_y = 137 \text{ in}^4$

$J = 3.4 \text{ in}^4$

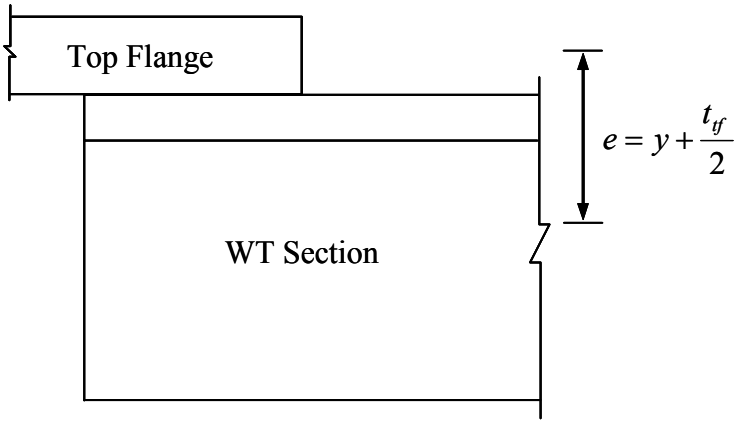

FIGURE D.4 ECCENTRICITY AT BRACE CONNECTION

(AISC F1-15)

$$B = +2.3\frac{d}{L_b}\sqrt{\frac{I_y}{J}} = 2.3\frac{10.76}{216.5}\sqrt{\frac{137}{3.4}} = 0.726$$

$$\phi M_n = \phi\frac{\pi\sqrt{EI_y GJ}}{L_b}\left[B + \sqrt{1+B^2}\right]$$

$$= (0.9)\frac{\pi\sqrt{(29{,}000)(137)(11{,}000)(3.4)}}{216.5}\left[0.726 + \sqrt{1+(0.726)^2}\right]$$

$$= 9867 \text{ k - in}$$

Check interaction Eqn.

$$\frac{382}{453} + \frac{8}{9}\left(\frac{(382)(2.86)}{9867}\right) = 0.94 \le 1.0 \quad \text{OK}$$

Therefore, WT10.5x55.5 satisfies compression strength limit state. Tension limit states should also be checked, but are not done in this example.

D.1.5 Stiffness Requirements

Find equivalent plate thickness of top-lateral truss

$$t_{eq} = \frac{E}{G}\frac{sw}{\frac{d^3}{A_d} + \frac{2}{3}\frac{s^3}{A_f}} = \frac{29{,}000}{11{,}000}\frac{(200)(83)}{\frac{(216.5)^3}{19.4} + \frac{2}{3}\frac{(200)^3}{30}} = 0.049 \approx 0.05 \text{ in.}$$

Bracing satisfies warping stiffness criterion. Therefore, secondary warping stresses should be less than 10% of bending normal stresses and need not be calculated explicitly.

For lateral stability requirements:

$$\beta_{lat} = \frac{4M_u C_d}{\phi L_b h_o} = \frac{4(7680)(12)(1.0)}{(0.75)(200)(54)} = 45.5 \text{ kips/in}$$

$$\beta_{\text{brace}} = \frac{AE}{L}\cos^2\theta = \frac{(19.4)(29{,}000)}{(216.5)}\left(\frac{83}{216.5}\right)^2 = 199 > 45.5 \text{ kips/in}$$

Note: the brace stiffness requirement, β_{lat}, could have been reduced by using the unbraced length, L_b, corresponding to reaching M_{max} (50 ft.). Larger brace stiffness is required when the actual unbraced length is used because the requirement is based on buckling between the actual brace points, which corresponds to a moment far greater than M_{max}. In this case, the required stiffness is easily satisfied by the brace area provided from the strength design criteria.

For girder rotation criteria assume differential girder displacement of 0.25 in. is required. The following calculations are based on the design method developed by Memberg (2002).

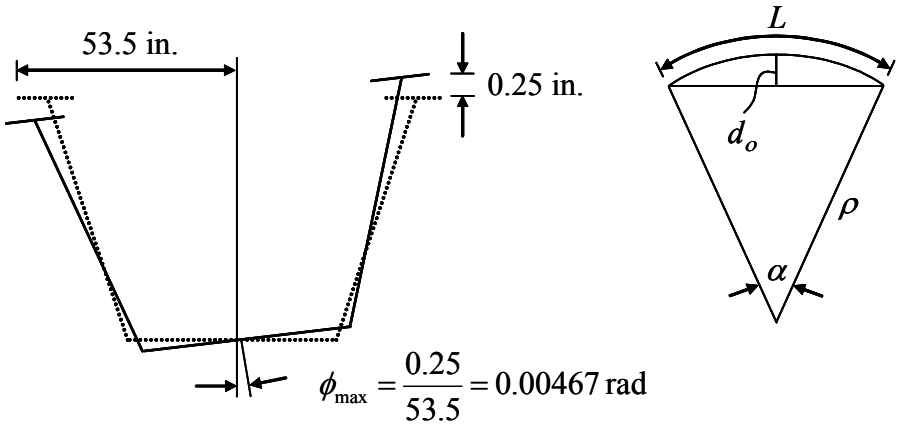

FIGURE D.5 GIRDER TWIST AND PLAN VIEW OF SECTOR

For a parabolic torque distribution

$$\phi(x) = \frac{wd_o x}{2GJ}\left[\frac{2x^3}{L^2} - \frac{8x^2}{3L} + L\right]$$

$$J = \frac{4A_o^2}{\sum \frac{b}{t}} = \frac{4(3753)^2}{2\frac{54}{0.5} + \frac{60}{0.75} + \frac{83}{0.049}} = 28313 \text{ in}^4 = 1.37 \text{ ft}^4$$

$$d_o = \rho\left[1 - \sin\left(90 - \frac{\alpha}{2}\right)\right] = (450 \text{ ft.})\left[1 - \sin\left(90 - \frac{150}{2(450)}\frac{180}{\pi}\right)\right] = 6.24 \text{ ft.}$$

$$\phi_{\max} = \phi\left(\frac{L}{2}\right) = \frac{7wd_o L^2}{72GJ} = \frac{7(2.72)(6.24)(150)^2}{72(11{,}000)(12)^2(1.37)} = 0.017 \text{ rad} > 0.00467 \text{ rad}$$

If no external diaphragms are used, the required top-lateral diagonal brace area would be 100 in^2, which is not practical. Therefore, use external diaphragms and find required spacing:

$$\phi(x) = \frac{wd_o x}{2GJ}\left[\frac{2x^3}{L^2} - \frac{8x^2}{3L} + L\right]$$

$$0.00467 \text{ rad} = \frac{7(2.72)(6.24)L^2}{72(11{,}000)(12)^2(1.37)}$$

$$L = 79 \text{ ft.} \rightarrow \text{use 1 external diaphragm at midspan}$$

D.1.6 Alternate Top-Lateral Brace Spacing

To illustrate the effect of using large top-lateral brace spacings, or acute brace angles, select 5 brace panels instead of 9. New panel spacing, s = 360 in., θ = 13 deg. The corresponding girder and diagonal forces change to

TABLE D.2 SUMMARY OF GIRDER AND DIAGONAL BRACE FORCES

Panel	Position [ft]	T [k-ft]	M [k-ft]	D_{tor} [kips]	D_{bend} [kips]
1	15.0	803	2758	475	-38
2	45.0	483	6435	-286	-89
3	75.0	0	7660	0	-106

$C_s = 2.8$ $\qquad$ $P_u = -545$ kips (comp)

$D_{LTB} = 171$ kips $\qquad$ $= 608$ kips (tension)

Thus, acute brace angle significantly increases the design brace forces while also increasing the unbraced length of the compression member.

Try WT 13.5x89, ϕP_n = 579 kips.

$A = 26.1\,\text{in}^2$

$y = 3.05$ in.

$e = 3.05 + \dfrac{1.25}{2} = 3.675$ in.

$d = 13.9$ in.

$I_y = 278\,\text{in}^4$

$J = 9.74\,\text{in}^4$

$$B = 2.3\frac{13.9}{370}\sqrt{\frac{278}{9.74}} = 0.462$$

$$\phi M_n = (0.9)\frac{\pi\sqrt{(29{,}000)(278)(11{,}000)(9.74)}}{370}\left[0.462 + \sqrt{1 + (0.462)^2}\right]$$

$$= 11{,}104 \text{ k - in}$$

Check interaction Eqn.

$$\frac{545}{579} + \frac{8}{9}\left(\frac{(545)(3.675)}{11{,}104}\right) = 1.1 \geq 1.0 \quad \text{NOT OK}$$

Try WT 15x105, ϕP_n = 745 kips.

$A = 31.0 \text{ in}^2$ actual area > assumed 30, change in P_u is negligible

$y = 3.40$ in.

$$e = 3.4 + \frac{1.25}{2} = 4.025 \text{ in.}$$

$d = 15.47$ in.

$I_y = 378 \text{ in}^4$

$J = 13.9 \text{ in}^4$

$$B = 2.3\frac{15.5}{370}\sqrt{\frac{378}{13.9}} = 0.50$$

$$\phi M_n = (0.9)\frac{\pi\sqrt{(29{,}000)(278)(11{,}000)(9.74)}}{370}\left[0.50 + \sqrt{1 + (0.50)^2}\right]$$

$$= 16{,}064 \text{ k - in}$$

Check interaction Eqn.

$$\frac{545}{745} + \frac{8}{9}\left(\frac{(545)(3.675)}{16{,}064}\right) = 0.85 \leq 1.0 \quad \text{OK}$$

For stiffness criteria

$$\beta_{lat} = \frac{4M_u C_d}{\phi L_b h_o} = \frac{4(7680)(12)(1.0)}{(0.75)(360)(54)} = 25.3 \text{ kips/in}$$

$$\beta_{\text{brace}} = \frac{AE}{L}\cos^2\theta = \frac{(19.4)(29{,}000)}{(369.4)}\left(\frac{83}{369.4}\right)^2 = 76.9 > 25.3 \text{ kips/in}$$

For warping stress criteria, t_{eq} = 0.03 in. To attain an equivalent thickness = 0.05 in. would require a diagonal brace area equal to 89 in^2. Thus, acute brace angles limit effectiveness lateral stiffness of diagonal and consequently increases forces from bending significantly. This is evidenced by the need for a WT15x105 vs. a WT10.5x55.5.

D.2 STRAIGHT GIRDER

Consider a straight girder with the same span, loading, and cross-sectional properties as the curved-girder example given in Section D.1. Design a top-lateral bracing system using metal deck only.

D.2.1 Stiffness Requirements

For the straight girder the only stiffness requirement comes from lateral stability of the top flanges. For single curvature $C_d = 1.0$.

$$h_o = 54 + \frac{0.75 + 1.25}{2} = 55 \text{ in.}$$

$$G'_u = \frac{4M_u C_d}{\phi\, b\, h_o} = \frac{4(7680)(12)(1.0)}{0.75(83)(55)} = 107.7 \text{ kips/in}$$

D.2.2 Strength Requirements

For lateral stability, metal-deck is not affected by shortening. Assume top flange out-of-straightness = 0.002. $C_s = 1.0$.

$$S_u = \frac{0.008 M_u C_d C_s}{b h_o} = \frac{0.008(7680)(12)(1.0)(1.0)}{(83)(55)} = 0.16 \text{ kips/in} = 1.9 \text{ kips/ft}$$

Initial selection of deck gauge and fastener layout can be made by referring to Table 7.1. Note, the shear strengths and stiffnesses are unfactored. For strength, the resistance factor of 0.75 is applied to the S_n values. The resistance factor for the stiffness, G', is present in the required stiffness formulation for G'_u. Using 16-gauge deck, end fasteners at every valley, and stitch fasteners at 6 in. spacing gives $\phi S_n = 2.2$ kips/ft and $G' = 127.3$ kips/in (case 3).

Check deck strength reduction due to horizontal force components from inclined webs. Calculate deck strength using Eqn. (7.11). Determine additional force per connector Q_2. Horizontal force component due to concrete load per unit length:

$$F_{lat} = \frac{2.1\,\text{k/ft}}{2}\left(\frac{1}{4}\right) = 0.26\,\text{k/ft}$$

$$N = \frac{5\,\text{fasteners}}{32\,\text{in.}}\left(\frac{12\,\text{in.}}{\text{ft.}}\right) = 1.875\,\text{fasteners/ft}$$

$$Q_2 = \frac{0.26\,\text{k/ft}}{1.875\,\text{fasteners/ft}} = 0.14\,\text{k/fastener}$$

Referring to calculations in Appendix B.3.2, all calculations are identical except those that depend on stitch fastener spacing. Using a spacing of 6 in. corresponds to $n_s = 13$.

$$n_s = 13$$

$$spacing = \frac{87\,\text{in.}}{n_s + 1} = 6.2 \approx 6\,\text{in.}$$

$$B = (13)(0.61) + \frac{1}{(32)^2}\left[0 + 4(640)\right] = 10.43$$

The modified design shear strength

$$\phi S_n = \phi\left(Q_f - Q_2\right)\sqrt{\frac{1}{\left(\frac{L}{2A(\lambda - 1) + B}\right)^2 + \frac{1}{N^2}}}$$

$$= (0.75)(2.78 - 0.14)\sqrt{\frac{1}{\left(\frac{7.25}{2(1)(0.69 - 1) + 10.43}\right)^2 + \frac{1}{(1.875)^2}}}$$

$$= 2.07\,\text{kips/ft.} \geq 1.9\,\text{kips/ft.} \qquad \text{OK}$$

Additional strength and stiffness requirements associated with torsion from unbalanced construction loads are not considered in this design example, but should be investigated.

REFERENCES

1. American Association of State Highway and Transportation Officials. (1998). *AASHTO LRFD Bridge Design Specifications*—2nd Edition, Washington, D.C.

2. American Institute of Steel Construction. (2001). *Load and Resistance Factor Design Specification for Steel Buildings*, Chicago, Illinois, December.

3. Basler, K. and Kollbrunner, C. F. (1969). *Torsion in Structures*. Springer-Verlag, Berlin, Germany.

4. Blank, D. (1973). "Stiffening Effects of Cold Formed Decks on Box Beam Bridges." Masters Thesis, University of Maryland, June, 170 pp.

5. Branco, F. A. and Green, R. (1984). "Bracing in Completed Box Girder Bridges." *Canadian Journal of Structural Engineering*, Vol. 11, No. 4, December, pp. 967-977.

6. Chen, B. S. (1999). "Top-Flange Lateral Bracing of Steel U-Shaped Girders." Masters Thesis, University of Texas at Austin, May, 106 pp.

7. Cheplak, B. A. (2001). "Field Measurements of Intermediate External Diaphragms on a Trapezoidal Steel Box Girder Bridge." Masters Thesis, University of Texas at Austin, May, 117 pp.

8. Currah, R. M. (1993). "Shear Strength and Shear Stiffness of Permanent Steel Bridge Deck Forms," Masters Thesis, University of Texas at Austin, August, 100 pp.

9. Dabrowski, Ryszard. (1968). *Curved Thin-Walled Girders*. Springer-Verlag, New York, 158 pp.

10. Ellingwood, B. E., MacGregor, J. G., Galambos, T. V., and Cornell, C. A. (1982). "Probability-Based Load Criteria: Assessment of Current Design Practice," *Journal of the Structural Division*, American Society of Civil Engineers, Vol. 108, No. ST5, May, pp. 978-997.

11. Fan, Z. and Helwig, T. A. (1999). "Behavior of Steel Box Girders with Top Flange Bracing." *Journal of Structural Engineering*, American Society of Civil Engineers, Vol. 125, No. 8, August, pp. 829-837.

12. *Guide Specifications for Horizontally Curved Highway Bridges*, American Association of State Highway and Transportation Officials, 1993.

13. Heins, C. P. (1975). *Bending and Torsional Design in Structural Members.* Lexington Books, Lexington, MA, 367 pp.

14. Heins, C. P. (1978). "Box Girder Bridge Design—State of the Art." *Engineering Journal*, American Institute of Steel Construction, Vol. 15, No. 4, Fourth Quarter, pp. 126-142

15. Heins, C. P. and Blank, D. (1973). "Box Beam Stiffening Using Cold Formed Decks." *Second Specialty Conference on Cold-Formed Steel Structures*, Oct 22-24, St Louis, MO, pp. 537-571.

16. Helwig, T. A. (1994). "Lateral Bracing of Bridge Girders by Metal Deck Forms," PhD Dissertation, University of Texas at Austin, August, 317 pp.

17. Jetann, C. A., Helwig, T. A., and Lowery, R. (2002). "Lateral Bracing of Bridge Girders by Permanent Metal Deck Forms. *Proceedings of the Structural Stability Research Council Annual Stability Conference*, Seattle, WA, April 24-27, pp. 291-310

18. Luttrell, L. D. (1981). *Steel Deck Institute Diaphragm Design Manual*, First Edition, St Louis, Missouri.

19. Luttrell, L. D. and Huang, H. T. (1981). *Steel Deck Diaphragm Studies*, Steel Deck Institute, St Louis, Missouri.

20. Luttrell, L. D. (1987). *Steel Deck Institute Diaphragm Design Manual*, Second Edition, Canton, Ohio.

21. MacDonald, R. E., Chen, Y., Yilmaz, C., Yen, B. T. (1976). "Open Steel Box Sections with Top Lateral Bracing." *Journal of the Structural Division*, American Society of Civil Engineers, Vol. 102, No. ST1, January, pp. 35-49.

22. Memberg, M. A. (2002). "A Design Procedure for Intermediate External Diaphragms on Curved Steel Trapezoidal Box Girder Bridges," Masters Thesis, University of Texas at Austin, August, 150 pp.

23. Ravindra, M. K. and Galambos, T. V. (1978). "Load and Resistance Factor Design for Steel," *Journal of the Structural Division*, American Society of Civil Engineers, Vol. 104, No. ST9, September, pp. 1337-1353.

24. Soderberg, E. G. (1994). "Strength and Stiffness of Stay-in-Place Metal Deck Form Systems," Masters Thesis, University of Texas at Austin, December, 159 pp.

25. Topkaya, C. (2002). "Behavior of Curved Steel Trapezoidal Box-Girders During Construction." PhD Dissertation, University of Texas at Austin, August, 108 pp.

26. Tung D. H. and Fountain, R. S. (1970) "Approximate Torsional Analysis of Curved Box Girders by the M/R-Method." *Engineering Journal*, American Institute of Steel Construction, Vol. 7, No. 3, July, pp. 65-74.

27. Winter, G. (1960). "Lateral Bracing of Columns and Beams," *Transactions,* American Society of Civil Engineers, Vol. 125, Part 1, pp. 809-825.

28. Yura, J. A. (1995). "Bracing for Stability—State-of-the-Art," *Proc. Struct. Congr. XIII*, ASCE, Boston, MA, Apr., pp. 88-103.

VITA

Brian Scott Chen was born in Bethlehem, Pennsylvania to Wai-Fah and Lily Chen in October of 1975. After graduating from West Lafayette High School in June of 1993, he entered Purdue University that same fall. In May of 1997, he received his Bachelor of Science degree in Civil Engineering with highest distinction.

In August of 1997, he enrolled in the graduate program in civil engineering at The University of Texas at Austin. He received his Master of Science degree in May of 1999 and continued his studies, obtaining his Doctorate of Philosophy in December of 2002.

Permanent address: 501 W. 26th St. #121
Austin, TX 78705

This dissertation was typed by the author.